Università degli Studi di Napoli Federico II

FACOLTA' DI INGEGNERIA

DIPARTIMENTO DI INGEGNERIA ELETTRICA

TESI DI DOTTORATO

Modelling for JET Vertical Stabilization System

Tutor: Dottoranda:
Prof. Raffaele ALBANESE   Ing. Teresa BELLIZIO

Coordinatore:
Prof. Guido CARPINELLI

Novembre 2010 (XXIII ciclo)

A nonno Carmine

Acknowledgements

Contents

5   The Vertical Stabilisation Simulator

6   Conclusions

References

Introduction

Nuclear fusion is, in a sense, the opposite of nuclear fission. Fission, which is a mature technology, produces energy through the splitting of heavy atoms like uranium in controlled chain reactions. Unfortunately, the by-products of fission are highly radioactive and long lasting. On the other hand, fusion is the process by which the nuclei of two light atoms such as hydrogen are fused together to form a heavier (helium) nucleus, with energy produced as a by-product.

Although controlled fusion is extremely technologically challenging, a fusion-power reactor would offer significant advantages over existing energy sources. In particular, there exists a sufficient fuel supply for several thousand years since the necessary hydrogen isotopes can be generated from water and abundantly available lithium during the reaction cycle. Like fission, fusion would produce no air pollution or greenhouse gases during normal operation since the fusion reaction product is helium. In contrast to fission, a fusion reactor poses no risk of a nuclear accident since a nuclear meltdown with a large, uncontrolled release of energy cannot occur. Most radioactive materials produced in a fusion reactor can safely and easily be disposed of within a few decades, in contrast to most fission by-products, which require special storage and handling for thousands of years.

The primary challenge of fusion is to confine a gas consisting of ionized hydrogen isotopes, called plasma, while it is heated and its pressure increases to initiate and sustain fusion reactions. The conditions for thermonuclear reaction are difficult and complex to implement, mainly because a very high temperature, of the order of 100 millions of degrees Centigrade, is necessary to pass the energy barrier opposing the fusion reaction due to the long range Coulomb repulsion. The number of particles in a particular region (density), and the amount of time they remain together (confinement time) are also important. There are three known ways to confine the

plasma: gravitational, inertial, and magnetic. Gravitational confinement, occurring naturally inside the sun and other stars, confines the plasma through large gravitational forces. Inertial confinement compresses the hydrogen gases through a controlled implosion, with inertia then holding the gases together long enough for fusion reactions to occur. Finally, magnetic confinement uses magnetic fields acting on hydrogen atoms that have been ionized (given a charge) so that the magnetic fields can exert a force on the moving particles.

This thesis is devoted to the control of tokamaks, magnetic confinement devices constructed in the shape of a torus (or doughnut). Tokamaks are the most promising of several proposed magnetic confinement devices.

Tokamaks of various sizes exist around the world. The largest tokamak is the Joint European Torus (JET) in Culham, England. There are roughly a dozen medium-sized tokamaks such as DIII–D. The medium and large tokamaks are usually funded by governments or consortia of governments and have a dedicated support staff (plus visiting scientists) of more than 100 people. Several smaller tokamaks are located at universities. ITER (International Thermonuclear Experimental Reactor) is an international experiment designed to show the scientific and technological feasibility of a fusion power reactor. It will be a tokamak with an elongated cross section able to produce 500 MW of fusion power, which will be more than the power required to maintain the plasma in steady state. Its design activities date back to the 80's and its construction started in 2008 at Cadarache, France.

The need to improve the performance of modern tokamak operations has led to a further development of the plasma shape and position control systems. In particular, extremely elongated plasmas, with high vertical-instability growth rate, are envisaged to reach the required performance for ignition. This request for better performance from the experimentalists' side has motivated the development of the new vertical-stabilization (VS) system at the JET tokamak, which has been proposed within the Plasma Control Upgrade project. The main aim of the project is to enhance the capabilities of the plasma vertical position control system in order to operate with very highly elongated plasmas in the presence of large perturbations. This thesis presents the activity carried out to increase the capability of the VS system and to understand the operational limits in order to assess what can be done to

improve the overall performance with the existing hardware and control system so as to minimize the impact on JET operation.

The first objective of this work is the analysis of the new diagnostic system and the influence of the mechanical structure on the magnetic measurements used as diagnostics by the VS controller; the main focus is on the influence on the controller performance in the presence of large perturbations. The second objective is to design a new controlled variable to increase the performance of the VS system. The third objective is to provide an equivalent model of an ELM (Edge Localized Mode), in terms of internal plasma profile parameters via best fit of the vertical velocity estimation. The last objective is to obtain a reliable and accurate model of the overall system, based on the new platform MARTe, developed at JET and useful also for other devices.

All the experimental activities described in this thesis have been carried out during my permanence at JET from June 2008 to September 2010.

A brief outline of the thesis is given below.

Chapter 1 gives an introduction to the fusion principles and describes the JET Tokamak, specifying notations and terminology used throughout the thesis. A detailed description of the poloidal field coils and the magnetic measurements is also given. Finally, the main goals of the Plasma Control Upgrade project are described.

Chapter 2 reports the plasma equilibrium equations and the model of the vertical instability in an elongated tokamak. Moreover, it deals with the study carried out to evaluate the effect of passive structures on the magnetic measurements. Finally, it presents the procedure developed to provide an ELM model schematised as an equivalent variation of internal plasma parameters identified from experimental data.

Chapter 3 firstly describes the approach used to design a new estimator of vertical velocity used as controlled variable by the VS system The main motivation of this study was the need of operating JET in future campaigns with the new ITER-like wall (ILW), which is expected to significantly shield some magnetic diagnostics. This study was also aimed at improving the VS capabilities by reducing the effect of edge localized modes (ELMs) on the vertical speed estimator. The alternative controlled variable was also planned to play the role of back-up solution in case of troubles with the standard one after the modifications of the radial field circuit. The

selection was made paying particular attention to robustness, reliability, and reduced impact on the ongoing experimental campaigns. The new controlled variable, denoted as OBS05, was successfully tested in JET on a variety of plasma scenarios and became the new vertical velocity estimator for VS system.

Chapter 4 gives an overview of the new software architecture of the new VS system and describes the modelling activities carried out to increase the performance with anew Enhanced Radial Field Amplifier (ERFA), and different sets of radial coil turns.

Chapter 5 describes the architecture of the new simulator of the VS system and presents the operational limits of the system in terms of largest rejectable disturbance.

Finally, the main conclusions are reported in Chapter 6.

1

Nuclear fusion and magnetic control

1.1 Fusion and tokamaks

This chapter describes the functionalities of a Tokamak fusion device. After a general introduction to the Tokamak operational space, the chapter focuses on the Joint European Torus (JET), the largest Tokamak device in the world. A detailed description of the magnetic actuators and magnetic measurements is given, mainly to introduce the vocabulary used in this thesis. Finally, the attention is moved to JET vertical stabilization system, and more precisely to the magnetic diagnostics and the poloidal field actuators that are used by this system. This chapter analyzes the technique used at JET to estimate the plasma vertical speed, which is used as feedback quantity by the VS controller, and describes the effect of noise and disturbances on the estimated quantity. Special attention is given to those disturbances that most affect the performance of the stabilization system. More precisely, the pick-up noise due to the switching power supplies, the magnetohydrodynamics (MHD) instabilities such as n=1 and n=2 modes, and Edge Localised Modes (ELMs) are treated.

1.1.1 Thermonuclear fusion

In nuclear fusion, two nuclei [1], [2], of light elements are brought together within the range of their strong interactions. As a consequence the nuclei react and melt together, forming new energetic particles. In order to bring the two nuclei together, the repelling Coulomb force has to be overcome over a relatively long distance. Consequently, high temperatures are required for fusion reactions.

The most accessible and promising reaction for a fusion plant is the one between two hydrogen isotopes: deuterium D and tritium T (see Figure 1.1). In this reaction both helium (4He)[1] an energetic neutron (n) are formed:

$$D + T \rightarrow \,^4He(3.5\ MeV) + n(14.1\ MeV) \tag{1.1}$$

Usually in the present experimental devices the use of tritium is avoided because of its radioactivity, therefore, for safety reasons, deuterium alone is used. In this case the produced energy is more than halved (7.3 MeV).

Most of the energy released in reaction (1.1) is carried by the high speed neutrons. The remaining energy goes to the alpha-particles (the fully ionized ^{4}He nuclei). In a thermonuclear fusion facility a jacket (or blanket) around the reactor would slow down the neutrons, converting their energy in heat. This heat could be extracted to produce steam for conventional electricity production.
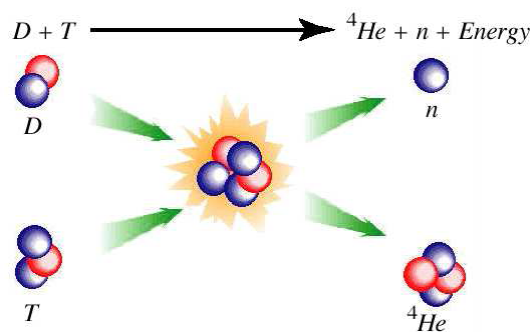

Figure 1.1 Illustration of the *D-T* reaction.

---

[1] He indicates the helium isotope with two protons and two neutrons.

It is worth noticing that deuterium is a common element which could be easily separated from water. Therefore, there is a virtually inexhaustible supply of deuterium in the oceans. In contrast, tritium does not occur naturally in significant quantities. Nevertheless it can be produced using reactions that occur between neutrons formed in the fusion reactions and the light metal lithium (Li).

Therefore, although the fusion reaction occurring in a reactor is between deuterium and tritium, the combustibles will be deuterium and lithium, as described by the following reactions[2]:

$$^{6}Li + n \rightarrow T + ^{4}He$$
$$^{7}Li + n \rightarrow T + ^{4}He + n$$
(1.2)

The world available lithium reserves are such that the present levels of electric power production could be maintained for several hundreds years, using fusion energy.

Since ions are positively charged, the Coulomb force of repulsion has to be overcome before the reactions (1.1) and (1.2) can occur. Therefore the nuclei have to be accelerated to a considerable energy in order to overcome the Coulomb barrier. For instance, the cross-section σ for the D-T reaction depends on the energy of the ions, reaching a peak around 100 keV.

A beam of deuterons from an accelerator cannot be used to have fusion reactions. In fact it can be shown that if the beam is directed at a target of solid tritium, most of the energy is lost in ionizing and heating the target and in elastic collisions. Hence the solution is to form a new state of the matter called plasma at a high temperature where the fastest particles undergo fusion reaction. This is the reason for the term *thermonuclear* fusion.

The power produced per cm^3 in a *D-T* reaction is:

$$P_r = n_D n_T \langle \sigma v \rangle \omega$$
(1.3)

where n_D and n_T are the deuterium and tritium densities, respectively, ω is the 17.6 MeV of energy released by reaction (1.1), and $\langle \sigma v \rangle$ is the product of the reaction

---

[2] ^{6}Li and ^{7}Li indicate two different lithium isotopes.

cross-section and the particles velocity averaged over the assumed Maxwellian distribution.

To maintain the plasma temperature, this power must exceed the amount lost. In fact, even if the plasma is perfectly confined, there is a loss of energy due to the radiation called bremsstrahlung. The bremsstrahlung power is given by:

$$P_b = 1.6 \times 10^{-40} n_e n_i Z_i^2 T_e^{1/2}$$

(1.4)

where n_e and T_e are the electron density and temperature, n_i and Z_i are the ion density and atomic number.

Note that both P_r and P_b vary as the squared density, but, due to the cross section σ rise, P_r increases more rapidly than P_b with the temperature.

The *ignition temperature* can be found equating P_r and P_b. For the *D-T* the ignition temperature is about 4 keV[3], while for the *D-D* reaction it is about 35 keV.

To produce by fusion more energy than the one required to heat the plasma and supply the losses, imposes a condition on the plasma density, the temperature and on the particle confinement time. The plasma kinetic energy W is given by the integral of the pressure over the plasma volume:

$$W = \frac{3}{2} k \int_V (n_e T_e + n_i T_i) dV$$

(1.5)

where k is the Boltzmann constant, and $T_{e,i}$ and $n_{e,i}$ denote, respectively, the temperatures and densities of electrons and ions. In an ideal plasma of hydrogen isotopes(with no impurities) $n_i = n_e$.

Process losses (due to Coulomb collisions, turbulence and escaped particles) tend to decrease W. To compensate these losses, an additional power P_{in} has to be deposited in the plasma. The process losses can be quantified in terms of a typical timescale called *energy confinement time* τ_E. At steady-state:

---

[3] Following the convention generally accepted in the fusion community, temperatures are written in electron-volts (eV). The temperature in electron-volts is defined by the potential difference in volts through which an electron must fall to acquire an energy equals to kT, where k is the Boltzmann constant and T is the temperature in degrees Kelvin. It follows that 1 $eV \sim 10000\ K$, thus 10 $keV \sim 100$ million degrees Kelvin.

$$\tau_E = \frac{W}{P_{in}} \tag{1.6}$$

In a steady-state reactor, to have a plasma that generates more energy through fusion reactions than the amount required to create and sustain it, the *Lawson criterion* [3] must be satisfied, that is:

$$n_i \tau_E > L \tag{1.7}$$

where L depends also on ion temperature T_i. For a D-T plasma [6], [7] at $T_i \sim 10 - 30$ keV, $L \sim 2 \times 10^{20} \ m^{-3}s$.

1.1.2 Magnetic confinement and tokamaks

The Lawson criterion (1.7) tells us that to achieve steady-state operations in a fusion reactor we must ensure high plasma density (n_i) and temperature (T_i) for enough time (τ_E). On the sun, gravity provides the force balancing the enormous pressure gradients leading to the conditions at which fusion reactions occur.

The main problem in the confinement of the plasma is to satisfy the Lawson criterion on the Earth. There are two different approaches:

- inertial confinement
- magnetic confinement

The inertial confinement approach seeks to fuse nuclei so fast that they don't have time to move apart. The two methods proposed for inertial confinement have been laser fusion and ion-beam fusion.

The magnetic confinement approach makes use of magnetic field to keep the charged particles for a long time far from the solid walls. In the linear devices the confinement was achieved thanks to the *magnetic mirror force* effect. In these devices the particles were reflected at the edges by the higher magnetic field (see Figure 1.3).

Toroidal geometry, opposed to linear, takes advantages from the avoidance of "*ends*". Among the several toroidal magnetic configurations that have been proposed,

the tokamak is leading the competition for higher values of the triple product $n_i\tau_E Ti$, thus it is the most promising device in the field of controlled nuclear fusion.

1.1.3 Tokamaks

The tokamak concept [2] was first developed in the former Soviet Union in the early 1960s. The name tokamak stems from the Russian words for toroidal chamber and magnetic coil (toroidalnaya kamera i magnitnaya katiushka).
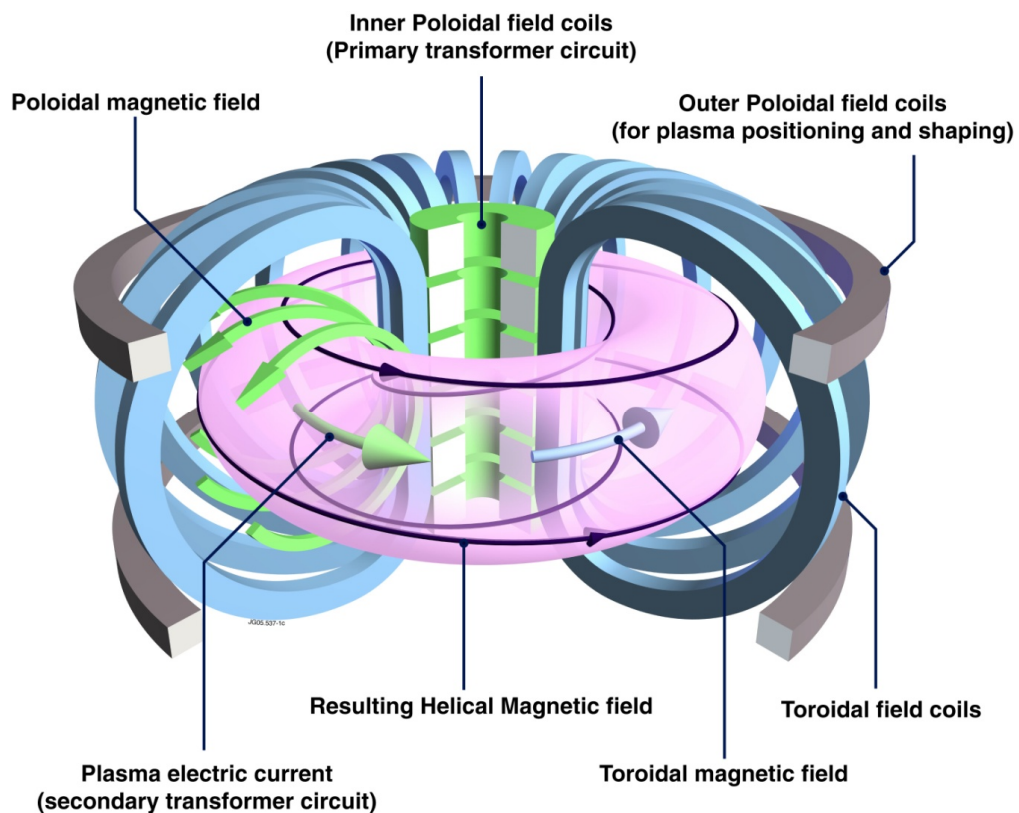
Figure 1.2 Tokamak magnetic configuration

The achievements of the tokamak are impressive: thermal energies are obtained up to 50 keV at reactor relevant densities (in the order of 10^{20} m^{-3}). Moreover several reactor relevant modes of operation have been identified and tested on tokamaks.

The Tokamak is a fusion device that uses magnetic fields to confine the plasma within a toroidal vacuum vessel, as Figure 1.2 shows. The main confinement is obtained by means of a set of toroidal field coils (Figure 1.2), which create a magnetic path for the charged particles that make a plasma. The control of the

plasma position and shape is obtained with a set of poloidal field coils. A dedicated subset of the poloidal field coils, referred to as central solenoid in Figure 1.2, is used to control the plasma current, by using the transformer principle. The remaining poloidal field coils are used to shape the plasma, control its position, and, in tokamak devices with an elongated plasma cross section, to stabilize the plasma vertical position. After the plasma is correctly confined and shaped, it needs to be heated to reach the temperatures at which the hydrogen nuclei start funding together.

The Ohmic heating due to Joule effect is significant for plasma currents of about 5 MA. The temperature that can be obtained in this way is very large, but it is not sufficient to approach the conditions needed for fusion reaction.

Systems for additional heating are:

Neutral beam injection (NBI) Beams of deuterium or tritium ions, accelerated by a potential of up to 1 MV, are injected into the plasma. In order to penetrate the confining magnetic field, the accelerated beams are neutralized. In the plasma, the beams become ionized and the fast ions give up their energy to the plasma.

Ion cyclotron resonant heating (ICRH) The plasma ions and electrons rotate around in the magnetic field lines of the tokamak. Energy can be transferred to the plasma through radio waves resonating with the ion rotation. Antennae in the vacuum vessel propagate waves (in the frequency range of 25-55 MHz for JET) into the core of the plasma to increase the energy of the ions.

Lower hybrid current drive (LHCD) Microwaves with several MW of power at frequencies in the range of 1-5 GHz accelerate the plasma electrons to generate a plasma current.

Neutral beam injection (NBI) as well as lower hybrid waves (LHCD) are capable to drive additional current (called *non-inductive*) into the plasma [4].

1.2   The Joint European Torus tokamak

An example of successful European collaboration, the *Joint European Torus* (JET) has been the world's foremost tokamak machine for 20 years. Built in the early eighties, JET was designed to allow the exploration of the plasma regimes in proximity of break-even, the condition at which the ratio between produced fusion power and input heating power is unity. At the time of its construction, JET was a large step in scale from existing experiments, even larger than the one envisaged for the construction of the International Thermonuclear Experimental Reactor (ITER) [5].

In 1997 16 MW of fusion power have been generated at JET by a heating power of 26 MW, corresponding to an *amplification factor* (Q)[4] of 0.6. This important result has been achieved using a *D-T* plasma.

At JET good results have been obtained using deuterium plasmas as well. Extrapolations have been carried out for these experiments, computing the amplification factors that could be achieved using a *D-T* mixture in place of pure deuterium.

1.2.1   The JET experiment

The JET magnetic configuration is characterised by a set of 32 toroidal field coils, and by 8 poloidal field coils. The toroidal field system is used to create a toroidal field that can reach up to 4 T at the centre of the JET vacuum vessel. Some of the poloidal field coils have turns reserved for different circuits, leading to a total of 10 circuits powered by 10 different power supplies.

JET Poloidal Field Coils

The JET poloidal field coils system is used to control the plasma shape, position and current. The overall poloidal system is divided into 10 circuits, each powered by a separate amplifier. The control system responsible to control the currents in each

---

[4]   The fusion performance of a power plant is denoted by Q, which is the ratio of the energy of the fusion products (alpha power plus neutron power for a *D-T* plasma) to that used to heat the plasma. Break-even corresponds to $Q = 1$, while ignition corresponds to $Q = \infty$. A *burning plasma* has $Q > 1$.

circuit is the Plasma Position and Current Control system (PPCC). More precisely, the PPCC is composed of the Shape Controller system (SC) and by the VS system, the first controlling the plasma shape and current in the low frequency domain, the latter stabilizing the plasma vertical position in the high frequency range.
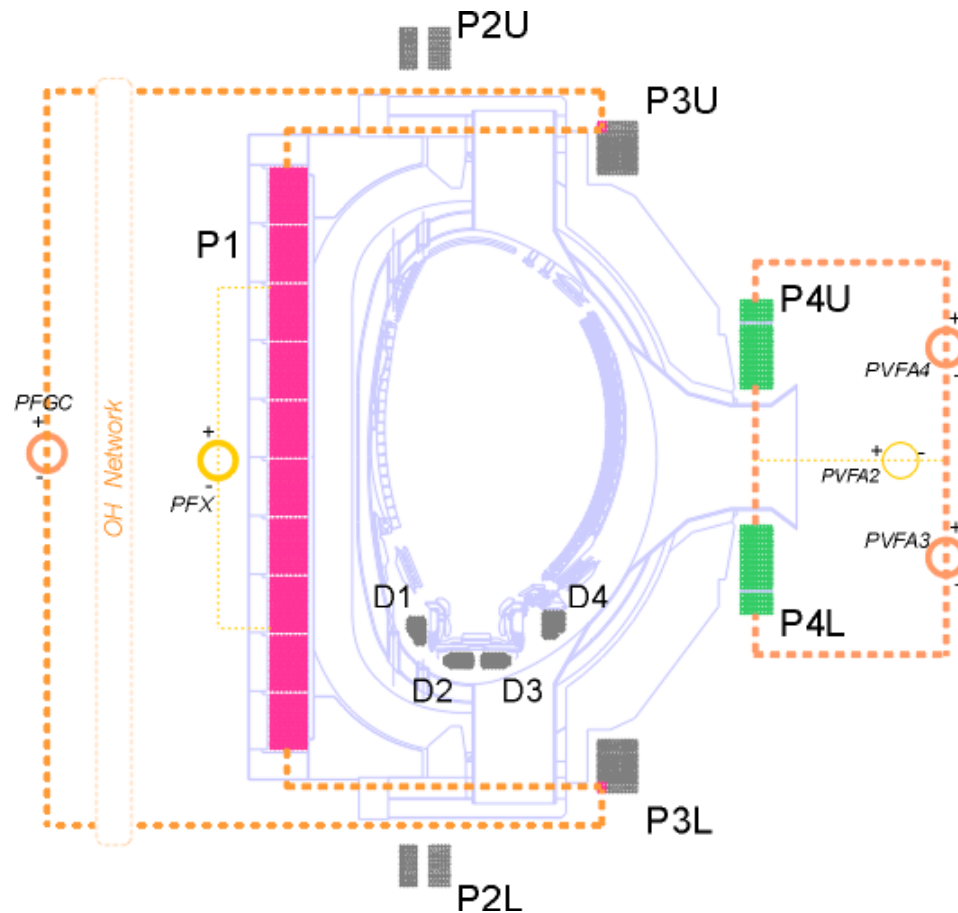
Figure 1.3 JET Poloidal Cross Section. The poloidal field coil system is composed of several circuits [8] (image courtesy of EFDA-JET).

Hereafter a brief description of the circuits is given.

Ohmic Heating Circuit The ohmic circuit is used to control the plasma current by using the transformer principle. This circuit is composed by the series of the central solenoid coils and some turns of the P3 circuit (normally referred to as P3M) acting as the primary winding of the transformer, whereas the plasma acts as the secondary winding. The physical connection of the ohmic circuit is shown in Figure 1.3. The circuit is powered by a flywheel generator, which is charged before the start of a JET experiment. The Ohmic heating circuit is designed so as to provide a small field in the plasma region and has negligible effects on the plasma shape. In order to act on

the plasma shape, a subset of the central solenoid has been connected to a power amplifier. This circuit is named as PFX circuit, where the name stands for poloidal field X-Point circuit.

Vertical Field and Imbalance Circuit The hoop force of the plasma has to be counteracted in order to keep the plasma within the vacuum vessel. This task is performed by the vertical field circuit, which is composed of the series of the P4 coils. The current flowing in this circuit has sign opposed to the sign of the plasma current, so creating in inboard force which counteracts the expanding hoop force of the plasma. This circuit is powered by a series of 4 amplifiers, of which 2 amplifiers are named the Booster amplifiers, and 2 are the vertical field amplifiers (these being represented in Figure 1.3). The booster amplifiers are only used during the very first phases of the plasma discharge, where the plasma current quickly increases. To control the vertical position of the plasma centroid, an amplifier which creates an imbalance current between the upper and the lower coils (P4U and P4L in Figure 1.3) is used. This circuit creates a radial field which acts on the vertical position of the plasma, and is normally referred to as the imbalance circuit.

Radial Field Circuit The radial field circuit is controlled by the vertical stabilization to stabilize the plasma vertical position. This circuit is composed of the series of some turns of the P2 and P3 coils, namely P2R and P3R, which are connected to create a mainly radial field. The radial field circuit is powered by a 5 kA-12kV IGBT amplifier, which is normally referred to as Enhanced Radial Field Amplifier (ERFA). This circuit is not used to control the plasma vertical position, but to keep the plasma vertical velocity around zero. The shape controller system uses the imbalance circuit to position the plasma in the vacuum vessel, while the vertical stabilization system uses the Radial Field circuit to stabilize the plasma around that vertical position.

Shaping Field Circuit The shaping circuit is used to change the plasma elongation. It is composed of the series of some turns of the P2 and P3 coils, namely P2S and P3S. To increase the plasma elongation, the circuit is connected in the way that the current in the P2 circuit has the same sign as the plasma current, while the P3 circuit has the current flowing in the opposite direction.

Divertor Circuits The position of the plasma strike points is controlled by means of the divertor circuits. JET has 4 divertor circuits (namely D1, D2, D3 and D4), each

powered by a different amplifier. Differently from all the other poloidal field coils, the divertor coils are placed within the vacuum vessel, as Figure 1.3 shows.

Effect of the Poloidal Field Circuits The influence and use of each of the poloidal circuits can be understood by observing Figure 1.4, where the effect of a single circuit on the plasma shape is displayed.
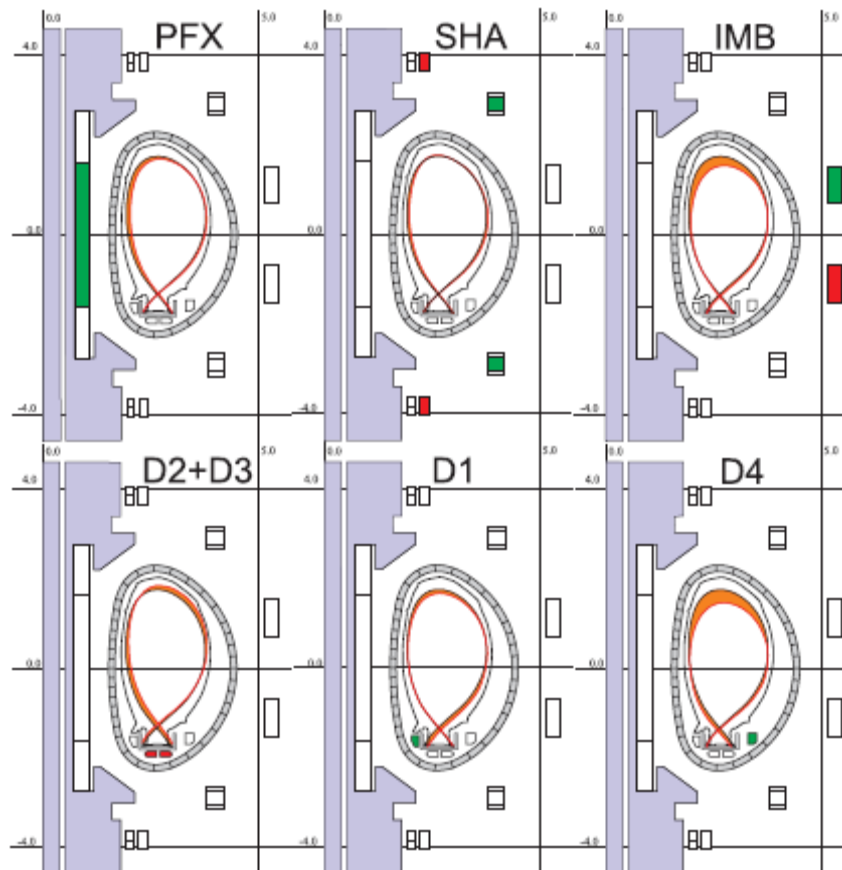
Figure 1.4 Effect of the poloidal field circuits on the plasma shape. The red area in the plasma characterises the effect of the variation of the current in a given circuit. The colour convention on the poloidal coil is red for a current flowing in the same direction as the plasma current, green for a current flowing in the opposite direction [8] (image courtesy of EFDA-JET).

Elongated plasmas, such as those experienced at JET, present a vertical instability that can lead to a sudden termination of the plasma experiment and could cause significant damage to the vacuum vessel and supporting structures. This event is normally referred to as a Vertical Displacement Event (VDE) and it is the task of the VS system to avoid its occurrence. The instability growth rate changes depending on the plasma elongation, where more elongated plasmas present a higher instability time constant. As Figure 1.5 shows, the overall effect of the poloidal field circuits is

to create currents of the same sign as the plasma current on the top and bottom of the plasma (Shaping circuit) and of the opposite sign on the inner and outer sides of the plasma (PFX and P4 circuits), so modifying the plasma elongation (ratio between vertical and horizontal dimension of the cross section) and triangularity (geometric parameter for D-shaped plasmas).
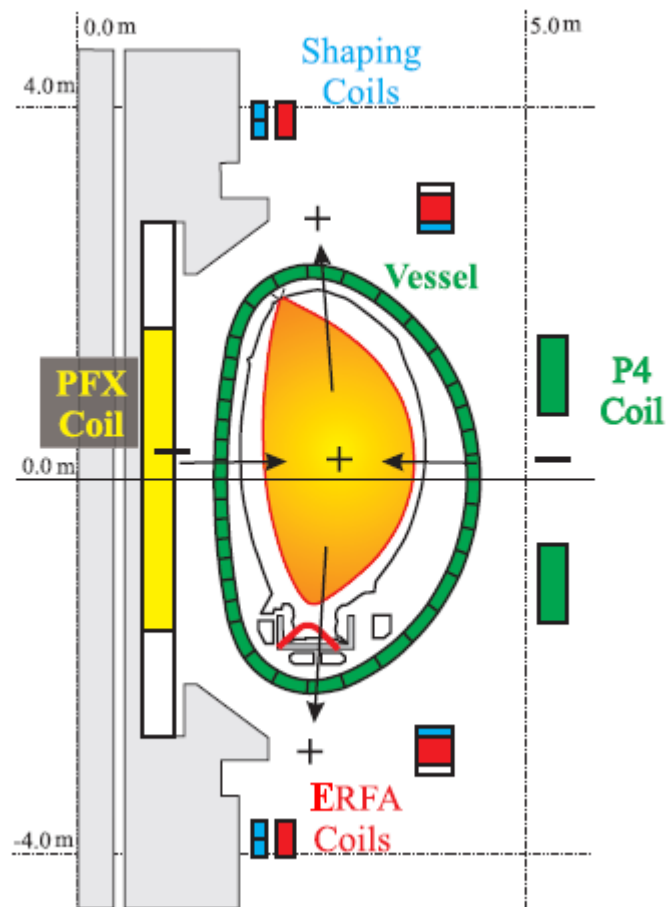
Figure 1.5 The plasma elongation can be modified by using different poloidal field circuits. The PFX and P4 circuits are used to *squeeze* the plasma, while the shaping circuit is used to change the elongation. Overall, the PFX and P4 circuit act by using a current of the opposite sign of the plasma, while the Shaping circuit uses a current of the same sign for the P2 coils and opposite for the P3 coils (image courtesy of EFDA-JET) [8].

The attraction forces between the upper (or the lower) shaping coils and the plasma increase as the distance decreases. Therefore, a vertical movement of the plasma in either direction increases the attraction force (in the same direction), hence triggering a vertical instability. The vertical stabilization system uses the ERFA circuit to

counteract the plasma movement by keeping the average of the estimated plasma vertical speed to zero.

1.2.2 Magnetic Measurement for Real Time Control

The information about the plasma position and shape is obtained by using a set of magnetic measurements located at different toroidal and poloidal positions. Depending on the quantity to be estimated, the magnetic measurements are integrated over time to produce a local measurement of the magnetic field and magnetic flux, or used non-integrated to measure the time derivatives of the magnetic field and flux.

Hereafter a description of the type of magnetic measurements used for real time applications and their toroidal and poloidal position is given.

Mirnov Coils, also known as pick-up coils, are a type of magnetic probe used to measure the local value of the time derivative of the magnetic field. The coil is made by several turns of wire wound around a small cross section area. The output voltage is proportional to the time derivative of the average magnetic flux concatenated by the windings. Given the small dimensions, these coils are used to measure the local value of the magnetic field component perpendicular to the coil cross section. JET is equipped with several Mirnov coils located at different poloidal and toroidal positions, as Figure 1.6 shows. The whole set of coils is classified according to the use and poloidal location. Figure 1.6 summarises the different naming conventions, and shows the toroidal and poloidal positions of the available coils.
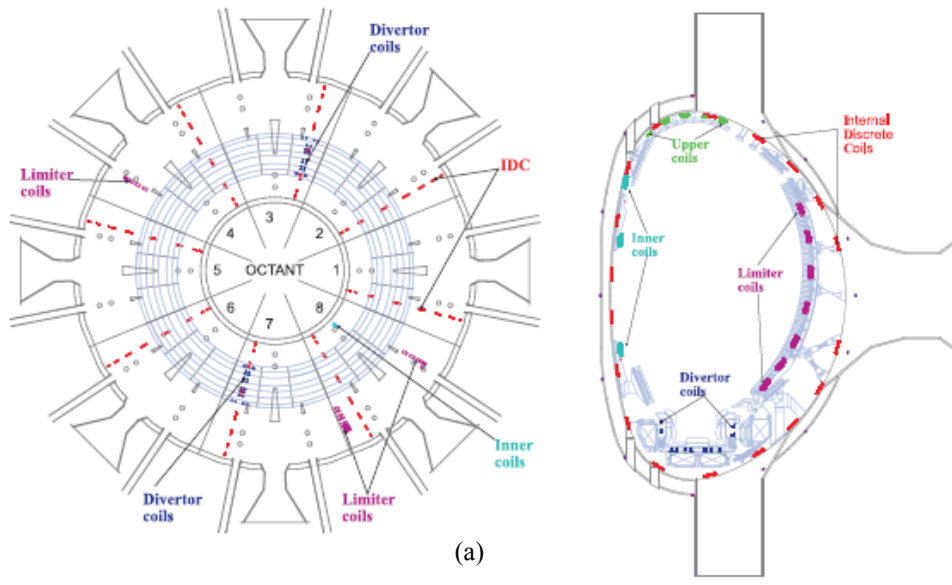
Figure 1.6 Toroidal (a) and poloidal (b) positions of the Mirnov coils. Only the coils displayed in red (Internal Discrete Coils) are used by the vertical stabilization system [8] (image courtesy of EFDA JET).

Saddle Loops The saddle loops are a type of magnetic probe which measures the time derivative of the magnetic flux on a large area. They are made by long wire placed on the external surface of the JET vacuum vessel to cover a one octant section of toroidal area. JET is equipped with 8 sets of 14 saddle loops, where the toroidal and poloidal location is shown in Figure 1.9.
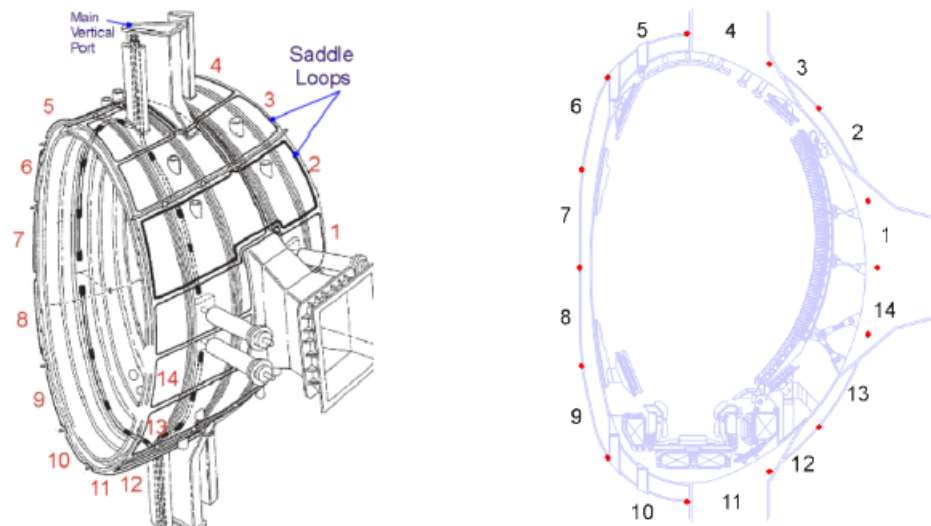
Figure 1.7 Poloidal location and view of an octant for the saddle loops installed at JET [8] (image courtesy of EFDA-JET).

1.2.3 Vertical Stabilization Magnetic Measurement

The VS system uses 18 poloidal field measurements provided by the internal discrete tangential field sensors, situated inside the vacuum vessel, and 14 saddle loops, measuring the average normal field to estimate the plasma vertical speed, which is used as the feedback quantity by the stabilization system. The technique that is used to compute the plasma vertical speed is derived from the current moment method, which was initially developed by Zakharov and later revised by Aikawa and Ogata. The starting equation is [9]:

$$\frac{d\left(Z_c I_\phi\right)}{dt} = \frac{1}{\mu} \oint_l \left[z\frac{dB_t(r,z)}{dt} - r\log\left(\frac{r}{R_0}\right)\frac{dB_n(r,z)}{dt} \right] dl \tag{1.8}$$

where I_ϕ is total toroidal current linked with the curve l, Z_C is the toroidal current vertical centroid, R_0 the major radius of the chamber, t the time, B_t and B_n are the tangential and normal components of the magnetic field measured on the line l, and r and z are the coordinates in the plane.

Assuming the l curve to be positioned on the JET vacuum vessel, the total toroidal current is given by the contribution of the plasma current, the current flowing in the divertor circuits and in the passive structures, namely the restrain rings and the divertor support structure. Discretising this equation with the finite number of measurements available, namely 18 tangential component of the magnetic field (B_t) measured by Internal Discrete Coils and 14 average values of the normal component (B_n) measured by the saddle loops, the relationship can be written as:

$$\frac{d\left(z_p\right)}{dt}I_p \approx \sum_{i=1}^{18} a_i \frac{dB_t(r,z)}{dt} + \sum_{i=1}^{14} b_i \frac{dB_t(r,z)}{dt} - \frac{d\left(I_p\right)}{dt}z_p - z_{pass}\frac{d\left(I_{pass}\right)}{dt} \tag{1.9}$$

with:

$$z_{pass}\frac{d\left(I_{pass}\right)}{dt} = \sum_{i=1}^{4} z_D(i)\frac{d\left(I_D(i)\right)}{dt} - z_{rr}\frac{d\left(I_{rr}\right)}{dt} - z_{mkII}\frac{d\left(I_{mkII}\right)}{dt} \tag{1.10}$$

In equation 1.9, I_p represents the plasma current, and $\dfrac{d(z_p)}{dt}$ the plasma vertical speed. The coefficients a_i's and b_i's are the weights obtained via discretization of equation 1.8 taking into account the poloidal positions along a closed poloidal line where the Mirnov coils and saddle loops are placed, while z_{pass} and I_{pass} represent the position and current of the passive structures. In particular, in equation 1.10 all the terms z and I at the right hand side specify all the z coordinate and the currents considered, with D indicating the four divertor PF coils, rr the restrain rings and $mkII$ the divertor support structure named Mark II.

The Vertical Stabilization (VS) system uses 32 magnetic measurements, coming from sets located in four different octant, each including 18 internal discrete tangential field sensors, situated inside the vacuum vessel and 14 saddle loops (namely CX01, …,CX18, SX01, …,SX14 where X=1,3,5,7 depending on the octant), originally utilized to estimate the vertical plasma velocity by means of the following relationships:

$$\frac{dI_P}{dt} = \frac{1}{\mu}\oint \frac{dB_t}{dt}\, ds \approx \sum_{k=1}^{Nmag} w_{0k} m_k \tag{1.11}$$

$$\frac{d(Z_P I_P)}{dt} = \frac{1}{\mu}\oint \left[Z\frac{dB_t}{dt} - R\log\left(\frac{R}{R_0}\right)\frac{dB_n}{dt} \right] ds \approx \sum_{k=1}^{Nmag} w_k m_k \tag{1.12}$$

where I_P is the plasma current, Z_P the vertical position of its centroid, R the radial coordinate, Z the vertical coordinate, R_0 the major radius of the chamber, t the time, B_t and B_n the tangential and normal component of magnetic flux density, respectively.

With a finite number, $Nmag$, of magnetic measurements, m_k, of time derivatives of magnetic fields, line integrals (1.11)-(1.12) can be approximated as linear combinations of these signals with suitable weights w_{0k}'s and w_k's. After the introduction of the divertor coils D1-4 and the installation of MK2 conducting structure inside the vessel, the magnetic measurements coming from magnetic field sensors placed on the lower part of the machine are not only behind currents flowing

inside the vessel but also significantly affected by the noise of the amplifier. The pick-up coils in the lower region were then discarded, and the remaining weights were readjusted. The resulting combination provides a rough estimate of (1.12) at slowly varying plasma current, denoted as ZPDIP, which is obviously inaccurate. Nonetheless, the VS system successfully works with feedback on ZPDIP, which is an output correlated to the unstable mode.

In principle, additional magnetic measurements located at different positions in the poloidal plane R-Z might be used for VS diagnostics. However, these additional in-vessel sensors are located at only two toroidal locations and it is not possible therefore to compensate for non-axisymmetric n=2 plasma perturbations.

Attempts at VS control have been done at JET using nonmagnetic measurements, e.g. soft X-rays [9]. The so-called full current moment method was also tested [10], based on (1.11)-(1.12) with suitable correction terms taking into account the contributions from the in –vessel currents. However, there was a prejudice that these techniques would not be reliable enough for routine operation or would deal with ELMs and therefore the idea was not followed up beyond the first test.

(a)   (b)
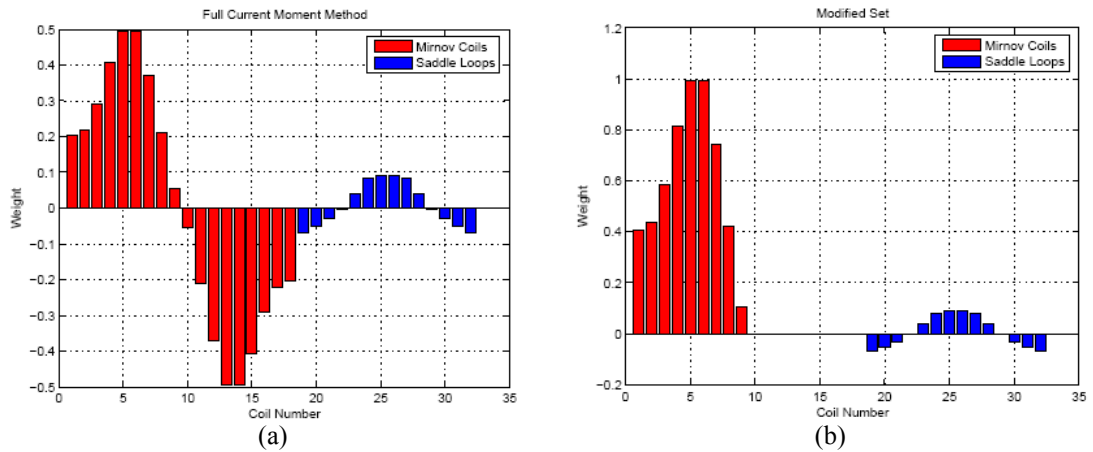
Figure 1.8 Spatial distribution of the Full Current Moment Method weights (a), and the standard set (yielding the ZPDIP signal), differing from the full current method so as to take in account the new divertor structure installed at JET. The first 18 weights correspond to the Mirnov coils (red), while the remaining 14 to the saddle loops (blue).

The weights obtained by the full current moments are thus used only during the early phases of the plasma formation while a different set of weights, heuristically adjusted after the mechanical modifications, has been applied so as to improve the stabilizing capability of the VS controller. In particular, during the main flat-top phase, JET uses

a standard set of weights (yielding the ZPDIP signal) that has doubled the original values relative to the Mirnov coils placed in the upper part of the vessel, while ignoring the measurements of the pick-up coils placed in the lower part of the machine, and keeping the same values for the saddle coils (Fig. 1.8 b). In addition, the last two terms of equation 1.9 are neglected.

The resulting combination provides an incorrect estimation of the plasma vertical speed, which is used during the main steady-state phases of the experiment as feedback to the VS system. It has been verified that the standard vertical speed estimator (ZPDIP) is inaccurate for future JET experimental campaigns with the new ITER-like wall (ILW), which is expected to significantly shield some magnetic diagnostics. This study was also aimed at improving the VS capabilities by reducing the effect of edge localized modes (ELMs) on the vertical position estimator. The selection was made paying particular attention to robustness, reliability, and reduced impact on the ongoing experimental campaigns.

In Chapter 3 the design of the alternative controlled variable is described.

1.2.4 MHD Activities

The plasma equilibrium is often affected by the presence of Magneto Hydro Dynamic modes [11], which reduce the plasma performances and cause a reduction of the signal to noise ratio of the estimated plasma vertical speed. The perturbation of the plasma toroidal symmetry is often decomposed in perturbations of the shape on the poloidal plane (M modes) and toroidal plane (N modes) components. For what concerns the VS system, only the N modes are considered, even if in reality the perturbation presents both M and N components. A graphical representation of the N modes is shown in Figure 1.9.
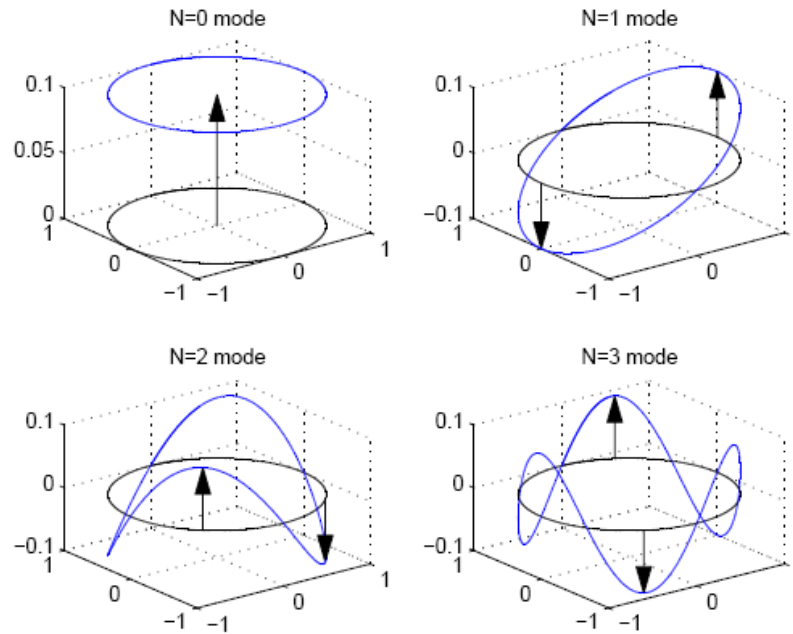
Figure 1.9 Graphical representation of the N modes. The modes are compared to the plasma equilibrium, which is represented by the black dashed line. While the N=0 mode, which essentially corresponds to a vertical displacement of the plasma, is controlled by the VS system, the other modes act as a disturbance.

To understand how the N modes affect the vertical speed estimation, let us consider an unrealistic case where only an N=2 mode is present. Since the modes rotate with the plasma, measurements placed in 2 opposite octants would measure the same field derivative and hence produce a vertical speed estimation that is equivalent to a plasma vertical displacement (N=0). The controller reacts to the measurement by requesting the activation of the amplifier, even if the plasma did not present any real vertical displacement. Moreover, since the modes rotate at high speed around the torus, the request sent by the controller to the amplifier is in the range of kHz, which has the consequence of overheating the amplifier. If the mode sustains for long periods, the amplifier gets into self protection to avoid thermal damage of the switching components, with the consequent lost of the vertical position of the plasma. To avoid the occurrence of the overheating of the power supply, the vertical stabilization system has been modified to include measurements from 4 opposite octants, so reducing the effect of the N=2 modes. An experimental example of this case (where also other modes appeared) is shown in Figure 1.10.
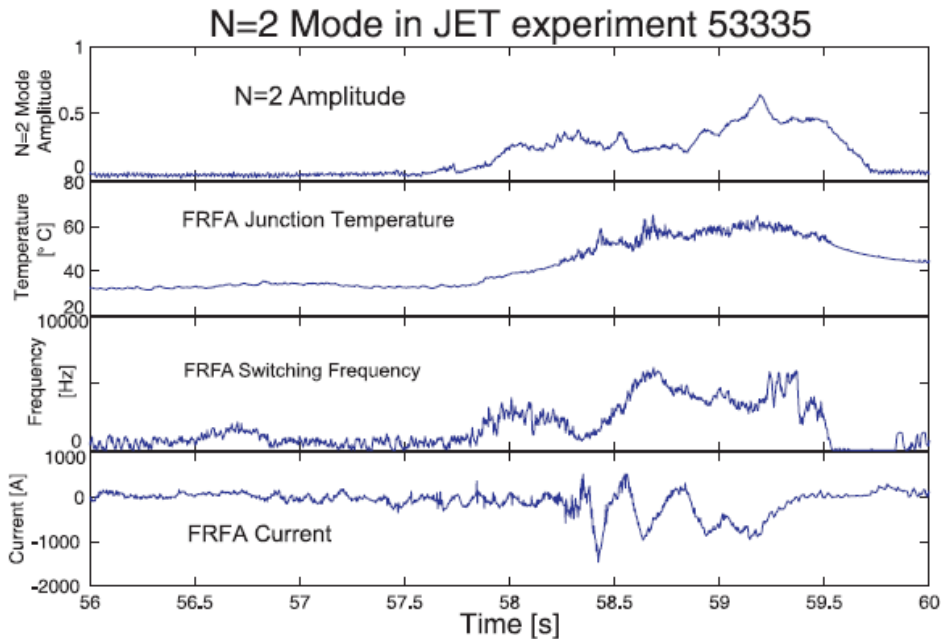
Figure 1 10 Example of amplifier overheating due to N=2 MHD activity. The top figure reports the mode amplitude, the second figure shows the FRFA junction temperature, the third figure shows the measured ERFA switching frequency and the bottom figure shows the ERFA current evolution. It is worth noticing that the normal ERFA switching frequency spans between 500 Hz to 800 Hz, while during the N=2 mode the measured switching frequency reaches the value of 5kHz.

1.2.5 Edge Localized Modes

Edge Localised Modes [12], [13] are MHD instabilities that occur when operating the plasma in the so called H-mode scenario. The H-mode is a type of plasma scenario where the pressure profile presents a steep gradient on the edge of the plasma, reducing the plasma transport to edge and hence increasing the plasma pressure (Figure 1.11). The physical phenomenon responsible for the H-mode scenario is the presence of a plasma transport barrier at the plasma edge (Edge Transport Barrier ETB). When a steep physical parameter gradient is observed, an instability is observed.

This instability (ELM) is responsible for the collapse of the ETB, thus reducing the plasma internal pressure and performance. ELMs manifest themselves as strong magnetic perturbations associated with a burst of D-alpha radiation and a loss of particles and energy from the plasma periphery.
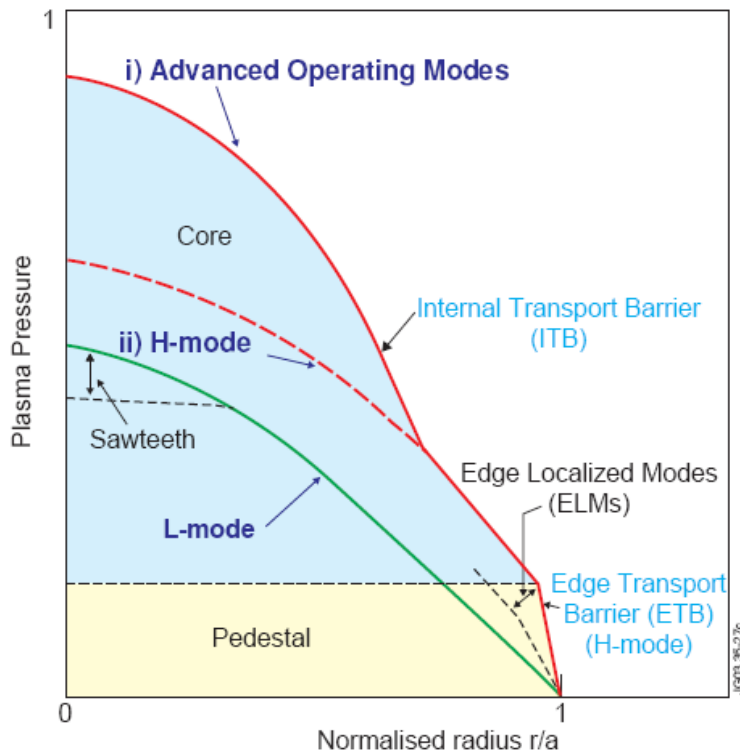
Figure 1 11 L mode and H mode pressure profile. The ELM instability occurs at the plasma edge where a steep pressure gradient is induced by the presence of an Edge Transport Barrier. [8] (image courtesy of EFDA-JET).

The phenomenon is roughly periodic with an intensity which is inversely proportional to the period. Energy pulses of more than 1 MJ can be discharged by the plasma at a rate of about 1Hz. This phenomenon is to some degree understood, but the lack of accurate measurements means that the exact details of what happens to the plasma are not known.

The following classification of ELMs is now standard [8]:

- *Type I ELMs*: the D-alpha radiation shows large isolated bursts and, therefore, Type I ELMs are also called 'large' or even 'giant' ELMs. The instability is pressure driven, and as the heating power is increased, the ELM repetition frequency also increases. The degradation of the plasma confinement is smaller than with other ELM types.

- *Type II ELMs*: these are observed only in strongly-shaped plasmas, i.e. with high elongation and triangularity of plasma cross-section. Also the plasma density needs to be rather high. The magnitude of the ELM bursts is lower

31

and the frequency is higher than that of type I ELMs, while the confinement stays almost as good. Type II ELMs are often called 'grassy' ELMs.

- *Type III ELMs*: the bursts are small and frequent. Therefore, another name for type III ELMs is 'small' ELMs. The instability is driven by electric current, and appears when plasma resistivity is rather high. The ELMs repetition frequency is found to decrease with the increasing heating power.

Since the ELMy-H-mode is the operating scenario that has been chosen for ITER (International Thermonuclear Experimental Reactor), studying how ELMs affect the performance and the controllability of the plasma is one of the most active fields of fusion research. This thesis proposes a model of an ELM event to study its effect on the VS system.

1.3 The Plasma Control Upgrade Project

The Plasma Control Upgrade [14] (PCU) project aimed at upgrading the performance of the Vertical Stabilization (VS) system [15]. The project was divided into three main areas of research aimed at improving the vertical stabilization system both from the performance and maintainability point of views. The first task aimed at improving the modelling techniques currently used for the analysis of the vertical instability and at producing a reliable plasma model that can be used to design improved control system techniques. The second part of the project studied the hardware and software requirements needed to increase the system flexibility so as to allow the maintainability of the overall system and the commissioning of new control techniques in parallel to the JET experimental campaign. The third task of the project studied and designed an enhanced radial field amplifier (ERFA) that should have increased the power delivered to the plant.

The modelling activity was focused to the optimization of the simulation tools, in order to tune the VS system so as to provide its best performance after the 2009-10 shut down. It also intended to provide an adequate support from modelling and control groups to the engineering design and commissioning of the new enhanced radial field amplifier (ERFA) [16], supposed to replace the previous one (FRFA). The main achievements include:

- the development of a closed loop model of the VS system, including ERFA as well as the coupling between VS and the plasma Shape Control (SC) [17], which in some cases yielded undesired oscillations;

- the choice of the turns to be used in the control coils, taking into account the parameters of ERFA.

2

Modelling for magnetic control

2.1 Ideal magnetohydrodynamics

The Ideal magnetohydrodynamics (MHD) [18], [19], model describes the time evolution of a plasma magnetically confined in equilibrium configurations [20]. The model is derived from the quasi-stationary Maxwell's equations:

$$\nabla \times \boldsymbol{E} = -\frac{\partial \boldsymbol{B}}{\partial \boldsymbol{t}} \tag{2.1}$$

$$\nabla \times \boldsymbol{H} = \boldsymbol{J} \tag{2.2}$$

$$\nabla \cdot \boldsymbol{B} = \boldsymbol{0} \tag{2.3}$$

with the constitutive relationships:

$$\boldsymbol{B} = \mu \boldsymbol{H} \tag{2.4}$$

$$\boldsymbol{J} = \sigma\left(\boldsymbol{E} + \boldsymbol{v} \times \boldsymbol{B} + \boldsymbol{E}_i\right) \tag{2.5}$$

where $\boldsymbol{E}$ is the electrical field, $\boldsymbol{B}$ is the magnetic flux density, $\boldsymbol{t}$ is the time, $\boldsymbol{H}$ is the magnetic field, $\boldsymbol{J}$ is the current density, $\boldsymbol{\mu}$ is the magnetic permeability, $\boldsymbol{\sigma}$ is the

electric conductivity, **v** is the velocity, and E_i is the impressed field, namely, the force per unit charge due to external sources.

The plasma velocity is determined by the momentum balance:

$$\rho \frac{D\boldsymbol{v}}{Dt} = \boldsymbol{J} \times \boldsymbol{B} - \nabla p \tag{2.6}$$

where ∇ is the *nabla* operator and p is the kinetic pressure, $\frac{D}{Dt} = \frac{\partial}{\partial t} + \boldsymbol{v} \cdot \nabla$ the substantial derivative. Pressure, velocity, and density are coupled by thermodynamic and fluid equations.

With the assumption of a single, non-dissipative fluid involving adiabatic behaviour and entropy conservation, the thermodynamic equation has the form:

$$\frac{D}{Dt}\left(p\rho^{-\gamma} \right) = \boldsymbol{0} \tag{2.7}$$

where ρ is the mass density and γ is the gas adiabatic exponent. Finally, mass conservation approximation yields the continuity equation:

$$\frac{D\rho}{Dt} + \rho \nabla \cdot \boldsymbol{v} = \boldsymbol{0} \tag{2.8}$$

In axisymmetric geometry with cylindrical coordinates (*r, φ, z)*, the vectors and can be expressed in terms of two scalar functions, namely, the *poloidal magnetic flux* and the *poloidal current*.

The poloidal flux $\Psi(r,z)$ is the magnetic flux linked with the circumference obtained by revolving the point (*r, z*) around the axis *z*. The vertical component of *B* is given by $\boldsymbol{B}_z = (\partial\Psi/\partial r)/2\pi r$, as shown in Fig. 2.1 considering the differential magnetic flux $d\Psi = \Psi(r + d\boldsymbol{r},z) - \Psi(r,z)$.

$$B_z \qquad \Psi (R+dR,Z)$$
$$\Psi (R,Z)$$

(a)

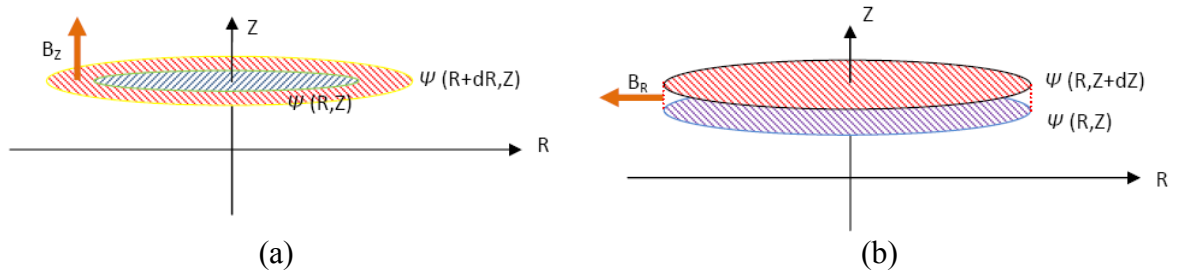$$B_R \qquad \Psi (R,Z+dZ)$$
$$\Psi (R,Z)$$

(b)

Figure 2.1 Evaluation of B_z (a) and B_r (b) using the poloidal flux per radiant Ψ.

The poloidal flux per radian $\Psi(r,z) = \Psi(r,z)/2\pi$ is more frequently used to simplify the expressions, yielding $B_z = (\partial\Psi/\partial r)/r$ (Fig.2.1a). In addition the divergence-free condition (2.3) yields the radial component $B_r = -(\partial\Psi/\partial z)/r$, since the differential flux $d\Psi = \Psi(r,z+dz) - \Psi(r,z)$ is exactly balanced by the magnetic flux across the lateral cylindrical surface, where B_r is the normal component and dz is the height (Fig. 2.1b). Using Ampère's law (2.2) and the constitutive equation (2.4) the total current linked with the circumference obtained by revolving (r, z) around the z axis is given by the $I_{pol}(r,z) = \dfrac{2\pi r B_\phi(r,z)}{\mu(r,z)}$.

If we introduce the poloidal current function $f = \mu I_{pol}(r,z)/2\pi = rB_\phi$ to simplify the expression, the magnetic flux density can be expressed as:

$$B = \frac{1}{r}\nabla\Psi \times i_\varphi + \frac{f}{r}i_\varphi \qquad (2.9)$$

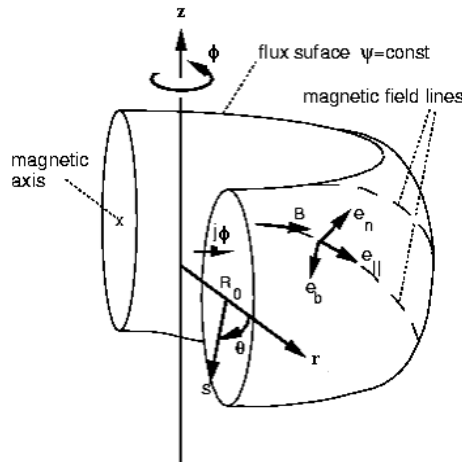where i_φ is the unit vector in the toroidal direction (Fig, 2.2).

Figure 2.2 Reference coordinate system

A similar expression can be derived for the current density:

$$\boldsymbol{J} = \frac{1}{r}\nabla\left(\frac{f}{\mu}\right)\times \boldsymbol{i}_{\varphi} - \frac{1}{\mu_0 r}\Delta^*\Psi \boldsymbol{i}_{\varphi}$$

(2.10)

where μ_0 is the permeability on the vacuum, and the poloidal components $\boldsymbol{J}_r = -\left(\partial I_{pol}/\partial z\right)/2\pi r$ and $\boldsymbol{J}_z = \left(\partial I_{pol}/\partial r\right)/2\pi r$ are expressed in term of f.

The toroidal component is related to the second-order differential operator Δ^* defined by:

$$\Delta^*\Psi \equiv r\frac{\partial}{\partial r}\left(\frac{1}{\mu_r r}\frac{\partial\Psi}{\partial r}\right) + \frac{\partial}{\partial z}\left(\frac{1}{\mu_r}\frac{\partial\Psi}{\partial z}\right)$$

(2.11)

where $\mu_r = \mu/\mu_0$ is the relative magnetic permeability, which is equal to one in a vacuum and in non-magnetic media like air and plasma. Equation 2.11 is obtained from the toroidal component of Ampère's law 2.2 using the constitutive equation 2.4 and the magnetic flux expression 2.9 in terms of Ψ.

If we make the assumption of single plasma fluid with $\sigma \to \infty$ and $\boldsymbol{E}_i \to \boldsymbol{0}$, we obtain $\boldsymbol{E} + \boldsymbol{v}\times \boldsymbol{B} = \boldsymbol{0}$ and the ideal MHD equations. At equilibrium, with the assumption of stationary conditions $\partial/\partial t = 0$ and static conditions $\boldsymbol{v} = \boldsymbol{0}$, the plasma momentum balance (2.6) becomes $\boldsymbol{J}\times \boldsymbol{B} = \nabla p$:

$$\begin{cases} \boldsymbol{J}\times \boldsymbol{B} = \nabla p \\ \nabla\times \boldsymbol{B} = \mu_0\boldsymbol{J} \\ \nabla\cdot \boldsymbol{B} = \boldsymbol{0} \end{cases}$$

(2.12)

This expression yields $\boldsymbol{B}\cdot\nabla p = \boldsymbol{0}$, which means that the magnetic surfaces are isobars, and $\boldsymbol{J}\cdot\nabla p = \boldsymbol{0}$, which indicates that the current lines lie on the magnetic surfaces.

In axisymmetric plasmas, taking into account expressions (2.9 – 2.10) and that $\mu = \mu_0$, we obtain $\nabla p \times \nabla \Psi = \nabla p \times \nabla f = 0$, thus $\nabla f \times \nabla \Psi = 0$. The equilibrium condition $\boldsymbol{J} \times \boldsymbol{B} = \nabla p$ becomes:

$$-\frac{\Delta^*}{\mu_0 r^2}\nabla\Psi - \frac{f}{\mu_0 r^2}\nabla\Psi = \nabla p \tag{2.13}$$

If we assume that the flux surfaces are nested, then $\boldsymbol{f} = \boldsymbol{f}(\Psi)$ and $\boldsymbol{p} = \boldsymbol{p}(\Psi)$, obtaining the *Grad- Shafranov* equation:

$$\Delta^*\Psi = -f\frac{df}{d\Psi} - \mu_0 r^2 \frac{dp}{d\Psi} \tag{2.14}$$

where Δ^* is defined by (2.11).

2.1.1 Solution of Grad-Shafranov equation via finite element method

If we consider the toroidal component of Ampère's law (2.2) we obtain the following equation [21], [22], [23], [24]:

$$\Delta^*\Psi \equiv r\frac{\partial}{\partial r}\left(\frac{1}{\mu_r r}\frac{\partial\Psi}{\partial r}\right) + \frac{\partial}{\partial z}\left(\frac{1}{\mu_r}\frac{\partial\Psi}{\partial z}\right) = -\mu_0 r J_\varphi \tag{2.15}$$

with:

$\Delta^*\Psi = -f\dfrac{df}{d\Psi} - \mu_0 r^2 \dfrac{dp}{d\Psi}$ in the plasma region,

$\Delta^*\Psi = -\mu_0 r J_{ext}(r,z,t)$ in the external conductors,

$\Delta^*\Psi = \boldsymbol{0}$ elsewhere

whit boundary conditions at $r = \boldsymbol{0}$ and regularity conditions at infinity:

$$\begin{cases} \Psi(0,z,t) = 0, \\[2em] \lim_{r^2+z^2\to\infty} \Psi(r,z,t) = 0. \end{cases}$$

Since there are no general solutions to the problem, numerical methods are used to obtain the poloidal flux map. A basic assumption made to obtain a form of the Grad-Shafranov equation, suitable for the purposes of current position and shape control, is that the plasma behaviour can be described using a small number of degrees of freedom [25]. From the knowledge of the external magnetic measurements it is possible to identify only a few plasma parameters, namely the total plasma current, the centroid of the plasma current and, for sufficiently elongated plasmas, the shape of the plasma separatrix, the poloidal beta (β_{pol}), and the internal inductance (ℓi), quantities that will be defined in section 2.2. On the other hand, for the understanding of magneto-hydrodynamics stability and transport phenomena, it is important to retrieve information on the internal plasma profile, such as the shape of the toroidal current density distribution and the internal profile of the safety factor q (the number of times a magnetic field line goes around a torus toroidally for each time poloidally). . For this task, the external magnetic measurements are not sufficient. Thereafter in the right hand side of the equation 2.15, the plasma current density profile is assumed to be a function of five parameters ψ_{axis}, $\psi_{boundary}$, I_p, β_{pol} and ℓ_i, which are the poloidal flux per radian at the magnetic axis, the poloidal flux per radian at the boundary, the plasma current, the poloidal beta and the internal inductance, respectively:

$$J_\varphi \equiv \lambda \left[\beta_0 \frac{r}{R_0} + (1-\beta_0)\frac{R_0}{r} \right] \left(1 - \overline{\psi}\right)^\alpha$$

where the parameters λ, β_0, α, are linked to the prescribed values of I_p, β_{pol} and ℓ_i, by 3 additional non-linear equations. The term $\overline{\psi}$ is given by $\dfrac{\psi_{axis} - \psi}{\psi_{axis} - \psi_{boundary}}$, while R_0 is a reference length, for example the major radius of the vacuum chamber. The nondimensional parameters β_{pol} and ℓ_i, related to the average kinetic and magnetic pressure are defined in Section 2.2.2.

Different numerical techniques are used to solve this set of equations. The most commonly used technique is the finite element method (FEM), where the solution domain is partitioned into a number of subdomains (finite elements).

Equation 2.15 can be used in the following form:

$$\Delta^*\Psi = \nabla \cdot \left(\frac{\nabla \psi}{\mu_r r^2} \right) = -\mu_0 r J_\varphi \qquad (2.16)$$

with the divergence operator in cylindrical coordinates for a 2D axisymmetric system. The solution can be obtained from equation 2.16 with boundary conditions on the domain of interest:

$$\begin{cases} \nabla \cdot \left(\dfrac{\nabla \psi}{\mu_r r^2} \right) = -\mu_0 r J_\varphi & \textit{in } \Omega \\ \\ \textit{boundary \quad condition \quad on} \quad \Omega \\ \\ \end{cases} \qquad (2.17)$$

with:

$$\Omega = \left\{ (r,z): r \in \,]0,+\infty] , \quad z \in \,]-\infty,+\infty[\right\} , \quad \left(d\Omega = 2\pi r dr dz \right)$$

Using axisymmetry and weighted residuals method, by multiplying equation 2.16 with an arbitrary test function and integrating on the Ω domain it becomes:

$$-\int_\Omega w \nabla \cdot \left(\frac{\nabla \Psi}{\mu_r r^2} \right) d\Omega = \int_\Omega w \mu_0 \frac{J_\varphi}{r} d\Omega \qquad (2.18)$$

where Ψ is constrained to be continuous and differentiable twice, whereas there are no constraints for the test function w.

Integrating by parts and applying Gauss's theorem the weak form is obtained:

$$\int_{\Omega}\left(\frac{\nabla w \cdot \nabla \psi}{\mu_r r^2}\right)d\Omega - \int_{\partial\Omega}\frac{w}{\mu_r r^2}\frac{\partial \psi}{\partial n}d\Sigma = \int_{\Omega}w\mu_0\frac{J_\varphi}{r}d\Omega \qquad (2.19)$$

In the weak form both ψ and w must be continuous and piecewise differentiable, i.e. constraints are introduced for w whereas the requirements for ψ are less stringent than the original boundary value problem. The weak form takes automatically into account the interface conditions at the discontinuity surfaces (continuity of the tangential components of H).

By applying the FEM technique with the Galerkin test functions equal to the shape functions u_k used for the approximation of the unknown variable, the problem reduces to the solution of a non-linear algebraic system of equations:

$$\underline{\underline{A}}(\underline{c}) \cdot \underline{c} = \underline{b}(\underline{c}, \underline{c}_{add}) \qquad (2.20)$$

where $\underline{c}$ are the coefficients that represent the coefficients of the expansion for the flux per radian $\psi = \sum_{k=1}^{N} c_k u_k$ (the nodal values with nodal shape functions $u_{k's}$), the matrix $\underline{\underline{A}}$ and vector $\underline{b}$ are obtained as:

$$A_{ik} = \int_{\Omega}\frac{\nabla u_i \cdot \nabla u_k}{\mu_r r^2}d\Omega, \qquad b_i = \int_{\Omega}u_i\frac{\mu_0 J_\varphi}{r}d\Omega \qquad (2.21)$$

The non linearity of the system arises from the fact that both the matrix A and the RHS of equations 2.20 depend on the solution of the system. Additional non linearity terms are there, in cases like JET, for the presence of ferromagnetic materials (JET iron core) for which $\mu_r \neq 1$ depends on the solution.

To evaluate the solution of the problem five additional non linear equations, (for ψ_{axis}, $\psi_{boundary}$, I_p, β_{pol}, l_i), and unknowns, $c_{add} = [\psi_{axis}, \psi_{boundary}, \lambda, \beta_0, \alpha]^T$, are needed.

Further equations (e.g., measurements or circuit equations) and unknowns (e.g., plasma parameters or circuit currents) are also needed in identification problems or transient analyses.

To solve the non linear system iterative techniques are applied, e.g. fixed point iterations or Newton-Raphson Method.

The FEM approach to the solution of the Grad-Shafranov equation is widely used both for the solution of direct and inverse problems. The software tools that are used within this thesis are the CREATE-L and the CREATE-NL equilibrium code solvers, which have been successfully validated with experimental data as well as against different linear and non linear equilibrium reconstruction codes for JET and other tokamaks [26], [27]. An example of equilibrium is shown in Fig. 2.3.
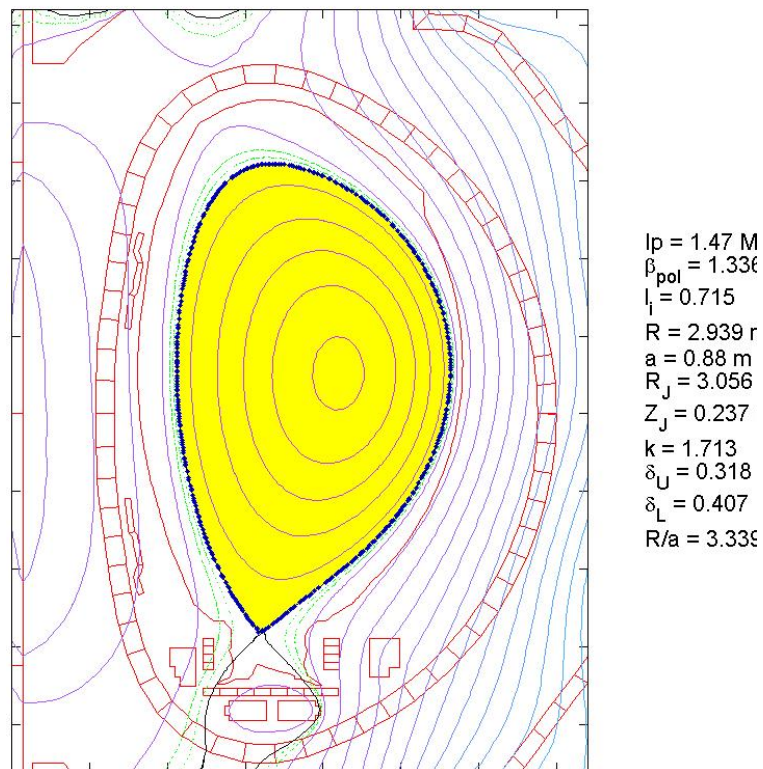

Figure 2.3 Equilibrium flux-map graphical reconstruction of CREATE-NL code for JET pulse #78452 at 55s.

2.2 Modelling approaches of the Plasma Vertical Instability

Tokamak plasmas with elongated poloidal cross-section, such as those experienced at JET, present better fusion performance than the standard circular Tokamak plasmas. On the other hand, elongated plasma are vertically unstable, with a growth rate that depends on its configuration and the surrounding conducting structures, thus requiring a vertical stabilisation system to operate the device [28], [29], [30].

The poloidal cross-section of the plasma is stretched to maximize the performance/cost ratio by reaching large volume and pressure plasma confinement. To elongate the plasma a force distribution, provided by a quadrupole field, with zero total contribution (Fig 2.5), is needed. A vertical movement in either directions increases the attraction force (in the same direction), hence triggering a vertical instability.
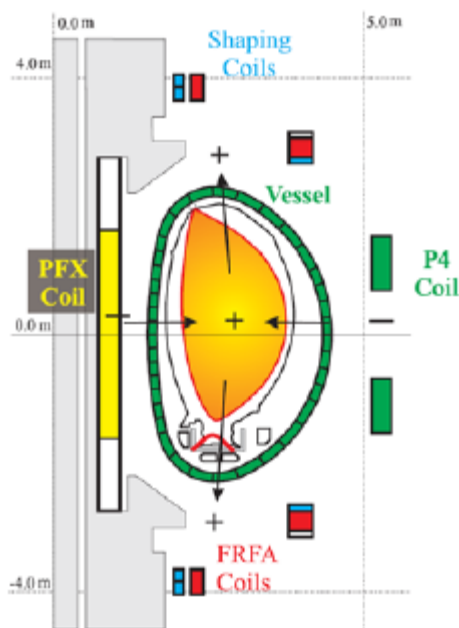

Figure 2. 4 The plasma elongation at JET can be modified by using different poloidal field circuits. The PFX and P4 circuits are used to squeeze the plasma, while the shaping circuit is used to change the elongation. Overall, the PFX and P4 circuit act by using a current of the opposite sign of the plasma, while the Shaping circuit uses a current of the same sign for the P2 coils and opposite for the P3 coils [8]

The control of the plasma shape at JET is performed by the shape controller system, as already mentioned in the first chapter. The Shaping Field circuit is used to create up-down symmetric currents so as to modify the plasma elongation and triangularity while the PFX and P4 circuits are used to create currents with the opposite sign of the plasma on the inner and outer sides of the plasma (Fig. 2.4). The vertical position of the plasma is stabilized by the VS system that uses the ERFA circuit to counteract the plasma movement by keeping the average of the estimated plasma vertical speed to a reference value. The next two sections illustrate the numerical techniques that are used in plasma physics
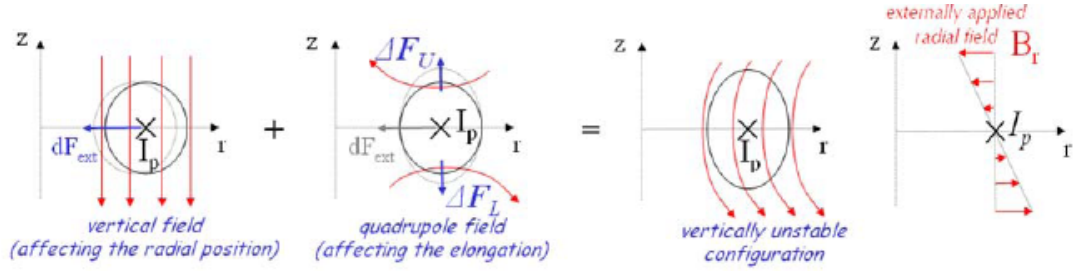
to model the plasma vertical instability.

Figure 2.5 To elongate the plasma is needed a force distribution, provided by a quadrupole field, with zero total contribution, in addition to the radial field used to guarantee the radial equilibrium. In the resulting configuration a slight plasma displacement directed upwards δz>0 would give rise to a net force directed upwards δFz>0 triggering the vertical instability.

2.2.1 Rigid displacement model approach

The rigid displacement model [31], [32], describes the plasma column as a single filament, or a rigid set of filaments, carrying constant current. The model also assumes that the plasma has only one degree of freedom, which is given by the vertical position of the filament, or the vertical position of the current centroid for the rigid set of filaments, namely z_p.

The mathematical model is obtained combining the circuit equations, which describe the current evolution in the poloidal field coils and the passive structure, and a vertical force balance equation, which describes the interaction between the externally produced magnetic field and the plasma filaments.

The model equations are:

$$\dot{\Phi}\big(I(t), z_p(t)\big) + RI(t) = U(t) \tag{2.22}$$

$$m_p \ddot{z}_p(t) = -2\pi r_p B_r\big(I(t), z_p(t)\big)I_p \tag{2.23}$$

Equation 2.22 describes the time evolution of circuit currents, where Φ is the set of fluxes linked with the circuits, R the resistance matrix, I the set of circuit currents, and U the set of applied voltages, which are zero for the passive circuits. Equation 2.23 is the force balance, where I_p, m_p, z_p and r_p are the plasma current, mass,

vertical position and radial position, respectively. B_r is the radial field acting on the plasma filaments. The linearized model:

$$\delta\dot{\Phi}\left(\partial I(t), \delta z_p(t)\right) + R\delta I(t) = \delta U(t) \qquad (2.24)$$

$$m_p\delta\ddot{z}_p(t) = -2\pi r_p\delta B_r\left(\delta I(t), \delta z_p(t)\right)I_p \qquad (2.25)$$

can be rewritten in terms of δI, variation on circuit current (with δI_p=0), and δz_p, variation on plasma vertical position:

$$\frac{\partial\Phi}{\partial I}\partial\dot{I} + \frac{\partial\Phi}{\partial z_p}\partial\dot{z}_p + R\partial I = \partial U \qquad (2.26)$$

$$m_p\partial\ddot{z}_p(t) = -2\pi r_p I_p\left(\frac{\partial B_r}{\partial I}\partial I + \frac{\partial B_r}{\partial z_p}\partial z_p\right) \qquad (2.27)$$

The terms of equation 2.26 can be renamed as:

$$\begin{cases} \dfrac{\partial\Phi}{\partial I} = L \\ \\ \dfrac{\partial\Phi}{\partial z_p} = I_p\dfrac{\partial M}{\partial z_p} = g \end{cases} \qquad (2.28)$$

while the terms of equation 2.27 can be rewritten as:

$$\begin{cases} -2\pi r_p I_p\dfrac{\partial B_r}{\partial I} = I_p\left(\dfrac{\partial M}{\partial z_p}\right)^T = g^T \\ \\ -2\pi r_p I_p\dfrac{\partial B_r}{\partial z_p} = F' \end{cases} \qquad (2.29)$$

where L represents the circuit inductance matrix, M the plasma circuits mutual inductance, g the stabilizing efficiencies and F' is the destabilizing force. Using these notations the linearized model becomes:

$$L\delta\dot{I} + g\delta\ddot{z}_p + R\delta I = \delta U \tag{2.30}$$

$$m_p\delta\ddot{z}_p = g^T\delta I + F'\delta z_p \tag{2.31}$$

This can be written in a form where only the derivatives of the poloidal field circuits currents appear, by multiplying equation 2.31 by g and eliminating δz_p:

$$-\frac{m_pL}{F'}\delta\dddot{I} - \frac{m_pR}{F'}\delta\ddot{I} + \left(L - \frac{gg^T}{F'}\right)\delta\dot{I} + R\delta I = \delta U - \frac{m_p}{F'}\delta\ddot{U} \tag{2.32}$$

If we consider the simplified case of a single poloidal field circuit and a single plasma filament model, equation 2.32 reduces to a differential equation with a single unknown:

$$-\frac{m_pL}{F'}\delta\dddot{I} - \frac{m_pR}{F'}\delta\ddot{I} + \left(L - \frac{g^2}{F'}\right)\delta\dot{I} + R\delta I = \delta U - \frac{m_p}{F'}\delta\ddot{U} \tag{2.33}$$

The characteristic polynomial of the equation 2.33 is:

$$P(\lambda) = -\frac{m_pL}{F'}\lambda^3 - \frac{m_pR}{F'}\lambda^2 + \left(L - \frac{g^2}{F'}\right)\lambda + R \tag{2.34}$$

From the analysis is possible to verify that exists at least one real unstable eigenvalue, in fact for $F' > 0$ and $R > 0$ we have:

$$\begin{cases} P(0) = R > 0 \\ \\ \lim_{\lambda\to+\infty} P(\lambda) = -\lim_{\lambda\to+\infty}\frac{m_pL}{F'}\lambda^3 = -\infty \end{cases} \tag{2.35}$$

which demonstrates that exist at lest one positive value of λ for which $P(\lambda) = 0$.

If the plasma mass is considered negligible, equation 2.34 is furthermore simplified yielding a first order linear differential equation:

$$\left(L - \frac{g^2}{F'}\right)\delta\dot{I} + R\delta I = \delta U \tag{2.36}$$

For a vertically unstable plasma (with a positive destabilizing force derivative $F'>0$), the massless model can be used only if the term $\left(L - \dfrac{g^2}{F'} \right)$ is negative, and the stability margin $m_s = g^2 / F'L > 1$, otherwise the unstable mode artificially disappears. If $m_s > 1$ the vertical instability growth rate time is given by $\tau_g = (m_s - 1)L/R$, which is comparable to the resistive time scale $\tau = (L/R)$. Otherwise, with $F'>0$ and $m_s <1$, the plasma mass must be taken into account and the vertical instability growth rate is on the Alfven time scale, which is much shorter $\left(\tau_A = \sqrt{m_p / F'} \right)$.

The massless model that takes in accounts multiple external circuits and the effect of passive structures can be used considering the following equation:

$$\left(L - \frac{gg^T}{F'} \right)\delta \dot{I} + R\delta I = 0 \tag{2.37}$$

If we introduce the modified inductance matrix $L^* = \left(L - gg^T / F' \right)$, equation 2.37 becomes $L^* \delta \dot{I} + R\delta I = 0$. It is possible to consider the open loop system in free evolution:

$$\dot{x} = Ax \qquad with \begin{cases} x = \delta I \\ A = -\left(L^* \right)^{-1} R \end{cases} \tag{2.38}$$

The estimation of the vertical instability growth rate is obtained by analyzing the unstable eigenvalues of the matrix A. In particular, $Ax_u = \lambda_u x_u$, where x_u is the unstable growth mode corresponding to the growth rate, i.e., the positive eigenvalue $\gamma_u = \lambda_u > 0$.

The main limitations of the rigid displacement model are related to an approximate reconstruction of the magnetic diagnostics used for the VS systems and an inaccurate estimation of the growth rate. In particular, the assumption that the plasma motion can be represented by a rigid displacement of a set of filamentary constant currents is not consistent with the local MHD equilibrium and does not take in account the plasma shape modifications during the vertical movements, bringing to an incorrect

estimation of the growth rate especially for plasmas with a high triangularity. The perturbed equilibrium model introduced in the following section overcomes some of these drawbacks .

2.2.2 Perturbed equilibrium approach

The perturbed equilibrium approach [26], [33], [34], combines the circuits equations with the Grad-Shafranov constraint to obtain an MHD-consistent plasma equilibrium. A set of assumptions used for the plasma behaviour are here listed:

- The inertial effects are neglected, so as to assume the plasma to evolve through a sequence of MHD equilibria, i.e. the plasma is considered massless.
- The plasma is toroidally axisymmetric, and its equilibrium evolution is determined only by the magnetic field averaged along the toroidal angle.
- The plasma current density profile is parameterized with only 3 degrees of freedom: the total plasma current I_p, the poloidal beta β_{pol} and internal inductance ℓ_i.

The poloidal beta and the internal inductance of the plasma are defined as:

$$\beta_{pol} = 4\frac{\int_{V_P} p\,dV}{\mu_0 R_o I_p^2}, \qquad \ell_i = 4\frac{\int_{V_P} \dfrac{B^2}{2\mu_0}dV}{\mu_0 R_o I_p^2} \qquad (2.38)$$

where R_0 represent the radius of the torus measured from the centre of the chamber. The poloidal beta is related to the ratio between plasma pressure and poloidal magnetic field pressure; the internal inductance gives a measure of how peaked the plasma current profile is.

A set of assumptions are also taken for the circuits and the conducting structures:

- The mathematical model for the conducting structures is the standard eddy current model, i.e., the quasi-stationary Maxwell equations (no displacement currents: $\partial\mathbf{D}/\partial t \rightarrow 0$).
- The time evolution of the currents is described by the standard circuit equations, where the applied voltage for the passive structures is zero.

It is worth noticing that the use of integral formulations for the conducting structures allows a unified treatment of circuits and eddy currents, even in the 3D case [36]. The perturbed model approach equations can be written in symbolic form:

$$\frac{d\Phi}{dt} + \mathbf{R}\mathbf{I} = \mathbf{U} \tag{2.39}$$

$$[\psi, \mathbf{Y}] = \eta(\mathbf{I}, \mathbf{W}) \tag{2.40}$$

where in equation 2.39 $\boldsymbol{\Phi}$ is the vector of fluxes linked with the circuits, $\boldsymbol{R}$ is the resistance matrix, $\boldsymbol{I}$ is the vector of currents, which includes the poloidal field circuit currents and the plasma current, and $\boldsymbol{U}$ is the vector of voltages applied to the circuits, which is zero for the passive structures. In Equation 2.40 $\boldsymbol{Y}$ is the output vector, which includes the magnetic equilibrium flux map, plasma shape parameters (plasma current centroid coordinates, gap measurements ...), integrated magnetic measurements (magnetic field B and magnetic poloidal flux), and $\boldsymbol{W}$ is the vector of disturbances, namely poloidal beta and internal inductance $[\beta_{pol}, \ell_i]^T$.

Equation 2.39 describes the current evolution in the poloidal field circuits and passive structures, while 2.40 represents the Grad-Shafranov constraint in a symbolic form, which takes in account the plasma shape and current profile modifications during the vertical displacements. The Grad-Shafranov constraint is imposed numerically, for a given machine geometry, material and circuit connections, by specifying the poloidal field circuit currents, the plasma current, the poloidal beta and the internal inductance. After solving the Grad-Shafranov equation using numerical methods, for instance Finite Element Methods (FEM), the MHD magnetic equilibrium is linearized around the equilibrium point to describe the influence of the external circuits currents and the internal plasma parameters β_{pol} and ℓ_i on the plasma shape and vertical instability. The following notations are defined:

$$\mathbf{I} = \mathbf{I}_0 + \mathbf{i}, \quad \mathbf{U} = \mathbf{U}_0 + \mathbf{u}, \quad \mathbf{W} = \mathbf{W}_0 + \mathbf{w}, \quad \mathbf{Y} = \mathbf{Y}_0 + \mathbf{y} \tag{2.41}$$

where with the lower-case are defined the perturbing quantities, while with subscript '0' are define the reference quantities. Using these notations the linearized model equations can be written as:

$$L^* \frac{di}{dt} + Ri = u - L_E^* \frac{dw}{dt} \qquad (2.42)$$

$$y = Ci + Fw \qquad (2.43)$$

where $L^* = \partial\Phi/\partial I$, $L_E^* = \partial\Phi/\partial W$, $C = \partial Y/\partial I$ and $F = \partial Y/\partial W$. We can finally write the model in the state space form:

$$\dot{x} = Ax + Bu + E\dot{w} \qquad (2.44)$$

$$y = Cx + Fw \qquad (2.45)$$

with $x = i$, $A = -\left(L^*\right)^{-1} R$, $B = \left(L^*\right)^{-1}$, $E = -\left(L^*\right)^{-1} L_E^*$.

Matrices A, B, C describe the linear dependence of the states, inputs and outputs (there is no direct algebraic link between inputs and outputs of equation 2.43), while matrices E and F describe the influence of the disturbances, namely β_{pol} and ℓ_i. All the state-space matrices depend on the plasma configurations and may present discontinuity during transition from limited to diverted configuration.

Like for the massless rigid displacement approach, the estimation of the vertical instability growth rate is obtained by analyzing the unstable eigenvalues of the matrix A. The advantage of the perturbed equilibrium approach is in a more realistic estimation of the plasma growth rate, and moreover, the use of the Grad-Shafranov equation forces the model to verify MHD equilibrium laws, considering changes both in the plasma shape and in the plasma current profile. The study of the vertical instability considers both the effect of externally applied magnetic fields and the changes in the plasma current and of the plasma internal profile (via modifications of the β_{pol} and ℓ_i parameters). Changes in β_{pol} and ℓ_i affect both the state evolution equation 2.44 and the output equation 2.45.

The overall model therefore takes into account the changes of the plasma shape due to externally applied field, i.e. a radial field "kick" from an external circuit, and changes in the internal parameters due to the injection of additional heating power or the occurrence of MHD phenomena such as ELMs, which can be modelled as equivalent changes in β_{pol} and ℓ_i.

The models used in the next sections have been obtained with the software tools CREATE-L and CREATE-NL, which have been successfully used as support during the commissioning of the new radial field amplifier and the new controller architecture

2.3 JET Mechanical structure

The mechanical structure at JET supports the poloidal and toroidal field coils (Fig. 2.6). It consists of inner cylinder, upper and lower ring and collar and outer shell. The interface between the structure and coils is made by the fluted inner cylinder along the straight nose section, by collar and ring teeth at top and bottom and by wedges in the outer shell casting.
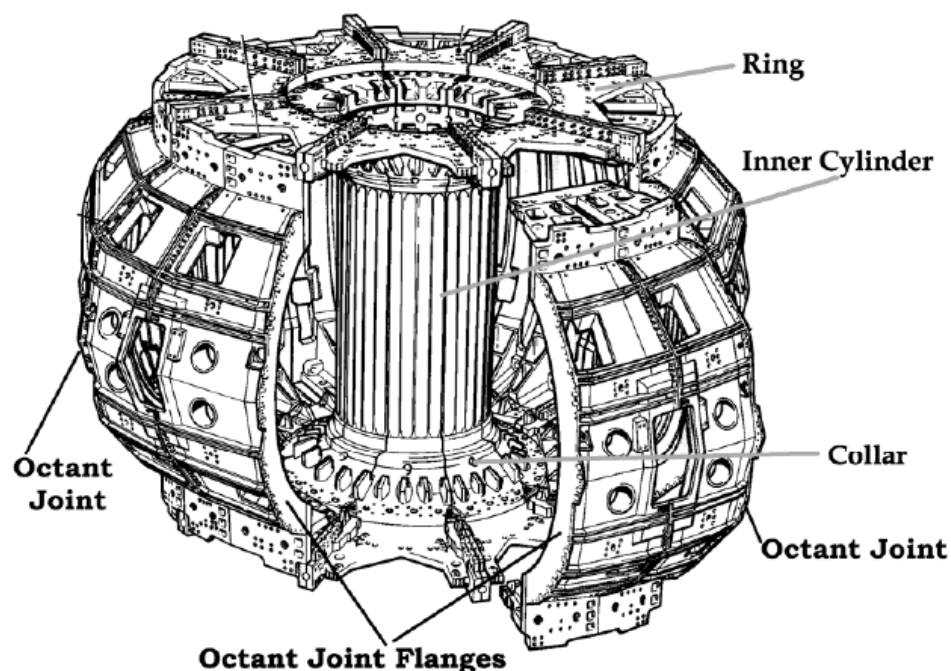

Figure 2. 6 View of the JET mechanical structure.

It has been designed in modular components, each component representing one octant of the machine. From a toroidal point of view, the mechanical structure is composed of eight sectors joined together to form the mechanical shell. The top and bottom part of the shell, named top and bottom rings at JET, join the external supports to the central support column (via the collar), and are as well divided into eight sectors, one for each octant. In order to reduce the effect of the eddy currents in the mechanical structure, which would have delayed the magnetic field penetration, each octant is divided into four parts, two top parts and two bottom parts, which are electrically insulated from each other. A similar insulating solution is applied to the

junction between different octants, between the octant and the top-bottom rings, and between the rings and the collar of the central support column.

The mechanical structure is modelled in the FEM model of JET as shown in Figure 2.7. Since the mechanical structure is not axisymmetric, an equivalent model that takes into account also the main 3D effects of the eddy currents is used. Each component of the simplified mechanical structure is schematized as a set of axisymmetric conductors.
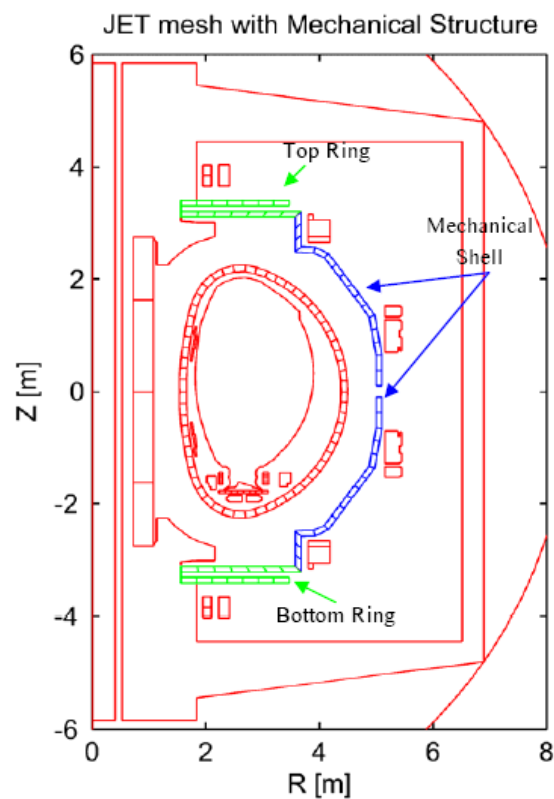

Figure 2.7 JET mesh. The different parts of the mechanical structure are shown.

To account for 3D eddy currents, each conductor is connected to the neighbour blocks via an artificial component with different value of resistance and inductance. The connections are such that the total toroidal current in each component is zero. The connection between the top part of the mechanical structure and the bottom part is not implemented since the mechanical structure design has introduced insulation materials between these components. The same technique is applied to the top and bottom rings of the structure.

2.3.1 Effects of passive structures on magnetic sensors

A closer analysis shows that the INCONEL dump plate structure of the first wall in JET placed on the top of the machine has a shielding effect with an electromagnetic time constant of about 1ms.

Internal discrete coils CX05 and CX06 are placed behind the INCONEL dump plate structures. Figure 2.8 shows the response of magnetic sensors C105 and C106, which measure the time derivative of the flux density in Octant 1, to a voltage step applied to the external radial field circuits. For magnetic sensor C104, which is not behind the plate, the time behaviour is completely different in the two cases with and without the plasma. On the other hand, internal discrete coil C105 does not see the movement of the plasma for about 350 μs. Moreover, a 2D analysis carried out by using the CREATE-L perturbed equilibrium approach [26] confirms the effect of the dump plate structure on pick-up coil C105.
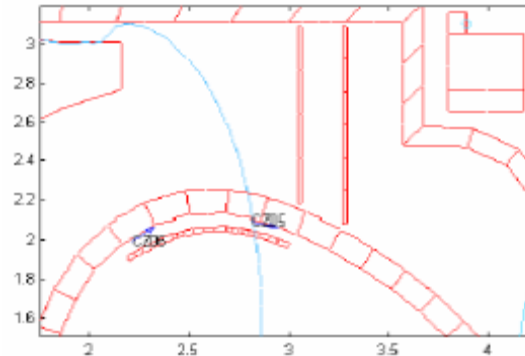

Figure 2.8 Position of dump plate on JET mechanical structure.

Figure 2.9 shows the time response of internal discrete coils C104 and C105 to a voltage step applied to the radial field circuit. The motion of the plasma, which is perceived immediately by other diagnostics, affects the time behaviour of coil C105 only after about 350 μs, in which the time behaviour is similar to a plasmaless pulse since the signal is mostly dominated by the field trapped between vessel and dump plate.
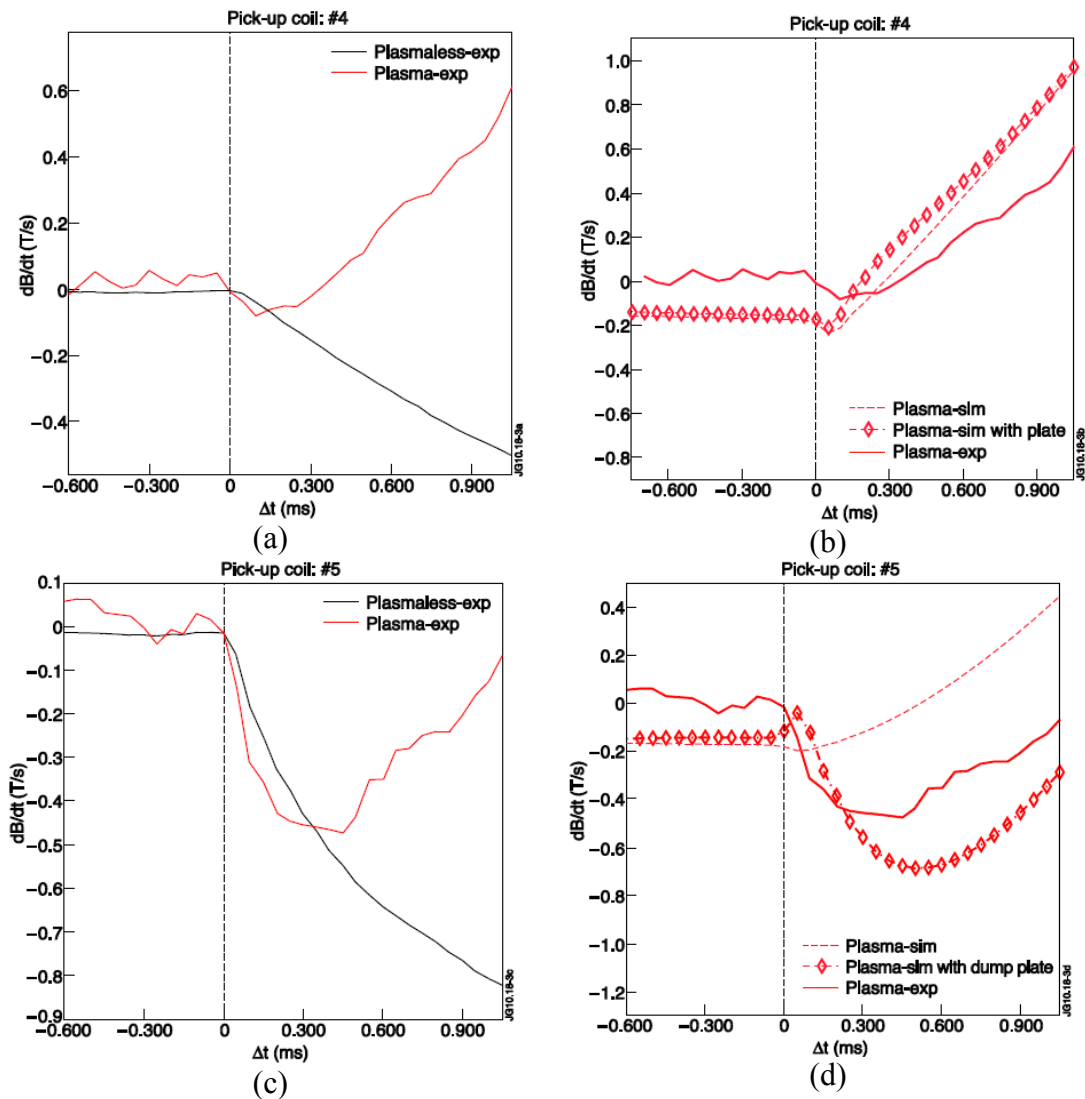
54

Figure 2.9 Response of internal discrete coils #4 and #5 to a voltage step applied to the radial field circuit at Δt=0 ms, showing the effect of the INCONEL dump plate structure: a) coil #4 signal in a plasmaless pulse; b) coil #4 signal in a plasma pulse; c) coil #5 signal in a plasmaless pulse; d) coil #5 signal in a plasma pulse. The motion of the plasma, which is perceived immediately by other diagnostics, affects the time behaviour of coil #5 (behind the structure) only after about 350 μs, in which the time behaviour is similar to a plasmaless pulse. This is confirmed by numerical simulations. The experimental data refer to plasmaless pulse #76241, in which Δt=t−38.1141s, and to the 2 MA plasma pulse #76196, in which Δt=t−18.3280s.

In the future a full replacement of JET first wall materials is planned, with beryllium in the main wall and tungsten in the divertor region [35]. This has a potential impact on the diagnostics and control of JET vertical stabilization system. The effect of the new tiles in the divertor region on pick up coils in the divertor could be significant for shape control. However, for reason given earlier, these are not used for vertical stabilization and therefore need not be considered further. The limiter tiles are rather

small, and attached to the existing INCONEL beams. In addition to the INCONEL support structure of the dump plates considered above, the beryllium tiles are mounted on new thick INCONEL carriers. Even where there are no beryllium tiles the original INCONEL support structure is protected by new thick INCONEL plates. The beryllium tiles, about 40 mm thick, will form two rails, but they will be castellated, hence an equivalent thickness of 20 mm can be assumed (Fig. 2.10).
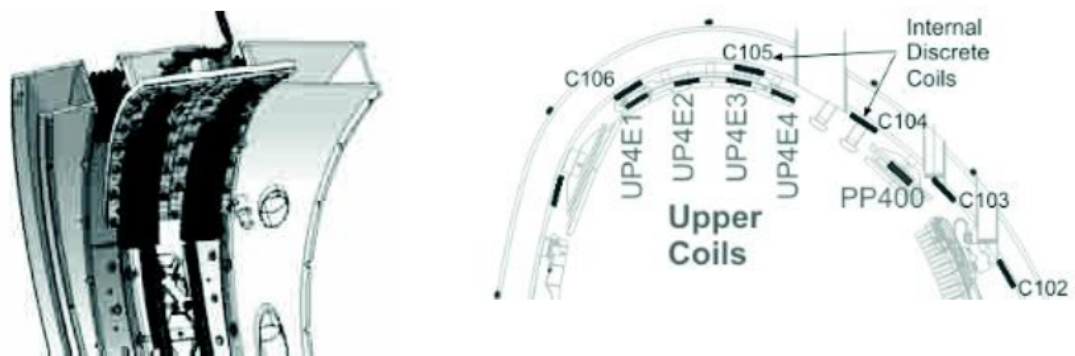
JG10.18-4c

Figure 2.10 Dump plates and beryllium tiles to be installed at JET (left) and position of the discrete coils used by the vertical stabilization system (right). Internal discrete coils C105 and C106 are behind the existing dump plate [8].

The electromagnetic time constant of a dump plate with the beryllium tiles has been estimated to be about 7 ms by CARIDDI [36]. In principle, there is cause for concern, as the vertical stabilization system has to work on a time scale much faster than 1 ms. Although the impact on the VS system was not expected to be dramatic, the PCU project explored the possibility of having a valid alternative to the controlled variable ZPDIP, a linear combination of magnetic measurements, used for several years. The new controlled variable, denoted as OBS05 does not makes use of the magnetic sensors behind the plates. The design and the commissioning of the new controlled variable are described in Chapter 3.

2.4 Edge Localized Modes identification

Because the perturbation affects the magnetic fields creating a strong variation in the plasma speed measurement, with an ELM the VS system observes a rapid increase of plasma speed followed by a rapid inversion and a slower decay. This causes the firing of ERFA and a resulting vertical excursion of the plasma, in some cases associated with loss of control. For these reason it is very important to characterize the behaviour of the VS system in term of type I ELMs. Moreover because an ELM event is a fast phenomenon, a fast acquisition of the magnetic signals is needed. From the viewpoint of the VS system, an ELM event can be schematized as a disturbance for the system, consisting in a variation of poloidal beta and internal inductance. In particular, by using the CREATE-L model, a representation of the plant behaviour is given in the state space form. A characterization of ELMs by means of poloidal beta and internal inductance variations has been carried out via simulation.
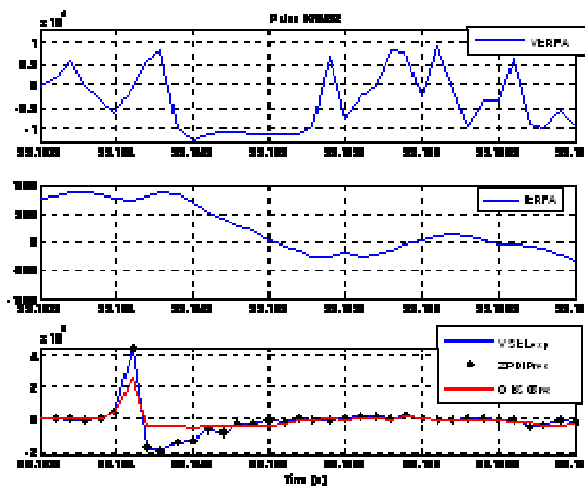

Figure 2.11 Effect of an ELM event on the Vertical Stabilization system: ERFA voltage (upper diagram), ERFA current (mid), and diagnostics related to the vertical speed (lower).

2.4.1 Description of modelling procedure

This section describes the procedure adopted for the identification of the ELMs in terms of waveforms of internal plasma profile parameters: poloidal beta β_{pol} and

internal inductance ℓi. This activity has been carried out using the CREATE-L model, via best fit of the vertical velocity estimation, during an ELM phase.

The vertical velocity estimation is a linear combination of the magnetic diagnostics that are the time integrated outputs. To obtain the time derivatives of these quantities, a derived state space model is used:

$$\begin{cases} \dot{x} = A\,x + B\,u + E\,\dot{w} & (2.41) \\ \dot{y} = C\,\dot{x} + D\,\dot{u} + F\,\dot{w} & (2.42) \end{cases}$$

where matrices C and F consider only the equations relative to the 32 magnetic coils used by VS system, among all the other possible outputs. If the state evolution equation 2.41 is substituted into the output equation 2.42 the following model is obtained:

$$\begin{cases} \dot{x} = A\,x + B\,u + E\,\dot{w} \\ \dot{y} = CA\,x + CB\,u + (CE + F)\,\dot{w} \end{cases} \quad (2.43)$$

If the disturbances are considered inputs to the system the model can be rearranged as follows:

$$\begin{cases} \dot{x} = A\,x + [B,E] \cdot [u,\dot{w}]^T \\ \dot{y} = CA\,x + [CB,(CE+F)] \cdot [u,\dot{w}]^T \end{cases} \quad (2.44)$$

where the outputs represent the time derivatives of the probes and the vertical velocity estimation is a linear combinations of these outputs. The system matrices and the input variables can be grouped for convenience, yielding to the equations:

$$\begin{cases} \dot{x} = AA\,x + BB\,\xi \\ \dot{y} = CC\,x + DD\,\xi \end{cases} \quad (2.45)$$

where:

$$\begin{cases} \xi = [u, \dot{w}]^T \\ AA = A \\ BB = [B, E] \\ CC = C \cdot A \\ DD = [C \cdot B, (C \cdot E + F)] \end{cases} \quad (2.46)$$

System 2.45 can be rearranged in the following way:

$$\begin{cases} \dot{x} = AA \ x + BB_p \ \xi_p + BB_{np} \ \xi_{np} \\ y = CC \ x + DD_p \ \xi_p + DD_{np} \ \xi_{np} \end{cases} \quad (2.47)$$

Where the suffix "*p*" indicates the prescribed inputs, for which fast experimental measurements are available, like the fast radial field amplifier voltage V_{ERFA}. The suffix "*np*" indicates the non prescribed quantities, as $d(\beta pol \cdot Ip)/dt$ and $d(\ell i \cdot Ip)/dt$, which have to be identified. Using an implicit time derivative scheme, it is possible to write:

$$\begin{cases} \dfrac{(\overline{x}_{n+1} - \overline{x}_n)}{\delta t} = AA \ \overline{x}_{n+1} + BB_p \ \overline{\xi}_{(n+1)p} + BB_{np} \ \overline{\xi}_{(n+1)np} \\ \overline{\eta}_{n+1} = CC \ \overline{x}_{n+1} + DD_p \ \overline{\xi}_{(n+1)p} + DD_{np} \ \overline{\xi}_{(n+1)np} \end{cases} \quad (2.48)$$

where the change of variables $\eta = w \cdot \dot{y}$ has been adopted to indicate the combination of the magnetic measurement, with a prescribed weights *w*, to obtain the vertical velocity estimation. Equation 2.48 can be rewritten as:

$$\begin{cases} \overline{x}_{n+1} = M_1 \ \overline{x}_n + M_2 \ \overline{\xi}_{(n+1)p} + M_3 \ \overline{\xi}_{(n+1)np} \qquad\qquad (2.49) \\ \\ \overline{\eta}_{n+1} = N_1 \ \overline{x}_n + N_2 \ \overline{\xi}_{(n+1)p} + N_3 \ \overline{\xi}_{(n+1)np} \qquad\qquad (2.50) \end{cases}$$

where:

$$\begin{cases} M_1 = inv(I - \delta t AA) \\ M_2 = M_1 \delta t BB_p \\ M_3 = M_1 \delta t BB_{np} \end{cases} \quad (2.51)$$

and:

$$\begin{cases} N_1 = w \cdot CC \cdot M_1 \\ N_2 = w \cdot CC \cdot M_2 + DD_p \\ N_3 = w \cdot CC \cdot M_3 + DD_{np} \end{cases} \qquad (2.52)$$

The non prescribed inputs are calculated as:

$$\overline{\xi}_{(n+1)np} = \left(N_3\right)^+ \cdot \left(\overline{\eta}_{n+1} - N_1 \overline{x}_n - N_2 \overline{\xi}_{(n+1)p}\right) \qquad (2.53)$$

where the unknown quantities ξ_{np} are obtained by solving equation 2.53 and the state equation 2.49 at each step, in the desired time range. The left hand side variables $\overline{\eta}_{n+1}$ and $\overline{\xi}_{(n+1)p}$ are the vertical velocity estimation and the amplifier voltages, respectively, both available as experimental data. The state variables $\overline{x}_n$ are set to zero for the first step of the procedure, which means that the systems starts with zero initial conditions on state variables, representing all the perturbed currents at the initial time. This condition is reasonable if the identification start from an equilibrium point before the ELM perturbation.

As shown in Fig. 7, two different identification procedures have been adopted:

- $d(\beta I_p)_u/dt$, $d(l_i I_p)_u/dt$ identified (without additional constraints) so as to fit both ZPDIP and Obs05 experimental data in simulation with the CREATE-L model giving VERFA, $d(\beta Ip)_u/dt$, $d(l_i Ip)_u/dt$ in input;

- $d(\beta I_p)/dt$, $d(l_i I_p)/dt$ obtained as linear combinations of $n=2$ and drift compensated V5 pickup coil signals 1 to 9, so as to fit $d(\beta Ip)_u/dt$, $d(l_i I_p)_u/dt$ so as to remove the drift of βI_p and $l_i I_p$.
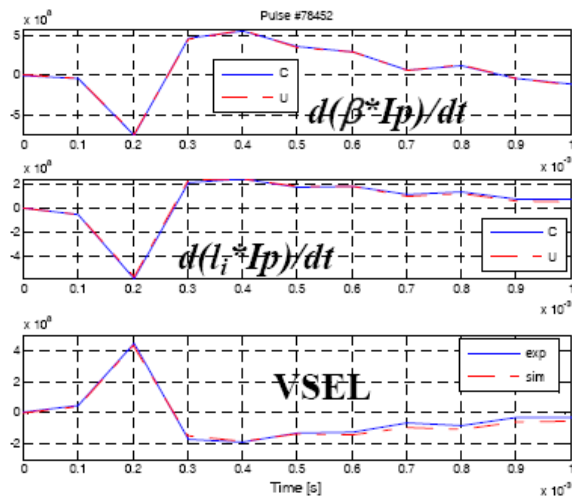
Figure 2.12 Different procedures adopted for the identification of the disturbances: poloidal beta and internal inductance. The red lines correspond to the procedure without constraints, the blue lines to the constrained procedure.

3

An Alternative Controlled Variable for JET Vertical Stabilization

3.1 Introduction

A major goal of the PCU enhancement project was to determine whether a better vertical velocity estimator could be designed compared to the semi-empirical ZPDIP used for many years [37]. This study was mainly aimed at improving the VS capabilities by reducing the effect of edge localized modes (ELMs) on the vertical position estimator. An additional motivation was the need of operating JET in future campaigns with the new ITER-like wall (ILW), which is expected to significantly shield some magnetic diagnostics [38]. The alternative controlled variable was also planned to play the role of back-up solution in case of troubles with the standard one after the modifications of the radial field circuit. The selection was made paying particular attention to robustness, reliability, and reduced time allotted for dedicated tests so as to limit the impact on the ongoing experimental campaigns. The new

controlled variable, denoted as OBS05, was successfully tested in JET on a variety of plasma scenarios and became the new vertical velocity estimator for VS system.

This paper presents the study that led to the implementation of the new controlled variable OBS05, selected using the technique presented in [39], paying attention to the following aspects: i) improvement of the procedure taking into account the range of frequencies of interest and using upgraded response model and experimental acquisition system; ii) reduction of the impact of in-vessel currents; iii) choice of a set of weights usable for a wide range of plasma configurations.

The controlled variable OBS05 was then selected so as to be not very different from ZPDIP in normal operating conditions. For this reason, it was derived only from magnetic diagnostics and aimed at giving an equivalent approximation of (1.12) as well. The selection of the OBS05 weights has been made using both computer models and experimental data. The models have been used to determine the range of frequencies of interest and to assess the validity of the choice for a variety of plasma configurations and operating conditions, so as to carry out the experimental tests safely. The selection of the weights has been carried out via pseudoinversion using the experimental data of a specific pulse in which oscillations were deliberately excited to estimate the phase margin and the crossover frequency of the VS stabilization loop.

Section 3.2 describes the procedure used for the selection of the weights. Section 3.3 illustrates the experimental results.

3.2   Selection of the VS controlled variable

The new VS controlled variable OBS05 should avoid the contribution of the magnetic signals coming from the sensors placed behind the dump plates and have scarce sensitivity to ELMs [12] and fast plasma movements that are not expected to excite the unstable mode, e.g. radial motion.

To minimize the impact on JET operation, it was decided to keep the same frequency response as the standard VS controlled variable ZPDIP so as to avoid redesign of the controller algorithm and gains.

The requirement that the response to the radial field circuit of OBS05 is the same as ZPDIP was then imposed via pseudo-inversion of experimental and/or simulated data in the time or frequency domain. The design procedure utilized to define the weights of OBS05 is similar to the technique presented in [39]. The controlled variable CREATE_A proposed in [39] was mainly aimed at verifying the design procedure and addressed the reduction of the influence of the ELMs for a particular plasma configuration. In contrast, the weights of OBS05 were selected so as to be usable for a wide range of plasma configurations, taking into account the range of frequencies of interest, using upgraded response model and experimental acquisition system, and reducing the impact of in-vessel currents.

3.1.1   Models and experimental data

The design procedure of the new VS controlled variable makes use of linearized response models and experimental data. The linearized CREATE-L plasma response model provides the response of the 128 magnetic signals (32 from each octant) to various inputs and as shown in Figure 3.1 the agreement between simulations and experimental data is good and adequate for the present study [39].
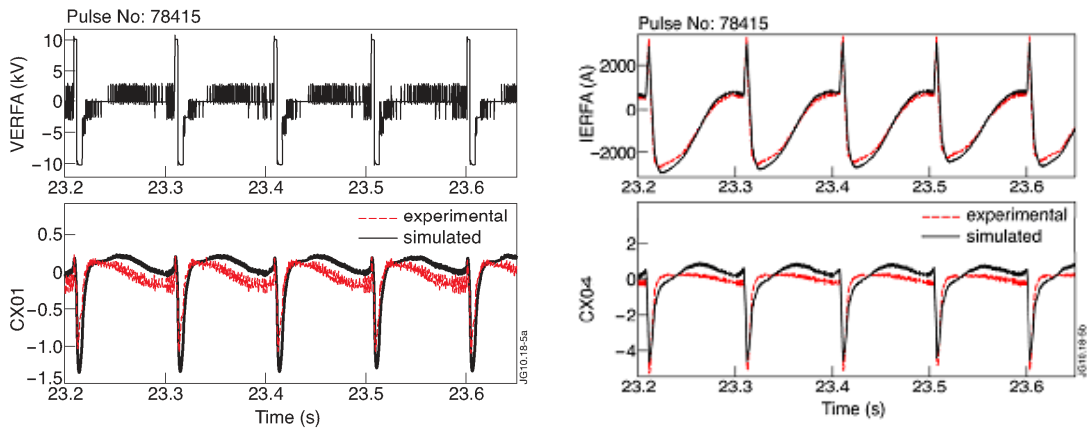
Figure 3.1 Time response of coil signals (T/s) and ERFA current to ERFA voltage in pulse #78415: comparison between simulations with the CREATE-L model and experimental data.

The linearized model is in some cases preferred to the use of experimental data because it is available for any configuration of plasma, the frequency domain analysis is straightforward and it is possible to split the different contributions acting on the plasma. The disadvantages when using the linearized model are the modelling errors, whereas the limitation of the experimental data is that they are available at a sufficiently high sampling rate only for experimental discharges carried out after the upgrade of the data acquisition system V5 (from pulse #76278). The modelling errors are essentially due to the equivalent axisymmetric approximation of 3D conducting structures and to the uncertainties in the plasma current profile parameters.

Taking account of the above merits and limitations, both experimental data and linear models were used for the present study.

The linearized CREATE-L [26] model was used especially for frequency analyses, whereas the experimental data were utilized in the time domain.

3.1.2 Requirements

The procedure illustrated in [39] requires the alternative controlled variable to have the same response as ZPDIP to the ERFA voltage, so as to maintain the closed-loop stability. This is not strictly necessary, since different transfer functions can be compatible with a suitable control scheme. However, this requirement was imposed for OBS05, because it was extremely useful to avoid redesign of the control system architecture and adaptive selection of the control gains.

The shielding effect expected by the ILW is significant only on the in-vessel pick-up coils. In addition, the possible improvements of the behaviour of the controlled variable are expected immediately after the occurrence of an ELM, i.e., on the fast time scale (about 1 ms) in which only the in-vessel pick-up coils are affected. For these reasons, it was decided to take the same weights as ZPDIP for the saddle fluxes, which are shielded by the eddy currents in the vessel.

A thorough analysis of the CREATE_A behaviour showed that:

- CREATE_A has not the same response as ZPDIP at the frequencies of interest for a wide set of plasma configurations (Figure 3.2);
- CREATE_A has nonzero weights (Figure 3.3a) for the sensors located in the lower part of the vessel, so it is very sensitive to a voltage kick applied to the divertor coils (Figure 3.3b), which is a capability of the new VS software [40].
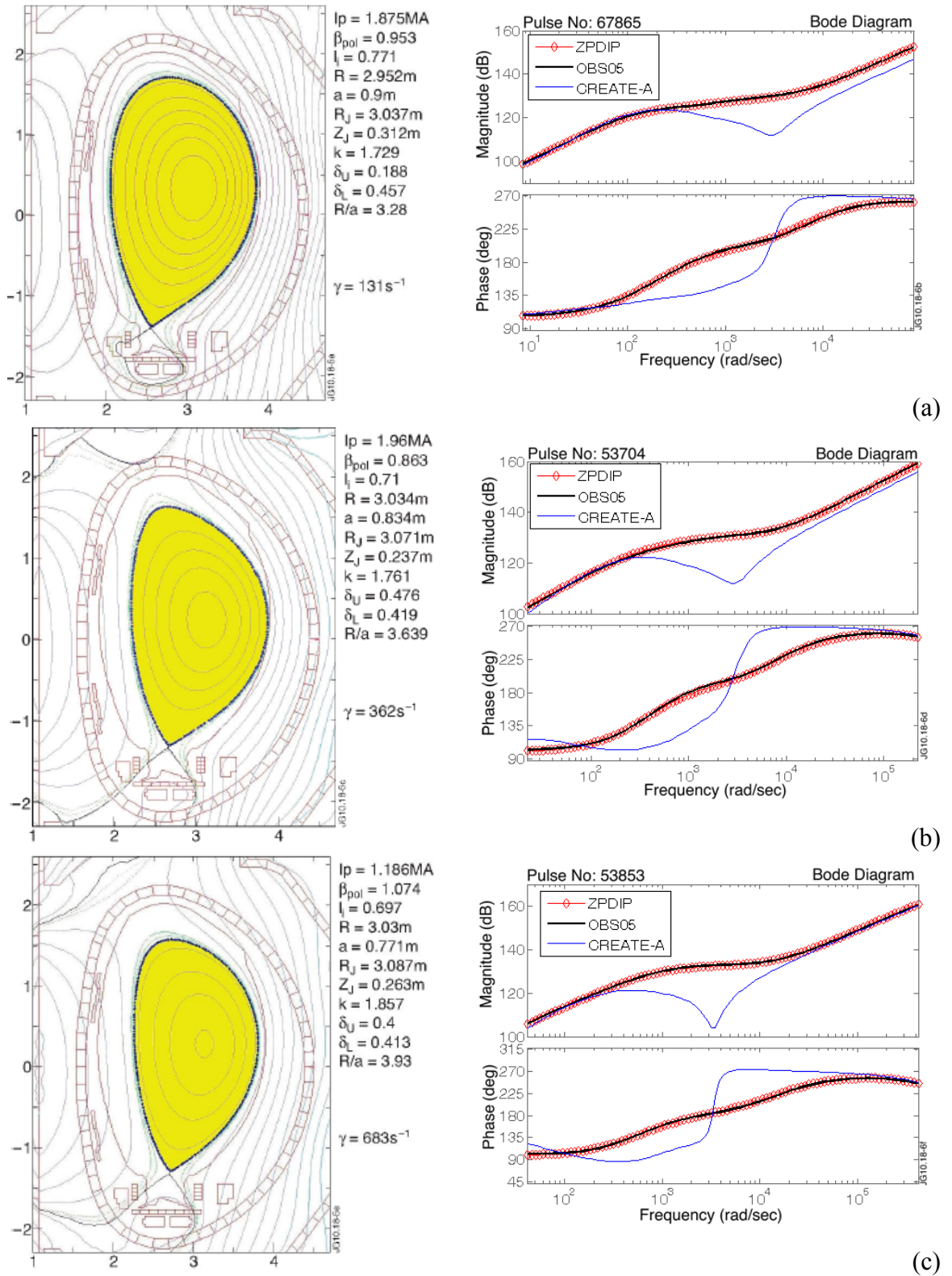
Figure 3.2 Bode plots: frequency response of ZPDIP, OBS05 and CREATE_A to VERFA for various configurations with different growth rates of the vertical instability: a) Pulse #67865 @ 8.490 s, $\gamma=131s^{-1}$; b) Pulse #53704 @ 22.840 s, $\gamma=362$ s^{-1}; c) Pulse #53853 @ 30.080 s, $\gamma=683$ s^{-1}.
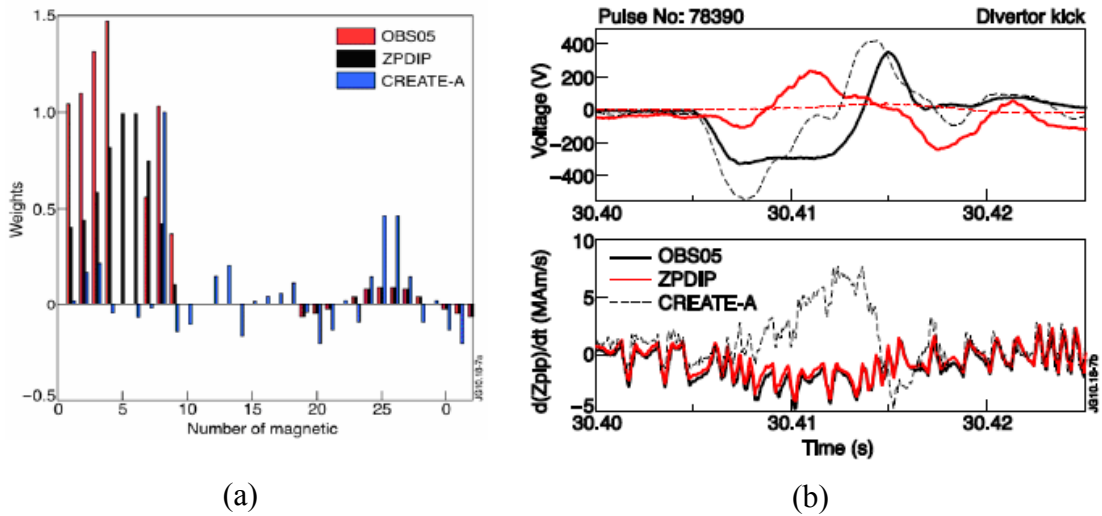
(a)　　　　　　　　　　　　　　　(b)

Figure 3.3 Comparison between ZPDIP, OBS05 and CREATE_A: a) weights applied to the signals coming from the 18 pick-up coils and the 14 saddle loops; b) response to divertor coil amplifier voltage inputs (VD1 solid black, VD2 dashed black, VD3 solid red, VD4 dashed red) in pulse #78390, in which the VS control loop was closed on ZPDIP.

Thus, the OBS05 weights (Figure 3.3a) were selected by imposing the following constraints:

- zero weights for the sensors placed behind the dump plates (CX05 and CX06) to avoid a shielding effect;
- zero weights for the sensors located in the lower part of the vessel (from CX10 to CX18), i.e. the same weights as ZPDIP, thus avoiding the shielding effect of divertor conductors and having low sensitivity to divertor kicks;
- same weights as ZPDIP for the saddle fluxes SX01 to SX14.

Moreover OBS05 should show behaviour as close as possible to ZPDIP:

- for a quiescent plasma, so as to have the same response as ZPDIP to the ERFA voltage when excited by ERFA amplifier (Figure 3.4a);
- during a vertical displacement event (VDE), so as to have the same sensitivity to the unstable mode (Figure 3.4b).
- during plasma current ramp up and ramp down phase (Fig. 3.4c);
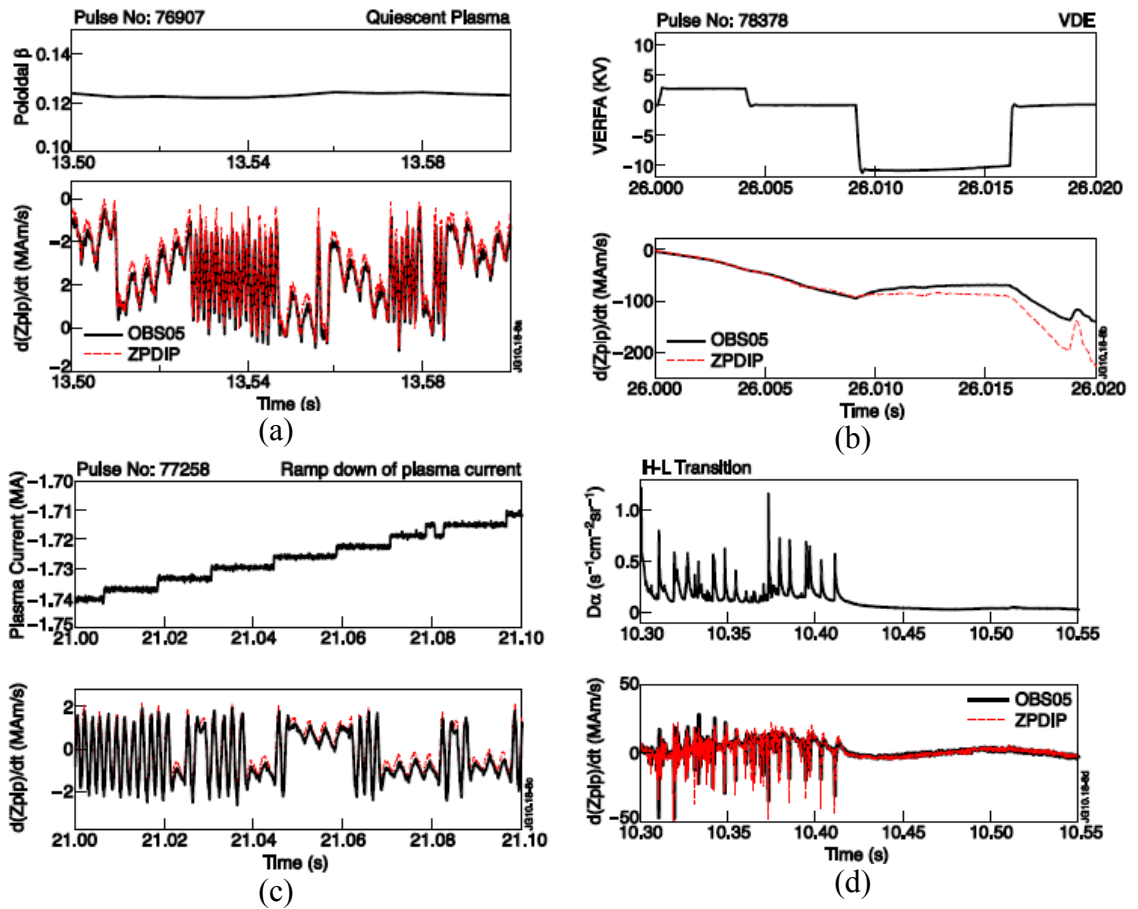- during H-L transitions (Fig. 3.4d).

Figure 3.4 Comparison between OBS05 (black) and ZPDIP (red) in conditions where the requirements asked for similar behaviours: a) quiescent plasma - pulse #76907; b) vertical displacement event - pulse #78378; c) ramp down of plasma current - pulse: 77258; d) H-L transition - pulse #76907. In all cases ZPDIP was the controlled variable.

Finally, to improve the capabilities of the VS system, OBS05 should have a better response to an ELM and be less sensitive to the divertor switching power supply noise at 300 Hz [39]. As shown in Figure 3.5a, the sign of ZPDIP is positive for a time interval $\Delta\tau \approx 300$ μs and then negative for much longer. This gives rise to an equivalent delay of $\Delta\tau_{eq} \approx 2\Delta\tau$ in the stabilizing action, as the ERFA voltage is saturated with the wrong sign for a time interval $\Delta\tau$. Figure 3.5b shows the 300 Hz noise due to the power amplifiers feeding the in-vessel coils in a plasmaless pulse when the ERFA voltage is zero. Therefore the weights of OBS05 should be selected so as to eliminate or at least reduce:

- the initial spike with the wrong sign shown by ZPDIP (Figure 3.5a).
- the divertor switching power supply noise at 300 Hz in plasmaless pulses (Figure 3.5b).
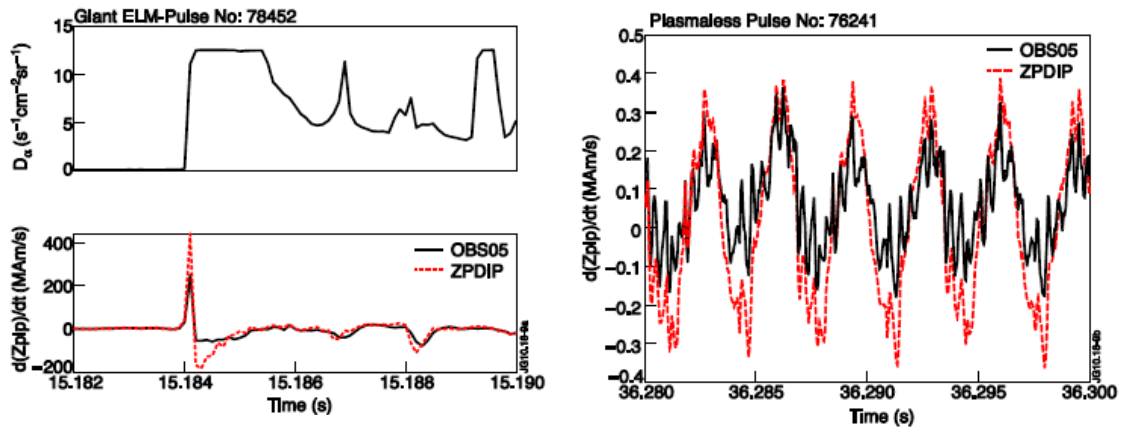
Figure 3.5 Different response of OBS05 and ZPDIP: a) to a giant ELM in pulse #78452 (the upper plot shows the Dα emission); to 300 Hz power amplifier noise in plasmaless pulse #76241.

3.1.3 Design procedure and expected performance

Due to the above constraints, the unknown weights are only seven. The determination of these weights was made paying particular attention at the typical VS operating frequencies. To this purpose, the experimental data of pulse #78398 with a 1.5 MA quiescent plasma having a growth rate of about 300 s^{-1} were extremely useful. This particular pulse was in fact aimed at estimating the phase margin and the crossover frequency of the VS stabilization loop [41].

It was then decided to maintain the closed-loop stability by imposing the time behaviour of OBS05 to match that of ZPDIP in the time interval from 26.03s to 26.08s of pulse #78398 (Fig. 3.6), in which plasma oscillations at the frequency of about 400 Hz were deliberately excited. The weights were selected via pseudoinversion taking into account only the first two singular values, as the ratio between the third and the first one did not exceed 12 %. The five independent combinations of weights obtained with the remaining singular values, were reserved as extra degrees of freedom to be used to match the dynamic response to ERFA voltage in other conditions as well as the additional requirements. However, this turned out to be unnecessary.

As shown in Figs. 3.2-3.4 in terms of dynamic response to voltage inputs applied to the radial field circuit and to divertor coils, there is a very good agreement between OBS05 and ZPDIP not only in pulse #78398 (Fig. 3.6), but also for a variety of configurations, scenarios, and conditions.
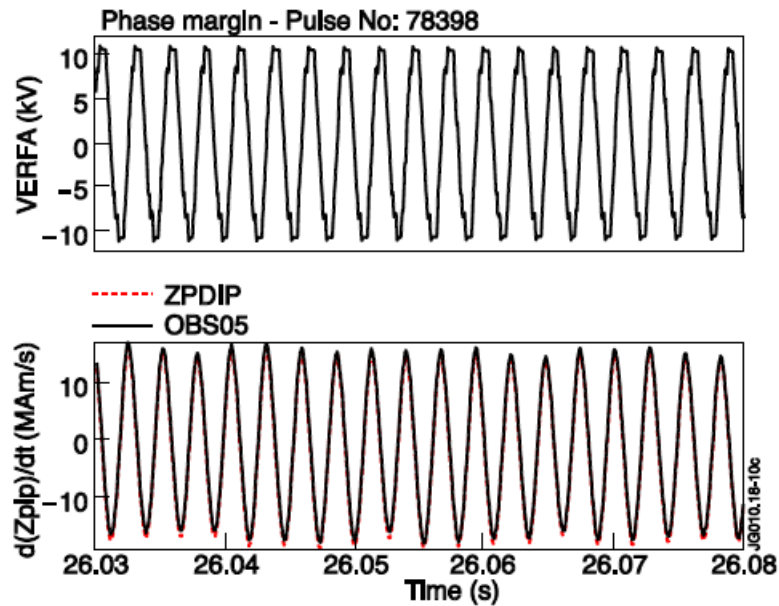
Figure 3.6 Phase margin experiment, JET pulse #78398: OBS05 and ZPDIP show a similar behaviour as requested by the design procedure at the frequency of about 370 Hz.

In particular Figure 3.4b shows that the difference between OBS05 and ZPDIP is within 7% till 26.02, when the plasma displacement is more than 40 cm; the sensitivity to the unstable mode has also been tested on the linearized models of Fig. 3.2 and the discrepancy between ZPDIP and OBS05 was within ±5%.

In addition, Figure 3.5a shows that after an ELM the positive spike of OBS05 is smaller than ZPDIP and that OBS05 is also less sensitive to the 300 Hz power amplifier noise. Consequently a lower excursion of ERFA current was expected when using OBS05 instead of ZPDIP, even if there is probably room for further optimization after a better understanding of the electromagnetic effects of an ELM on the VS system.

The time behaviours illustrated in Figs. 3.3-3.6 were of course reconstructed offline. The software of the new JET VS system allows online acquisition of different combinations of magnetic signals. After selection of the OBS05 weights, the online OBS05 signal was then acquired and compared to ZPDIP, which was still used as feedback variable, so as to test the validity of procedure (Fig. 3.7) and the correct implementation in the control system of JET, before closing the loop on OBS05.

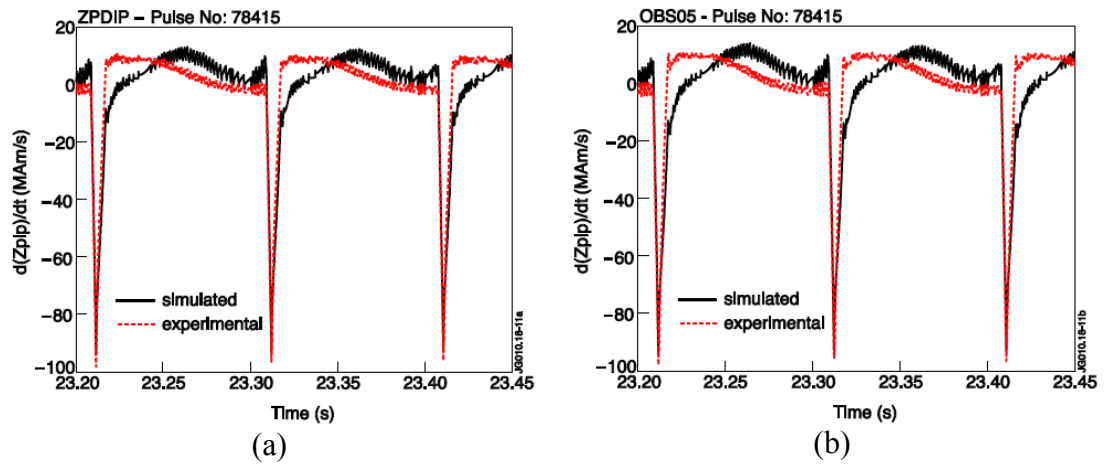**Figure 3.7** Response to radial field circuit voltage inputs: comparison between simulations and experimental values of ZPDIP and OBS05 in kick and recovery tests of pulse #78415. The values are obtained as linear combination of magnetic signals.

3.3 Experimental results

The alternative VS controlled variable OBS05 was then successfully tested in feedback during several VS experiments in JET. To minimize the impact on JET operation and to avoid dangerous disruptions, OBS05 was initially tested during ramp down at low plasma current (Fig. 3.8).

Afterwards, OBS05 was successfully tested for one second in the quiescent low beta current flat-top phase of a 1 MA discharge. The signals coming from OBS05 and ZPDIP were nearly coincident also using OBS05 as controlled variable.

The controlled variable OBS05 was finally tested during the H-mode phase. As expected from the analysis of giant ELMs (Fig. 3.5a), the behaviour of OBS05 was better than ZPDIP. This is demonstrated by the experimental data collected in the ELMy phases of pulses #78665 and #78666. The average excursion of ERFA current was about 40 % less in pulse #78665 after 16.5 s, i.e., when OBS05 replaced ZPDIP as feedback variable (Fig. 3.9a). This was confirmed in pulse #78666 (Fig. 3.9b), an experiment with the same scenario as #78665, with the only difference that after 16.5 s ZPDIP replaces OBS05.
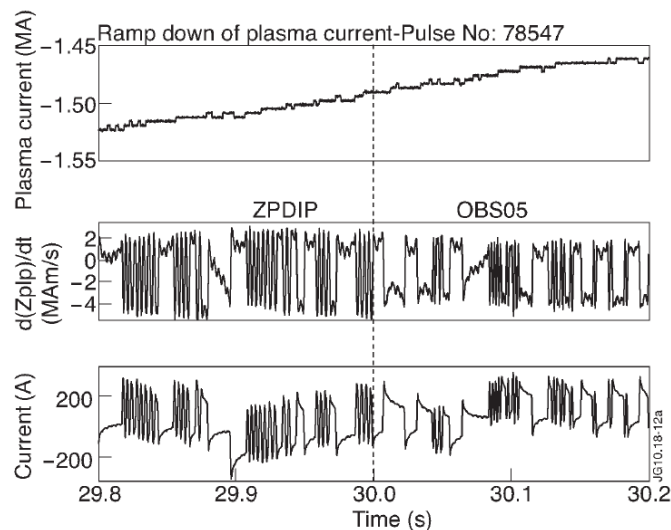
Figure 3.8 Experimental test of OBS05 in closed loop during ramp down (pulse #78547).
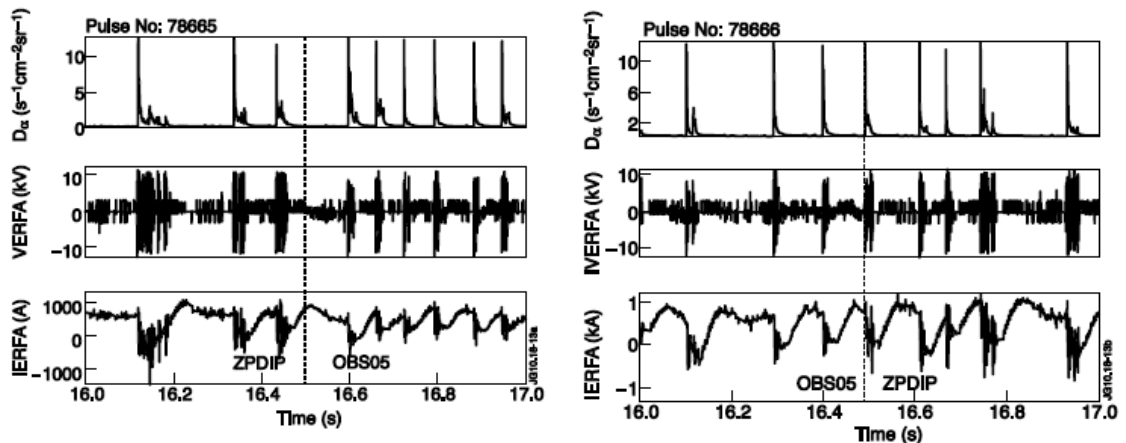
Figure 3.9 Experimental tests of OBS05 in closed loop in pulse #78665 after 16.5 s and in pulse #78666 before 16.5 s: Dα, radial field amplifier voltage and controlled variables. With OBS05 the stability is preserved and the radial field circuit current excursion on the fast time scale after an ELM is considerably smaller.

Indeed OBS05 was experimentally tested in a variety of scenarios and conditions: Fig.3.10 shows different pulses where OBS05 was the controlled variable for the VS system and ZPDIP was in open loop. All these experimental results confirm the predictions obtained using the modelling approach.

After these validation tests, in the remaining part of the JET experimental campaign OBS05 was used as preferred VS controlled variable.
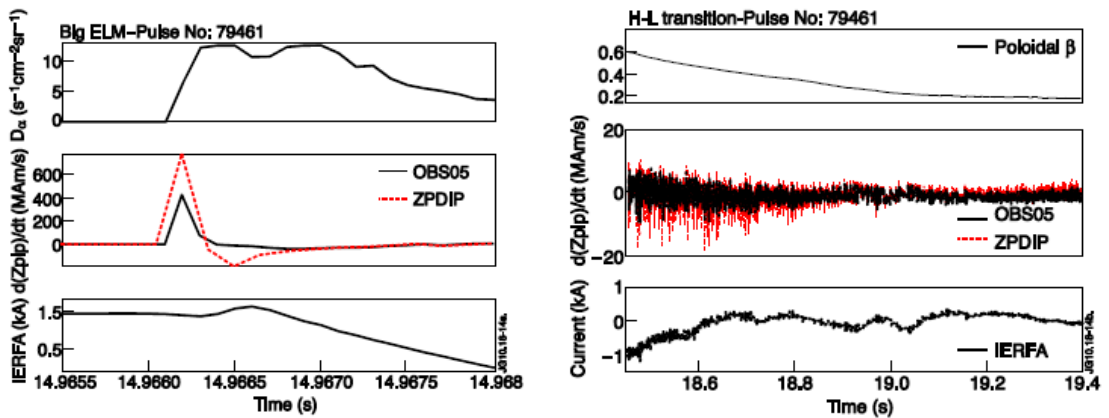
Figure 3.8 Experimental test of OBS05 in closed loop in pulse #79461: a) Large ELM; b) H-L transition.

3.4 Summary of the features of the new controlled variable

The new controlled variable OBS05 was successfully tested in JET experimental campaign on a variety of plasma scenarios and was then used as preferred VS controlled variable. To minimize the impact on the ongoing experimental campaign, OBS05 was required to reproduce the same behaviour as ZPDIP in most normal operation conditions, whilst reducing the sensitivity to the initial phases of ELMs, so as to avoid modification of VS controller architecture and gains.

The behaviour of OBS05 was better than ZPDIP in the ELMy phases of some pulses, yielding a significant reduction (about 40 %) of the excursion of ERFA current.

The selection of the weights was made via singular value decomposition exploiting experimental data and tested on both additional experimental data and simulations based on linearized plasma response models. The independent combinations of weights corresponding to the discarded singular values can be used as extra degrees of freedom for further optimization of the closed loop response. Further optimization and better estimation of the plasma vertical speed can be obtained using the approach suggested by Equations 1.9 - 1.10.

4

The new JET Vertical Stabilisation System

4.1 Introduction

The need of achieving better performance in present and future tokamak devices [68] has pushed plasma control to gain more and more importance in tokamak engineering [45]. High performances in tokamaks are achieved by plasmas with elongated poloidal cross-sections and diverted configurations [46]. Since such elongated plasmas are vertically unstable [47], position control on a fast time-scale is an essential feature of those machines. To achieve better performances, it is convenient to maximize the plasma volume within the available space. It turns out that the ability to control the plasma shape while ensuring good clearance between plasma and the facing components is an essential feature of any magnetic control system. Furthermore, plasma shape and position control in the ITER tokamak [35] will represent a challenge. In ITER, which is the next step toward the realization of electricity producing fusion power plants, the target operational scenarios can

approach plant controllability limits [45]. The VS system is one of the most critical ones in a tokamak, as it is responsible for avoiding vertical disruptions by guaranteeing zero plasma vertical velocity (on average). In JET and ITER, the VS controller is designed to vertically stabilize the plasma so that the shape controller can successfully control the plasma position and shape. The feedback signal is then related to the plasma vertical speed. The actuator is the Radial Field Amplifier (RFA) circuit shown in Fig. 4.1. To avoid saturating the current in the circuit, the VS controller also implements a current control loop.
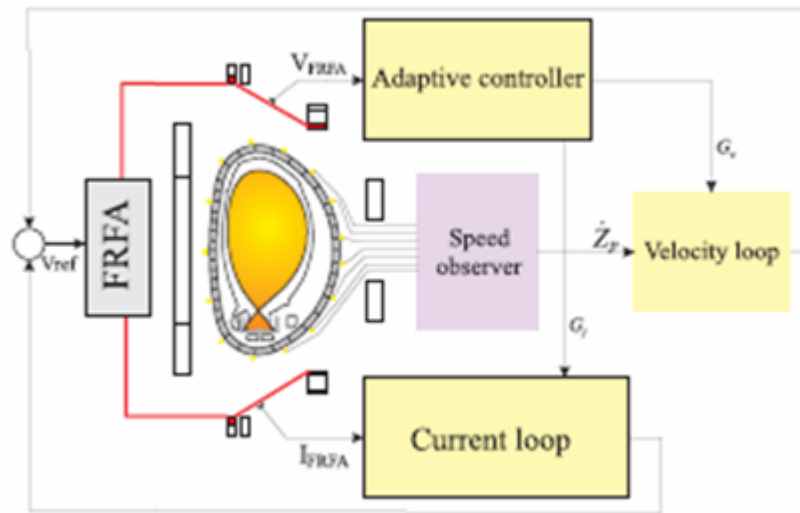
Figure 4.1 Simplified scheme of the JET Vertical Stabilization system

During the experiment, some plasma magnetic events act as disturbances for the VS control system. In particular, small and frequent edge localized mode (ELMs) [46] perturbations can cause the overheating of the RFA power supply, while giant ELMs create a large disturbance that puts the plasma far out of the equilibrium, sometimes causing a plasma disruption. The control system upgrade at JET has enhanced the VS system ability to recover from large ELM perturbations, especially for the case of plasmas with high elongation, i.e. plasmas with large vertical instability growth rate. The design of the new system has been carried out following a model–based approach [47], [42], which turns out to be essential when high performances and robustness are required. In particular, such an approach has been adopted for:

- the design of the new VS control algorithm, to optimize the controller parameters for the different operative scenarios.

- the design of the new power supply for the RFA circuit, called *Enhanced Radial Field Amplifier* (ERFA), to assess the system performance for different choices of the parameters, including nominal voltage and current;

- the assessment of the best choice for the turn setup of the coils; of the radial field circuit.

Thanks to the availability of reliable linear models for the plasma magnetic behaviour [26], a validation phase, including numerical simulations and then experimental tests and commissioning, has been carried out for each design step, from conceptual design to implementation.

In this work we focus our attention on the software architecture of the new VS control system, which is based on the Multi-threaded Application Real-Time executor (MARTe) [48], [49]. Indeed, the new VS system represents the first *MARTe based* control system that has been successfully developed and deployed at JET.

The chapter is structured as follows. The next section gives the general overview of the control system architecture and describes more in details both the main software components and the user interface which is strongly related with the VS software architecture. Section 4.3 presents the structure of the Enhanced Radial Field Amplifier and the model activities that has been carried out. Finally, Section 4.4 describes modelling and experimental activities carried out to assess the optimal number of radial field coil turns to increase the performance of VS system.

The main motivations that have driven both the design and the development of the new JET VS system are recalled in this section. Scenarios with highly elongated plasmas in presence of large ELM perturbations are envisaged to achieve better fusion performance in tokamaks. In these *extreme* scenarios a *general purpose controller* may not meet the requirements. Therefore, to improve the performance, it is a common practice to rely on a model–based design approach [42], [47], which ensures the needed control performance. In particular, for each plasma scenario, it is envisaged that the JET VS system could potentially use different estimations of the plasma vertical velocity, as well as different adaptive algorithms for the controller gains, in order to optimize the system behaviour.

The architecture proposed for the VS system is similar to the one adopted for the eXtreme Shape Controller at JET [50], [51], [52]. In particular, it permits to cope

with different scenarios during the same experiment in a simple manner. However, since the controllers are heavily optimized, a safety logic capable of switching to the general purpose controller in case of unexpected events must also be present, in order to get a safe termination of the experiment. Since control algorithms are usually developed in a modelling and simulation environment (e.g. Matlab/Simulink®), another requirement for the new VS software architecture concerns the possibility to check and validate the whole real-time code (including both the control algorithm and the auxiliary modules, i.e. communication interfaces with other systems, data acquisition, etc.) before testing it on the plant. To carry out this offline validation, real-time computational model of the plant based on detailed plasma linearized models [26], [27], [33] are needed.

Thus the adoption of flexible and modular software architecture is mandatory for the VS implementation, in order to successfully cope with the functional requirements summarized above. Indeed, the existing VS system [45], based on 4 Texas Instruments DSPs® (TMS320C40), was not flexible enough to satisfy the requirements. As an example, the present control system has been used to carry out some preliminary experiments aimed to confirm the simulation results. To perform these tests the needed modification have been applied as *patches* to the normal control mode, since it was not possible to isolate the control algorithm from the remaining part of the software. Unfortunately, given the limitations of the present architecture, every time a new functionality was required its implementation was not straightforward, mostly due to this lack of modularity.

These flexibility and modularity issues were accounted since the beginning of the conceptual design phase of the new architecture for the JET VS system. It is worth noticing that a modular architecture permits also to minimize the unavoidable interactions between software modules. Indeed, given a higher degree of *separation* it is possible to dramatically reduce the chance of errors when a single module is modified. In order to take into account all the functional requirements the new VS system has been developed exploiting the MARTe framework [49]. MARTe is built over a multi-platform library, i.e. it permits the execution of the same code on different operating systems, and provides the high level interfaces with hardware, external configuration programs and user interfaces, assuring at the same time hard

real-time performances. Within the MARTe environment, the end users are required to define and implement algorithms inside a well defined software block named *Generic Application Module* (GAM), which is executed by the real-time scheduler. The JET VS system has been implemented by using MARTe under the Real Time Application Interface (RTAI)/Linux operating system [48]. Thanks to this choice it has been possible to exploit the multi-processor ATCA4 based hardware architecture [49].

4.2 Software architecture

The VS software has been developed by using the MARTe framework. Within MARTe, the user application is a collection of GAMs, which are implemented by the users and executed by a real-time micro-scheduler. In particular, the user specifies the GAM inputs and outputs, as well as a number of parameters specific to each GAM. Each GAM is implemented using a standard Application Programming Interface (API), which has been designed taking into account all the peculiar needs when operating in a tokamak reactor. More details about MARTe can be found in [49]. A functional block diagram of the overall VS system software architecture is depicted in Fig. 4.2. The inputs to the VS cubicle from other JET subsystems are acquired via ADCs, which are managed by the *ATCA-ADC GAM*. The acquired measurements include all the magnetic measurements and some additional inputs, such as the plasma current.
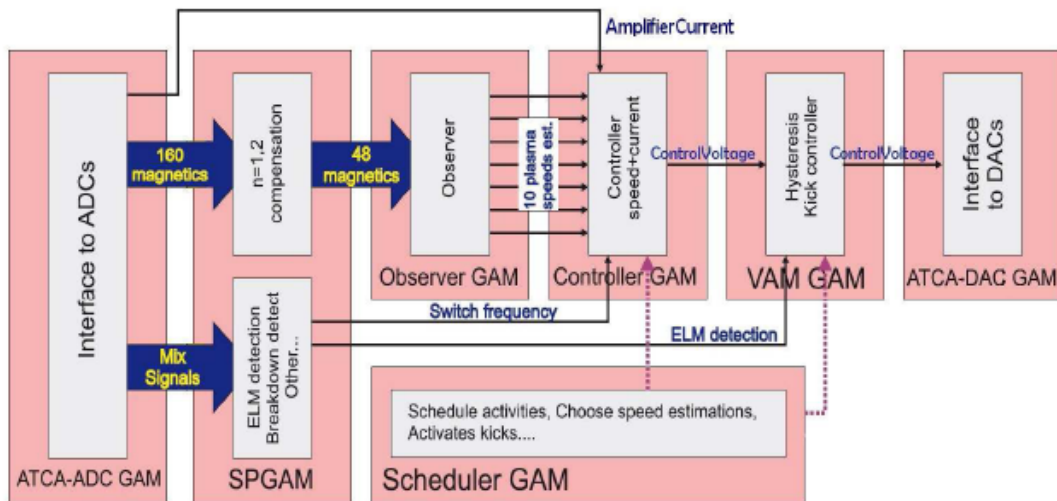
Figure 4.2 Software architecture of the new VS system.

Once the input signals have been acquired, they are available to all other GAMs. In particular the measurements are sent to the *Signal Processing GAM* (SPGAM) which computes the reference waveforms for the control loops (as specified in the user interface, see Section V) and the compensated magnetic measurements [56]. The compensated magnetic measurements are then sent to the *Observer GAM*, which

computes up to ten different estimations of the plasma vertical velocity. All these different estimations are available during the whole experiment. As a matter of fact, each estimation can be obtained as an output of a generic dynamic linear system. All the plasma velocity estimations, together with the power supply current and switching frequency, are sent as inputs to the *Controller GAM*, which contains four different control algorithms, and computes the voltage reference to the power supply. As for the planning of the experiment, every JET discharge is logically divided into a number of *time windows*. In each time window, all control algorithms receive all the plasma velocity estimations. The selection of the controlled variable is made on the basis of the signals provided by the *Scheduler GAM*. Although all the plasma velocity estimations are always computed, in each time window four out of forty possible paths are available. Such an architectural choice can be effectively exploited to minimize bumps during control algorithm transfer. Indeed to avoid control bumps the desired controlled variable can be selected as input to an inactive controller one time window before activating it.

Furthermore, in each time window, the *Scheduler GAM* instructs the *Vertical Amplifier Manager GAM* (VAMGAM) about which voltage request generated by the controllers should be sent to the power supply. Based on the signals received from the *Scheduler GAM*, the VAMGAM can also perform several additional functions. In the new VS system there is also the possibility to use the divertor coils for vertical stabilization purposes. In particular, the *Divertor Amplifiers Manager GAM* (DAMGAM) sends the voltage requests to the divertor power supplies. All the requests for the actuators (RFA and divertors power supplies) are sent to the DAC by the *ATCA-DAC GAM*.

4.2.1 Main software components

Following the main software modules previously introduced are described in details. In particular more details about the Observer, the Controller, the VAM and the DAM GAMs are given.

- ✓ **Observer GAM**: the architecture of the new JET VS system has been conceived to operate in advanced plasma scenario, where different estimations of the

plasma vertical velocity must be available in order to optimize system performance. For these reason, the Observer GAM has been designed as a container of ten different observers which run in parallel computing different estimations of the plasma vertical velocity. An observer receives as input a set of measurements and a transformation matrix. The resulting outputs can be used as inputs for other observers, in a daisy chain design, enabling the eventual reuse and optimization of some calculations. At the end of the production chain, a special observer produces a last signal, which is the result of a configurable linear combination of the output of all the observers. The observer computational interface can be extended and specialized in order to meet and model specific requirements, loosing in flexibility but leveraging configuration and functionality. One example is the state space model observer, where instead of specifying one anonymous matrix, the end-user is expected to provide the matrices with a direct correspondence to the observer dynamic model.

✓ *Controller GAM*: as for the Observer GAM, the Controller GAM has been conceived as a container of four control algorithms running in parallel during the whole pulse. Thanks to this choice, it is possible to meet the requirements in terms of disturbances rejection and thermal losses in the ERFA circuit, by selecting the *optimal* controller in each phase of the pulse. Furthermore this architectural choice permits to safely validate new control algorithms on the plant by running them in open-loop during the experiments. There are a number of inputs that are common to all the control algorithms. In particular each control algorithm receives as inputs all the plasma vertical velocity estimations computed by the Observer GAM, together with the current in the ERFA circuit and the current reference waveforms. Moreover, each algorithm can have its own input signals. The selection of the plasma vertical velocity to be used for the control is made on the basis of the scheduling signal provided by the Scheduler GAM. The control algorithms can implement any linear or nonlinear control algorithm, provided that the computational effort is achievable. However each control algorithm is assigned two basic tasks:

- control of the plasma vertical velocity, in order to achieve vertical stabilization;

- control the current in the ERFA circuit, so as to avoid current saturation and reduce the thermal losses in the circuit components.

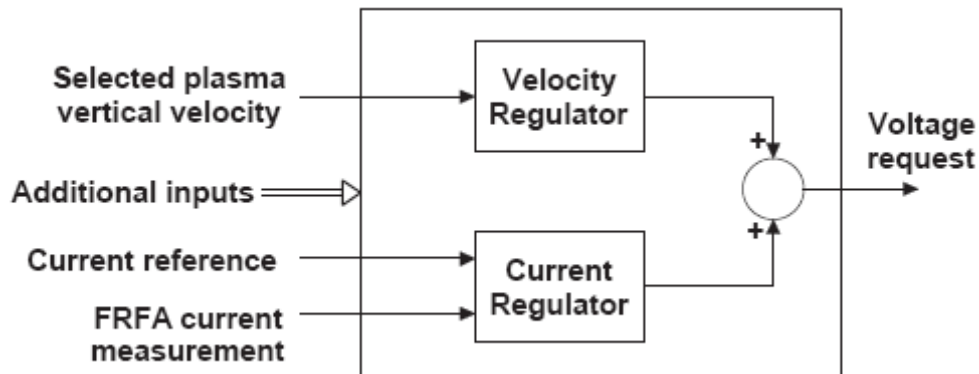Figure 4.3 shows the basic structure of a control algorithm contained in the Control GAM.

Figure 4.3 Basic structure of a control algorithm. Each control algorithm must provide a *Velocity Regulator* to achieve vertical position stabilization, and a *Current Regolator* to avoid current saturation and reduce the thermal losses in the actuator circuit.

✓ **Vertical Amplifier Manager GAM**: the VAMGAM selects the desired controller outputs, on the basis of the scheduler signals. Before sending it to the Enhanced Radial Field Amplifier (ERFA), the selected voltage request could be further processed by the following VAMGAM components: the Dither module, the Delay module, the Kicks module and the Relay Characteristic.

1) Dither: The Dither component adds a saw tooth waveform to the selected voltage request. This feature is used to reduce the effect of the voltage quantization. Indeed ERFA is composed of four units each rated 3 kV, 5 kA, which can be configured to deliver 12 kV, 5 kA [9].

2) Delay: The Delay module is used to delay the voltage request by a given number of time samples. The resulting delay introduced in the system is used to estimate the stability margins [21] during dedicated open-loop tests.

3) Kicks: The Kicks module is the most important component of the VAMGAM. It implements all the various types of kicks, which are voltage pulse of a given length and amplitude, and which can be specified by using the VS graphical user interface.

A kick logic is specified by using a kick waveform and a kick type. The former describes the voltage waveform to be applied by the kick component, while the latter decides when to apply the waveform itself. A kick waveform is defined as a sequence of time windows, each one specifying the following parameters:

- the length (in seconds) of the time window;

- the amplitude (in volts) of the window;

- the kick modality which can be set either equal to

  ◊ ON, so as to apply in feed-forward the amplitude of the current time window, substituting the value calculated by the controller;

  ◊ OFF, so as to ignore the amplitude specified and turn off the kick logic in the current time window;

  ◊ ADD, so as to add the amplitude specified to the value calculated by the controller);

- the time, which can set equal to

  ◊ DEFAULT, so as to use as length of the current time window the value specified by the length parameter;

  ◊ WAVEFORM, so as to use as length of the current time window the values specified by a given waveform.

By using the kick waveform and the kick type parameter a very high level of customization is achieved, allowing the user to specify:

- *timed kicks* which are kicks applied at a precise time during the experiment and used to simulate Vertical Displacement Events (VDEs) and perform halo currents studies [58], [59];

- *periodic kicks*, used for ELM pacing [60]; Figure 4.4 shows an example of 12 kV negative kicks;

- H_α *kicks* which are triggered at the occurrence of an ELM, and which are used to switch off the controller during an ELM phase;

- *saturation kicks*, which are used as protection system when the amplifier current reaches the safety threshold.
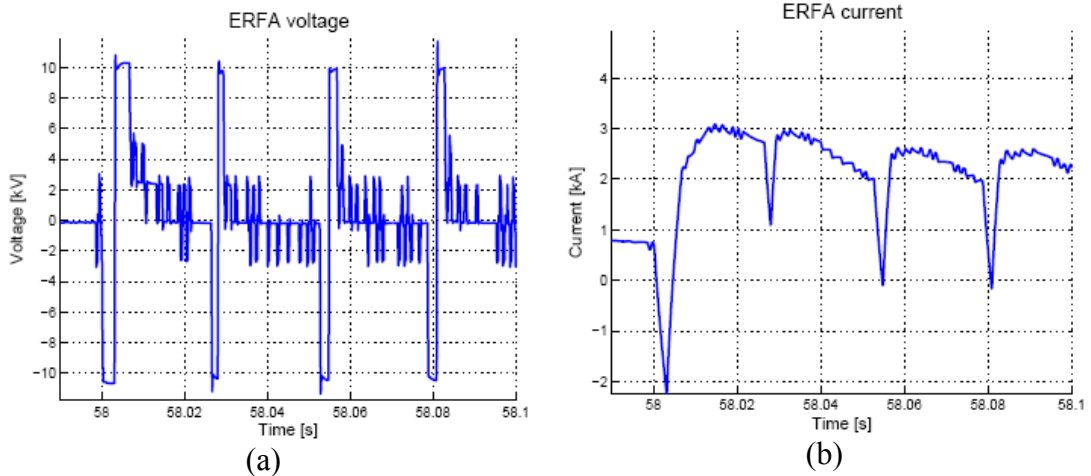
(a)	(b)

Figure 4.4 12 kV negative kicks applied during pulse #78951 starting from *t* = 58 *s*. (a) Amplifier voltage. Note that after each negative kick there is a positive counter kick due to controller reaction. (b) Amplifier current.

4) *Relay Characteristic:* the *Relay Characteristic* module implements the same variable hysteresis logic of the power supply ensuring that the correct voltage is applied by the amplifier even in presence of noise or not perfect calibrated DACs. Furthermore this block, if required, generates the digital word used to command the amplifier through the digital link.

✓ ***Divertor Amplifier Manager GAM:*** The DAMGAM is a module created in order to let the VS system act on the divertor coils, which are normally controlled by the Shape Controller [50]. In particular the DAMGAM made possible the application of voltage kicks to the divertor coils. A block diagram of the DAMGAM is shown in Figure 4.5, where P is a 4-by-4 invertible matrix which defines a linear transformation that maps the four divertor voltage requests received from the Shape Controller into a custom P-space.
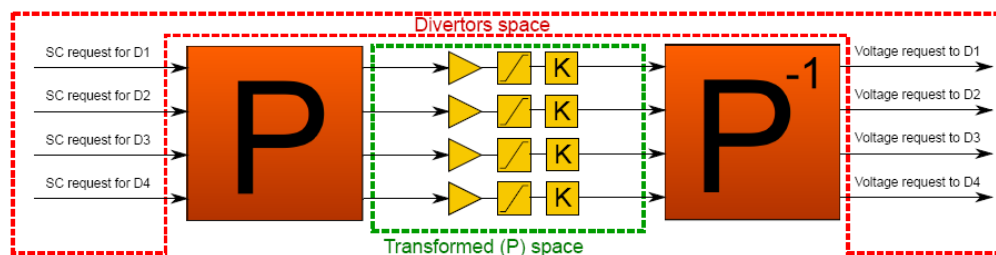

Figure 4.5 Block diagram of the DAMGAM module.

In this space a gain and a saturation can be applied to each signal, and the transformed signals pass also through a kick controller which works in almost

the same way as the VAMGAM module. Eventually the signals are transformed back in voltage requests to the divertor amplifiers. Thanks to its highly configurable structure the DAMGAM can effectively be used to explore all the possible interactions and advantages of using also the divertor coils for the task of the vertical stabilization. An example of use of the DAM is shown in Figure 4.6. In this experiment a full voltage kick on *D1*, *D2* and *D4* was applied by mean of a *P* matrix with the first row defined as [1 1 0 -1], corresponding to the linear combination of the divertor voltages that affects the plasma vertical movement. The other rows of *P* correspond to the linear combinations that less affect the vertical movement and have been computed through a singular value decomposition (SVD) decomposition. Figure 4.6(a) and 4.6(c) show the voltage input and output of the DAMGAM respectively, during the application of a 3 kV periodic kick (see Figure 4.6(b)).
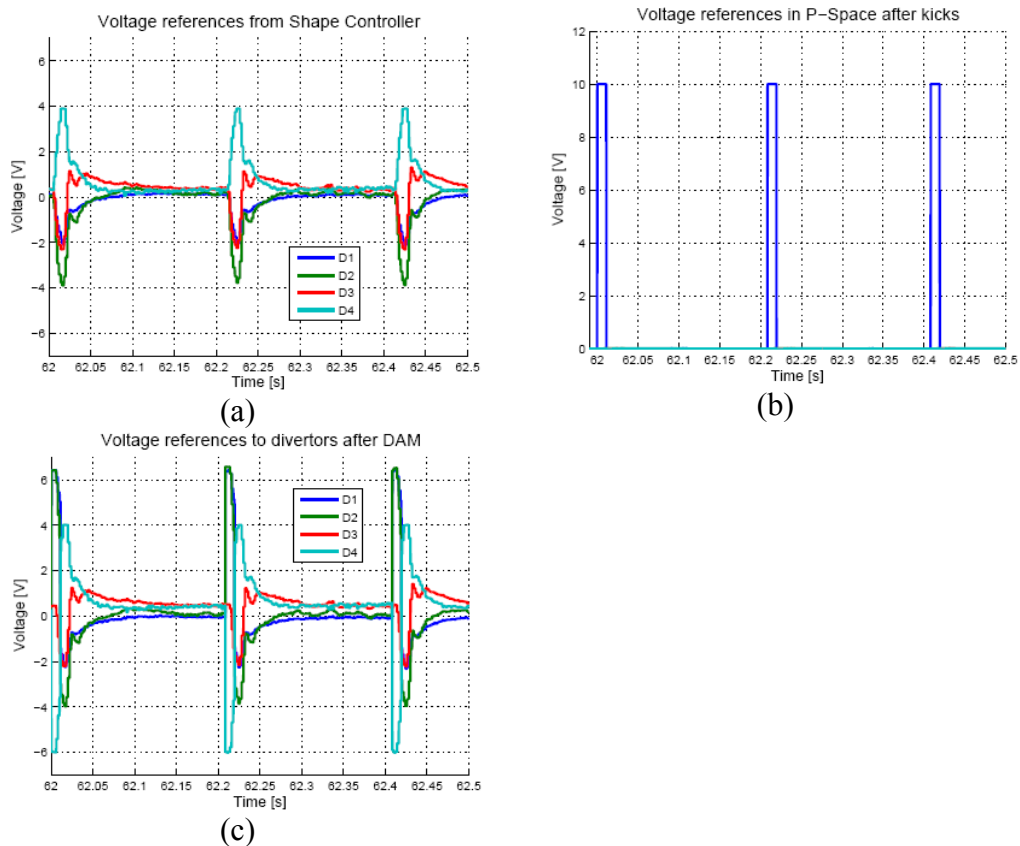

(a)

(b)

(c)

Figure 4.6 Example of periodic kicks in the DAM (pulse #78528). Note that ADC and DAC voltages are shown. These voltages range between [-10 V,+10 V]. (a) Divertor voltages as request by the Shape Controller. (b) Full voltage kick in the *P*-space. (c) Actual voltage applied to the divertor coils. As required, *D*3 does not receive any kick.

4.2.2 User interface

This section introduces the VS system user interfaces. Two main graphical interfaces are available, namely the Level 1 Interface (L1-Interface) and the Web Interface. The former allows the user to setup all the VS system parameters before the experiment, while the latter permits to monitor the state of the system during the experiment [61].

4.2.2.1 Level 1 Interface

The structure of the L1-Interface is made of several graphical layers each one corresponding to a different level of abstraction. Such layers are organized in two main levels:

◊ *Real-time executor level*, which allows the user permits to load the configuration of MARTe. In particular, the user can specify the GAMs to be executed together with their parameters, specifying them by means of a text files. It is important to note that this level is common to all the MARTe-based applications.

◊ *Application level*, which is customized for the VS system. This level is designed so as to allow the user to set each single parameter of the controller before the experiment.

The *Real-time executor level* is made of three different graphical pages:

• the *MARTe Layer* page, which allows to load the MARTe external and internal configuration files

• The *MARTe Thread Layer* page, where the user can load all the GAMs that make up the real-time system to be deployed. In particular for the VS system all the GAMs described in this work are loaded from this page, together with their configuration files.

• The *Patch* page, which is used when a change of the default system parameters (as they are specified in the configuration files) is necessary.

In general, the *Application level* depends on the particular system developed with the MARTe framework. The *Application level* deployed for the VS system is made of two graphical pages:

- The *General* page, which is used to set the parameters of the controller. In particular this page is organized in five subsections, each one corresponding to one of the following modules: SPGAM, Observer GAM, Controller GAM, VAMGAM and DAMGAM.

- The *Scheduler* page. This page is dedicated to the Scheduler GAM and allows the user plan the experiment by setting the VS behaviour in each of the 25 available time windows. For example, in each time window the user can choose the plasma vertical velocity to be controlled together with the desired control algorithm. This page also permits to set the desired VAMGAM and DAMGAM behaviours, and switch on the kicks performed by these two modules.

4.2.2.2 Web Interface

The *Web Interface* is based on the MARTe framework and it is automatically generated by the real-time application, i.e. by the VS system. This graphical interface allows the user to *navigate* into the GAMs structure so as to check the value of the parameters loaded in the VS system. Note that, while the L1-interface is a JET specific SunOS based application, the user can access to the Web Interface by using any system equipped with an internet browser.

4.3 The Enhanced Radial Field Amplifier

The radial field necessary for the vertical stabilisation of JET plasmas is generated by a dedicated set of poloidal field coils, denoted as P2R and P3R (Fig. 4.7), supplied by the old Fast Radial Field Amplifier (FRFA) [62], [63], based on Gate Turn-Off thyristors (GTO) and composed of four units rated 2.5 kA/ 2.5 kV, typically configured to deliver 10 kV / 2.5 kA. The design of a new amplifier was influenced by theoretical and modelling analysis of typical JET VDEs. Since control of a vertically unstable plasma following a perturbation depends both on the speed of the amplifier in producing the desired current in the coils, i.e. on the applied voltage, and on the available current the solution chosen for the new Enhanced Radial Field Amplifier (ERFA) has been an upgrade of about 20% of the output voltage to ± 12 kV, in four units rated ± 3 kV, and a doubling of the current capability to ± 5 kA.
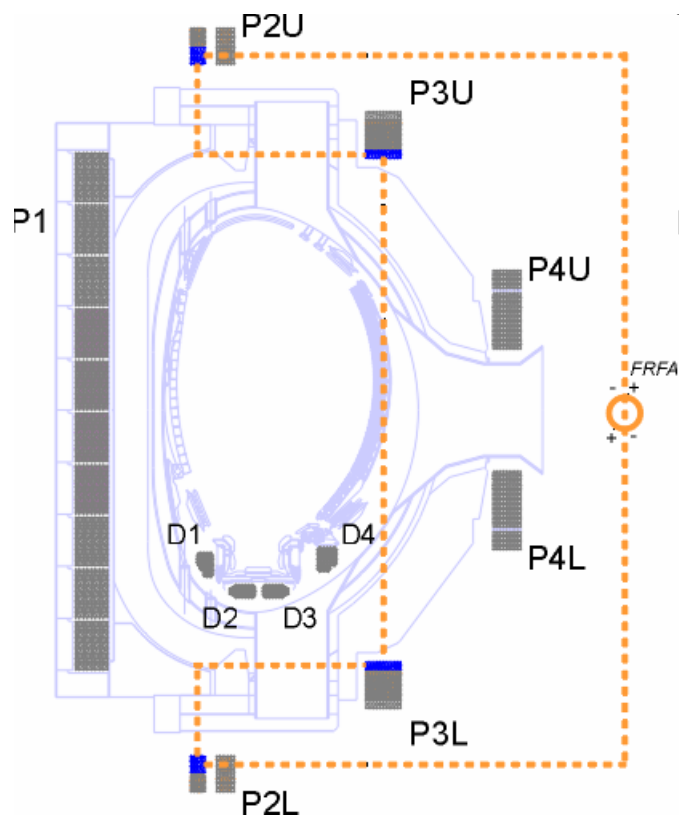

Figure 4 7 Radial field circuit [8].

4.3.1 Design of the amplifier

The requirement for the ERFA system (12 kV, 5 kA) can be satisfied by means of four units connected in series, each rated for 3 kV, 5 kA output. In principle, it would also be possible to have only two units rated for 6 kV, 5 kA, but this solution was judged not convenient because of the excessive amplitude of the voltage steps. A possible reconfiguration of the units to supply 6 kV, 10 kA is not considered of interest for JET. In conclusion the new ERFA amplifier [64] is composed of four 3 kV, 5 kA units connected in series at the output.

The structure of the unit, which is proposed to satisfy the requirements, is sketched in Fig. 4.8. It is composed of a transformer, an ac/dc thyristor converter with chokes on the dc side, a capacitor bank and a chopper then an H-bridge inverter, a filter for dV/dt limitation and a protection bipolar crowbar. This design assumes that the capacitor bank handles the high power peaks in transient conditions; in particular, during the current ramp-up phase of the load, generally lasting some ms, the energy is transferred from the bank capacitance to the coil inductance via the inverter, at the expense of the capacitor bank voltage.
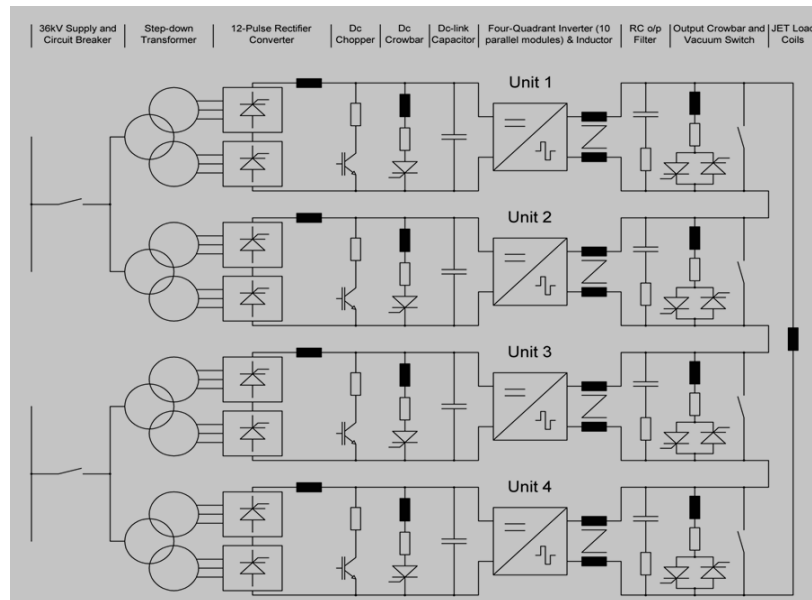

Figure 4.8 Scheme of the four units of the Enhanced Radial Field Amplifier

Conversely, in case of a decreasing load current, the energy stored in the coils is fed back to the capacitor bank, thus causing a corresponding voltage increase. In these

phases, in particular operating conditions, the capacitor voltage might become too high and require an overrating of the capacitor bank itself. To avoid this, one option is to feed the power back to the JET distribution system, but this choice would have required a very high power four quadrant converter to guarantee the power flow in the required short times. On the contrary, a chopper with series resistance and a fast hysteresis voltage control has been inserted in parallel to the capacitor bank. This allows limiting the capacitor voltage rating to that required by the normal operating conditions, as it provides dissipation of the excess energy.

The ac/dc converter has to supply only the pre-charging voltage to the capacitor bank and the power corresponding to the losses during the pulse.

With this design approach, the size of the capacitor bank is limited and the transformer and ac/dc converter power ratings can be greatly decreased. Moreover, a simple single quadrant operation is sufficient for the ac/dc converter thus simplifying significantly both the power and the control section.

The ERFA units have to be able to operate all together, as in normal operating conditions, but also independently. In fact, in case of fault of one unit, operation will continue with the other (nonfaulty) units. This means that each unit has a control section able to assure the independent operation and ERFA overall has a system control which provides for the common management of the units.

The ERFA control will be therefore divided in two sections:

- The control section which provides the ERFA system control, named *Supervisor* below;

- Individual control of each ERFA unit.

The Supervisor implements all the functions necessary for the correct amplifier operation both in Remote mode, under the PPCC control, and in Local mode from the supervisor panel for commissioning, maintenance and troubleshooting. In addition, four individual unit control systems are provided to assure the correct unit operation both under the Supervisor control and independently for single unit operation, namely the single unit commissioning.

To assure the best response time, operation of the ERFA under a voltage delta control with hysteresis seems the best choice. In particular as shown on Fig. 4.9 the

ERFA output voltage can assume nine (nominal) voltage levels (-12000 V, -9000 V, -6000 V, -3000 V, 0 V, 3000 V, 6000 V, 9000 V, 12000 V).
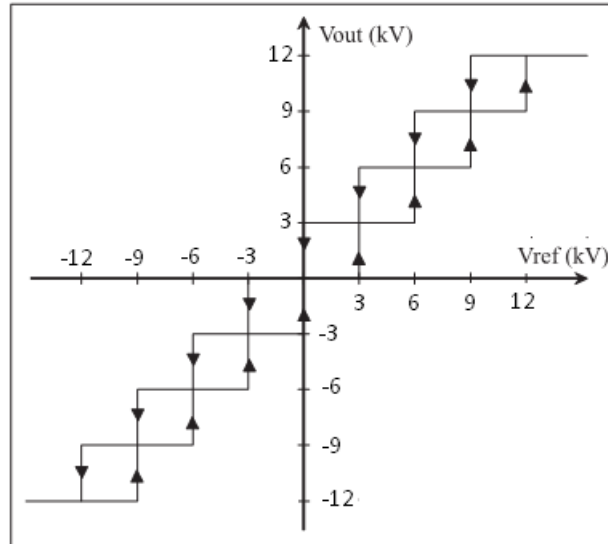

Figure 4.4.9 Hysteretic characteristic of the amplifier

The generation of the reference voltage will be assured by the Supervisor in local control and by PPCC in Remote mode.

In remote mode, the reference signal coming from the PPC Control can be analogue or digital. In case it is digital, PPCC will supply to ERFA a number corresponding to the desired output voltage among the nine possible discrete levels and the number will be directly used by ERFA to produce the corresponding output voltage:

- -4 All four ERFA units applying negative voltage
- -3 Three units applying negative voltage and one unit in zero state
- -2 Two units applying negative voltage and two units in zero state
- -1 One unit applying negative voltage and three units in zero state
- 0 All four units in zero state
- +1 One unit applying positive voltage and three units in zero state
- +2 Two units applying positive voltage and two units in zero state
- +3 Three units applying positive voltage and one unit in zero state
- +4 All four units applying positive voltage

In case PPCC will send an analogue reference signal (Vref from PPCC), ERFA will convert it to digital form via an A/D converter. The reference signal will be

converted in an integer number between -4 and +4 and the transitions between one number to another will be ruled by hysteresis logic with tuneable thresholds.

In open loop operation, there is no control of the output current, it is however required that a dynamic current limiter is implemented in the ERFA control; in this condition, ERFA is able to continue to supply the maximum current till other limits are reached.

In normal conditions with all the four units operating, ERFA can generate nine distinct voltage levels numbered among -4 and +4. It should be remarked that the two extreme values of the output voltage can be obtained with one possible combination of the switches, whereas the intermediate levels can be obtained with more than one combination in such a way that successive switching at the same output voltage level can involve different semiconductors, thus reducing the losses on the each device.

In case of one or more units becoming faulty before the pulse or during the pulse, the control system of the amplifier is able to apply in real time a different algorithm optimized for the number of available units. This function is performed by the block named "rotation logic" which will receive the number corresponding to the desired level of the output voltage as input signal and the information related to the number of available units. This block will produce four output signals, one for each inverter; each output signal will be an integer number between 0 and 4 representing a status of the inverter switches.

4.3.2 Modelling of the amplifier

To have a complete simulator for the Vertical Stabilization system a simplified model of the amplifier is needed. The proposed simplified circuits models the following functions:

- hysteretic characteristic of the amplifier;
- the saturation of the amplifier current.

The model of ERFA is derived in order to be coupled to the plasma control system on a bandwidth from 1 Hz to 1 kHz. The main approximation is on the voltage droop due to the capacitor discharge in case of relatively long (50 ms) activation of a single module without rotation. Figure 4.10 shows the model of the cable.
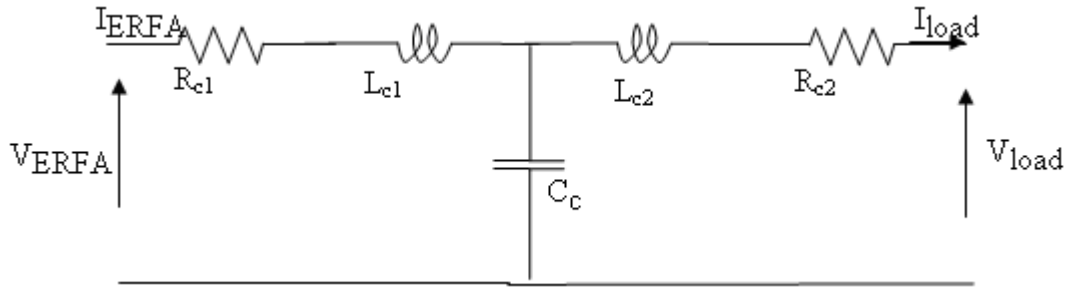
Figure 4.10 Cable model

where $R_{c1}=R_{c2}=10$ mΩ, $L_{c1}=L_{c2}=50\mu$H, $C_c=300$ nF, I_{ERFA} and V_{ERFA} are respectively the current and the voltage of the ERFA amplifier, V_{load} and I_{load} are respectively the voltage and the current on the coils.

Fig. 4.11 shows the model valid for a single ERFA unit. Every switching action dissipating an energy should properly be taken into account via an impulsive current generator in parallel to C_{bank}, which is not present in the following scheme.
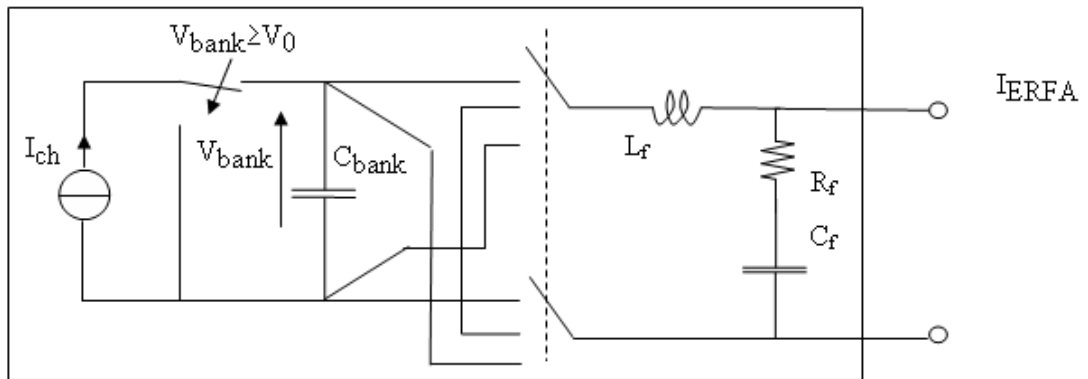
Figure 4.11 Model of a single ERFA model

where:

I_{ch}=125A, V_0=3kV, C_{bank}=75mF, L_f=200μH, R_f=8Ω, C_f=12μF

$$I_{ch} = \begin{cases} \min[K(V_{ref} - V_{bank}), 125A] & \textit{if } V_{bank} < V_{ref} \\ 0 & \textit{if } V_{bank} \geq 3kV \end{cases},$$

$V_{ref} = \sqrt{V_0^{\,2} - (C_{bank}/L_{load,nom})I_{load}^{\,2}/4}, \quad L_{load,nom} = 20mH$ with standard turns

The factor of 4 in the expression of V_{ref} is inserted by assuming that the energy returned from the load can be shared among the 4 modules. The simplified model of the overall ERFA amplifier is shown in Fig. 4.12
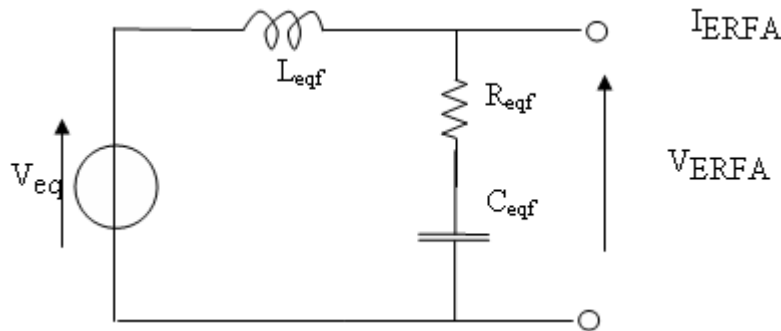
Figure 4.12 Simplified model of 4 units of ERFA

$L_{eqf} = 800\mu H$, $R_{eqf} = 32\Omega$, $C_{eqf} = 3\mu F$, $Veq = V_1 + V_2 + V_3 + V_4 = V_h \sqrt{1 - (L_{load,nom} I_{load}^2 / (4 C_{bank} V_0^2))}$

where $C_{bank} = 75mF, V_0 = 3kV$, $L_{load,nom} = 20mH$ with standard turns,

$V_h \in \{-12,-9,-6,-3,0,3,6,9,12 \text{ kV}\}$ is the voltage request downstream the hysteresis loop.

To validate the described models, the following circuits have been developed in PSIM$^®$. Fig. 4.13 shows the simplified model developed in PSIM$^®$, whereas Fig. 4.14 shows the complete model of the amplifier.
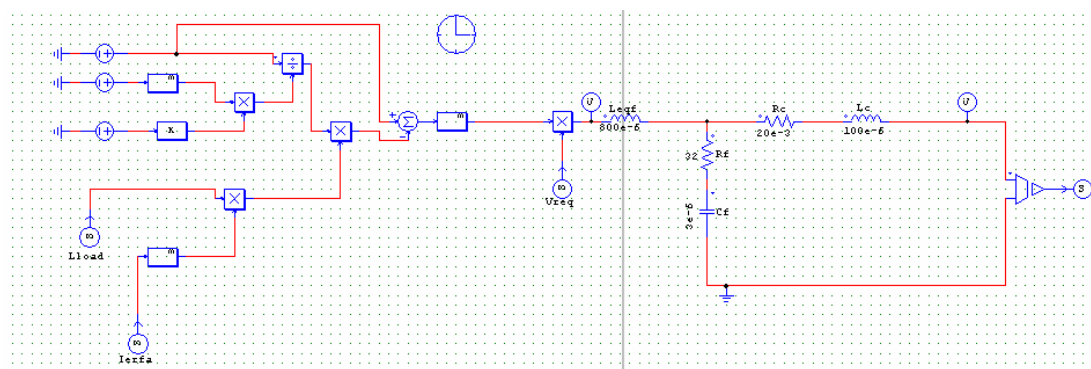
Figure 4.13 Simplified model of the Enhanced Radial Field Amplifier developed in PSIM$^®$

Figure 4.14 Complete model of the Enhanced Radial Field Amplifier developed in PSIM®

(a)   (b)
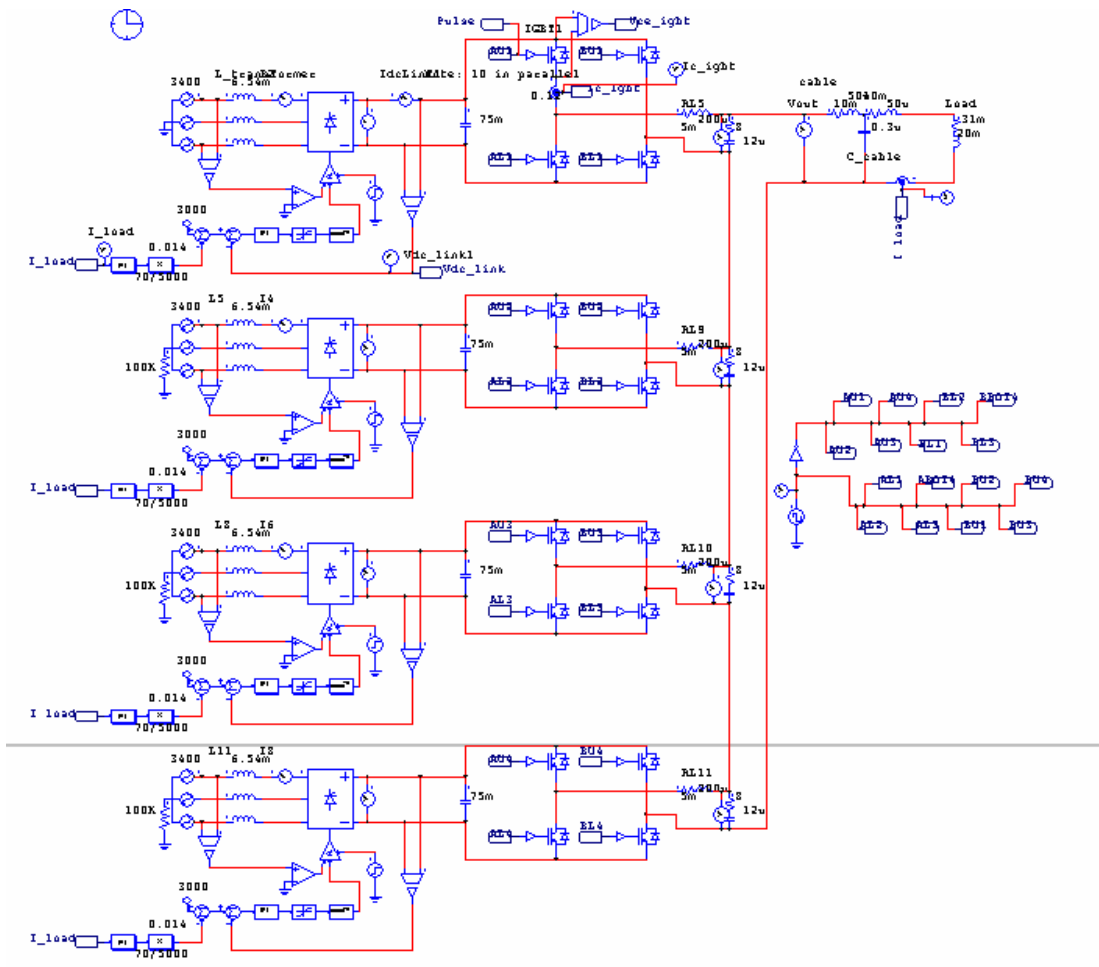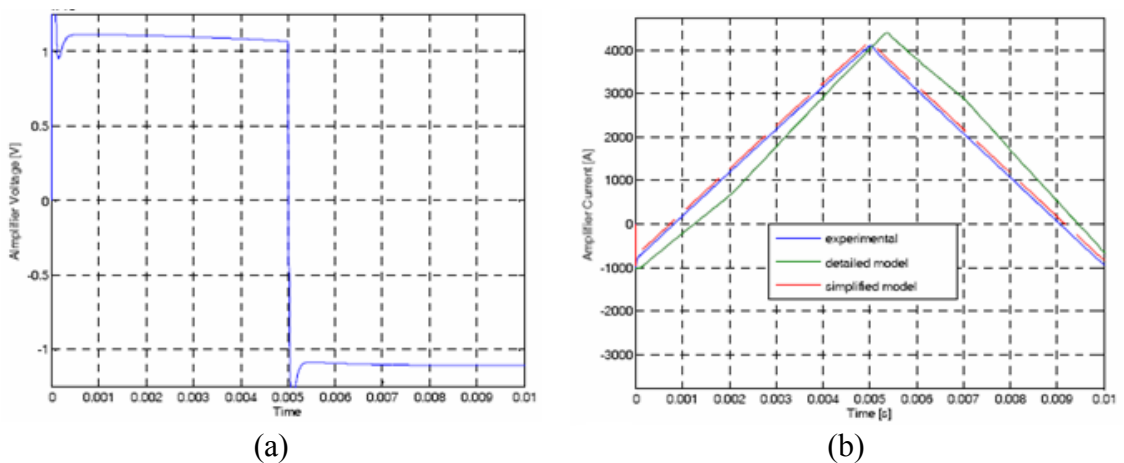
Figure 4.15 Validation of the simplified model. a) Amplifier voltage applied to the models. b) Comparison between experimental data (blue line), detailed model (green line), simplified model (red line).

4.4 Optimization of radial field coil turns

As discussed in the previous section, in order to increase the performance of the VS system a new radial field amplifier has been projected and installed at JET.

The radial field necessary for the vertical stabilisation of JET plasmas is generated by a dedicated set of poloidal field coils, denoted as P2R and P3R (Fig. 4.1), which were fed by the old Fast Radial Field Amplifier (FRFA) [63], composed of four units rated 2.5 kA/ 2.5 kV, typically configured to deliver 10 kV / 2.5 kA. The design of a new amplifier was influenced by theoretical and modelling analysis of typical JET VDEs. Since control of a vertically unstable plasma following a perturbation depends both on the speed of the amplifier in producing the desired current in the coils, i.e. on the applied voltage, and on the available current the solution chosen for the new Enhanced Radial Field Amplifier (ERFA) has been an upgrade of about 20% of the output voltage to ±12 kV, in four units rated ±3 kV, and a doubling of the current capability to ± 5 kA as discussed more in detail in the previous section. An additional improvement in the system performance could be obtained by the ability to operate continuously with a current bias of 2.5 kA, thus enabling a fast current swing of 7.5 kA. To better balance the upgrade of nominal current and voltage, the possibility of decreasing the inductance of the Radial Field Coils was explored. The variation of inductance of the Radial Field circuit was made possible by configuring the connection to the P2R/P3R coils with a variable number of turns. The standard configuration, characterised by 72 turns, is the reference with a differential inductance of ~ 20 mH. Since ERFA nominal voltage (12 kV) is 20% higher than FRFA whereas ERFA nominal current (5 kA) is twice as much as FRFA, coil turn reduction was expected to be advantageous to increase the voltage per turn and the time derivative of the stabilizing field. The price to be paid is the reduction of the Ampere turns, hence the maximum stabilizing field. To define the optimal number of radial field coils modelling activities have been performed. This activity is described in the next subsection. After a modelling activity with thorough analyses and simulations, three possible sets of optimum configuration have been proposed for experimental tests. Subsection 4.4.2 describes these experimental activities and illustrates the final choice of coil turns.

4.4.1 Modelling activities and results

The optimal configuration of turns mainly depends from the plasma current I_P and from the growth rate γ. Therefore, a set of plasma configurations and currents should be defined for this optimization, and in principle different coil turns could be used for different plasmas.

For each type of plasma all possible combinations of P2R and P3R have been analyzed. The possible values of P2R and P3R, compatible with technological constrains, are represented below (Fig. 4.16):

Figure 4.16 Turn Options compatible with technological constrains

By considering all the possibility in term of configuration of turn, plasma current and growth rate two different modelling procedures have been carried out with different criteria. The first procedure has as benchmark criteria the maximum initial vertical displacement, the second one has the maximum controllable ELM size.

The parameter ranges of the configurations analysed are:

$$1.2 \text{ MA} < I_p < 4 \text{ MA}, \ 111s^{-1} < \gamma < 695 \text{ s}^{-1}.$$

The tools for the analysis of the first procedure consist of a linearized model of the plasma coupled to a simplified model of ERFA amplifier, described in the previous section. The benchmark condition is defined in terms of maximum controllable

vertical displacement δZ_{0max}. To carry out the optimization, we analysed all admissible turn combinations under the following conditions:

- P2R turns= 0,8,16

  P3R turns= 0,2,4,6,…,18,20,

  with differential inductance $L_{load} \geq 10mH$;

- $\delta Z \leq 20cm$;

  $I_{ERFA}= \leq 5\,kA$;

The main outcome of this analysis is shown in Figs. 4.17-4.18 and Table 4.1. Additional analyses have been carried out to assess the effects of 2.5 kA prepolarization, limit displacements of 30 cm instead of 20 cm, and the possibility of keeping constant the ERFA current after saturation.

The main conclusions of the described modelling analysis are hereafter listed:

- The operational space analyzed is 1.2 MA<I_p<4 MA, 111 s^{-1}<γ<695 s^{-1} .The worst case analyzed is with a 4MA plasma with a growth rate of about 500 $s^{-1.}$

- Leaving the (16, 20, -16, -20) configuration of turns with ERFA would be not efficient at high growth rates; in the worst case there would be a gain factor of only 1.3 with respect to the present (16, 20, -16, -20) turns with FRFA .

- The optimal symmetric configuration of turns with ERFA is (8, 18, -8, -18); in the worst case there is a gain factor of about 1.7 with respect to the present (16, 20, -16, -20) turns with FRFA. The performance degradation with the symmetric configuration (8, 20, -8, -20), which is expected to be cheaper, is negligible.

- The optimal asymmetric configuration of turns with ERFA is (16, 20, -0, -4); in the worst case there is a gain factor of about 2.2 with respect to the present (16, 20, -16, -20) turns with FRFA. The performance degradation with the asymmetric configuration (16, 20, 0, 0), which is expected to be cheaper, is negligible. The (16, 20, -8, -2) asymmetric option replaced the (16, 20, 0, 0) initial more advantageous proposal, due to the risks related to the high voltage per turn.

- The beneficial effect of a 2.5 kA prepolarization is significant with optimal turns (10-15% with a growth rate around 300 s^{-1}).

- No significant performance improvements are obtained when maintaining constant the ERFA current after its saturation (less than 3% and even less with 2.5 kA prepolarization).

- The asymmetric configurations strongly interact with the shaping circuit.

- The solutions with 0 turns in the lower coils should be avoided for problems of insulations in the remaining coils, which would be subjected to a significant voltage.

- The suggested alternative turn configurations for P2RU - P3RU - P2RL - P3RL are then: 16-20-8-2 (11mH) and 8-20-8-20 (12 mH).
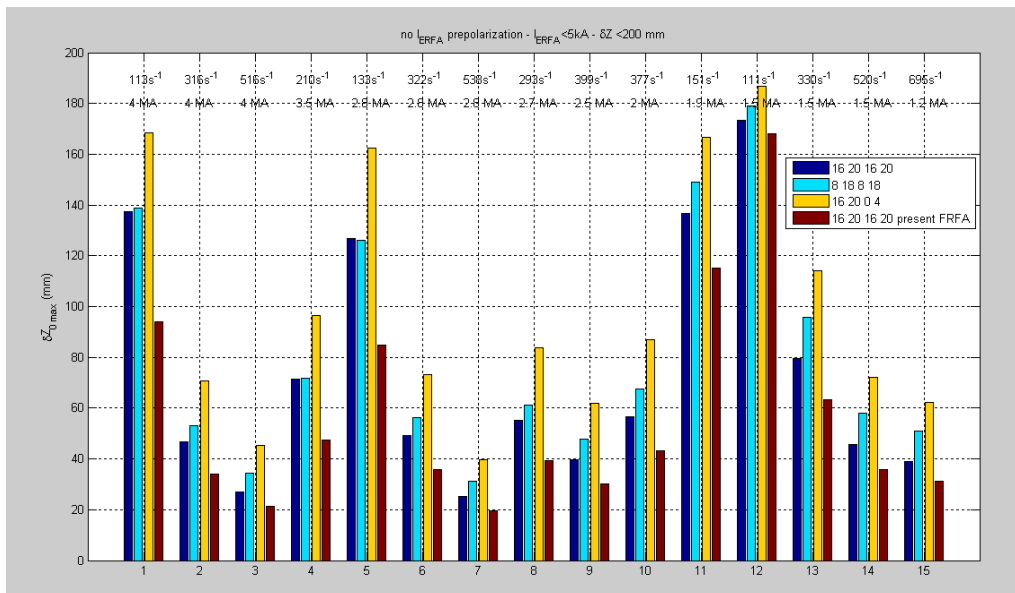

Figure 4.17 Values of δz_{omax} for plasmas with different I_p and γ (ERFA vs FRFA): effect of the number of turns.
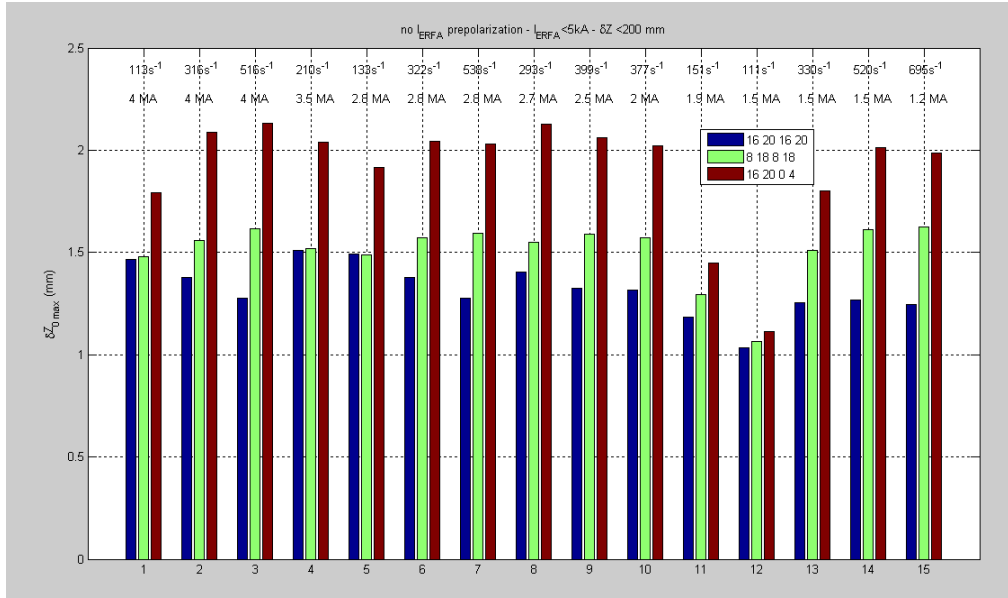
Figure 4.18 Relative improvement for ERFA with respect present FRFA in term of δz_{omax} for plasmas with different I_p and γ: effect of the number of turns.

I_P (MA)	γ (s^{-1})	$\delta z0max$ (mm) 16 – 20 – 16 -20 ERFA	$\delta z0max$ (mm) 8 – 18 – 8 – 18 (8-20-8-20) ERFA	$\delta z0max$ (mm) 16 – 20 – 0 -4 (16-20-0-0) ERFA	$\delta z0max$ (mm) 16 – 20 – 16 – 20 Present FRFA
4.0	113	138	139 (146)	168 (168)	94
4.0	316	47	53 (52)	71 (70)	34
4.0	516	27	34 (33)	45 (45)	21
3.5	210	71	72	97	47
2.8	133	127	126	162	85
2.8	322	49	56	73	36
2.8	538	25	31	40	20
2.7	293	55	61	84	39
2.5	399	40	48	62	30
2.0	377	57	68	87	43
1.9	151	137	149	167	115
1.5	111	173	179 (178)	187 (187)	168
1.5	330	80	96 (92)	114 (113)	63
1.5	520	46	58 (55)	72 (71)	36
1.2	695	39	51	62	31

Table 4.1 Values of $\delta zomax$ for plasmas with different Ip and γ and for the optimal number of turns (ERFA vs FRFA).

Particular care was devoted to the risk analysis and the measures to be taken whenever needed, so as to carry out ERFA commissioning safely. Essentially there are two sources of risk:

- modelling errors;
- impact on other subsystems.

The modelling errors are mainly related to the crude 2D model of the 3D mechanical structure used for this analysis. The 2D equivalent model utilizes two parameters tuned so as to fit the experimental response of I_{FRFA}, plasma and magnetic measurements to radial voltage inputs in the present configuration. The radial field circuit field pattern is certainly modified when changing the turns.

Moreover a possible impact on the following JET subsystems was considered:

- coupling with SC circuits;
- breakdown.

The asymmetric configurations strongly interact with the shaping circuit. However, the expected range of shape control current variation is in the same order of magnitude as the divertor currents in with the old FRFA (0-500 A). During the breakdown, a bias field is added to compensate the magnetic field produced by the eddy currents induced in the passive structures. In symmetric tokamaks, a vertical field is sufficient. Due to the presence of the divertor, the passive structures of JET are asymmetric, hence the FRF circuit is used during breakdown. If the turns of P2 and P3 are not reduced proportionally, which is the case of the suggested options, the present time behaviour of the radial field current would provide a different contribution to (radial and vertical) field in the breakdown region (Fig 4.19). This might cause problems and even prevent the breakdown.
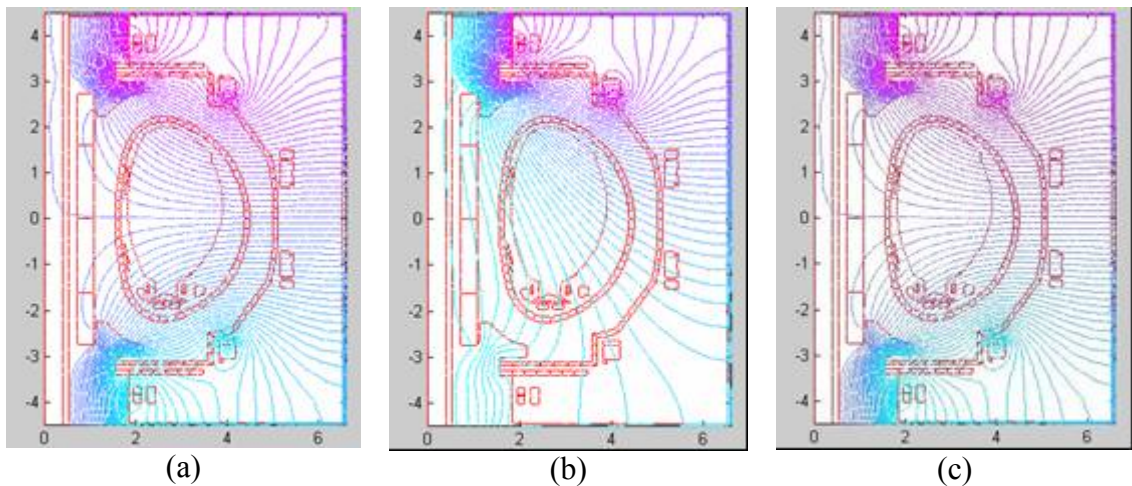
<div align="center">(a)   (b)   (c)</div>

Figure 4.19 Field configuration with various coil turns: a) standard configuration (16, 20, -16, -20); b) asymmetric configuration (16, 20, 0, 0); c) reduced configuration (8, 20, -8, -20);

To validate the obtained results an additional modelling verification with different benchmark criterion has been carried out.

As mentioned earlier an ELM event creates a strong variation in the plasma speed measurement. Indeed the maximum rejectable ELM can be considered as benchmark to study the performance of the VS system. From the viewpoint of the VS system an ELM event, being a variation of poloidal beta and internal inductance, can be schematized as a disturbance for the system. In particular, by using the ELM identification in term of internal plasma parameters, described in 2.4, and the simplified closed loop model of the VS system. By considering the identified quantities as disturbances for the system the closed loop simulations have been performed. In particular, as shown in Fig. 4.19 the inputs of the system are the amplifier voltage VERFA and the identified quantities, instead the output are the amplifier current IERFA and the estimation of the vertical velocity ZPDIP.
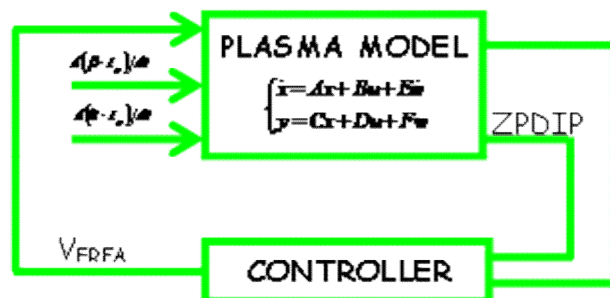

Figure 4.20 Closed loop simplified scheme

Thanks to these simulations it has been possible to find the maximum controllable ELM by multiplying the disturbances for a factor α. For each proposed radial turn configuration a comparison with the standard one has been made. This procedure confirms the results obtained with the first one.

As a conclusion of the modelling activities three different coil options of P2RU-P3RU-P2RL-P3RL turns were then proposed for experimental tests. The reduced symmetric option (8, 20, -8, -20) was obtained by reducing the coil turns of P2R, for which the allowed values are 16, 8, 0. For medium-high growth rate plasmas the expected gain G for medium-high values of the growth rate γ ranges from 1 to 1.2. Using 2.5 kA ERFA current offset G>1 also for lower growth rates. The (16, 20, -8, -2) asymmetric option replaced the (16, 20, 0, 0) initial more advantageous proposal, due to the risks related to the high voltage per turn.

4.4.2 Experimental activities

In order to study the effect of the different inductance configurations for the Radial Field coils, the performance of the new vertical stabilisation system has been assessed, in each radial turns configuration, on the basis of its response to controlled perturbations in as wide a range of equilibria as possible, thus covering a large range of vertical instability growth rates (γ ~ 100 − 1400 s^{-1}) and exploring the effect of parameters like plasma-wall clearance. The controlled perturbations were provided by so called "vertical kicks", i.e. an open loop maximum voltage pulse of varying length, either upwards or downwards, followed by closed loop recovery by the VS controller (Fig. 4.21). The 2D models were also capable to predict the maximum duration Δt_k of a kick, given by a simple relationship, i.e. $exp(\gamma \Delta t_k)<2$, in the absence of other sources, saturation effects and nonzero initial conditions. This is obtained by the simple first order model:

$$\frac{du_p}{dt} = \gamma \cdot u_p + B \cdot V_{ERFA}$$

where u_p is the vertical speed of the plasma, γ the growth rate, V_{ERFA} the amplifier voltage, and B a constant. Applying a kick at constant kick voltage V_k in $0<t<\Delta t_k$, and

then a constant recovery voltage V_r of the opposite sign for $t > \Delta t_k$, the vertical speed is:

$$
\begin{cases}
u_p(t) = [\exp(\gamma t) - 1] \cdot B \cdot V_k / \gamma & 0 < t > \Delta t_k \\
u_p(t) = [k_r \cdot \exp(\gamma t) - 1] \cdot B \cdot V_r / \gamma & t > \Delta t_k
\end{cases}
$$

with:

$$
k_r = \left[1 - (1 - V_r / V_k) \cdot \exp(\gamma \Delta t_k) \right]
$$

To obtain speed inversion, k_r has to be negative, yielding the simple condition:

$$
\exp(\gamma \Delta t_k) \leq 1 + |V_r| / |V_k|
$$

This permits to establish safe conditions for kicking the plasma when correctly estimating the growth rate in advance. In addition the above formulas can be used to have experimental estimates of the growth rate: i) lower and upper bounds simply testing whether the plasma disrupts or not; ii) more accurate estimates from the expression of kr and the experimental value of the time needed for speed inversion.

The response to ERFA kicks was compared in terms of:

- time needed to stop the plasma after the kick: Δt_{v0}
- ERFA current needed to stop the plasma: ΔI_{ERFA}
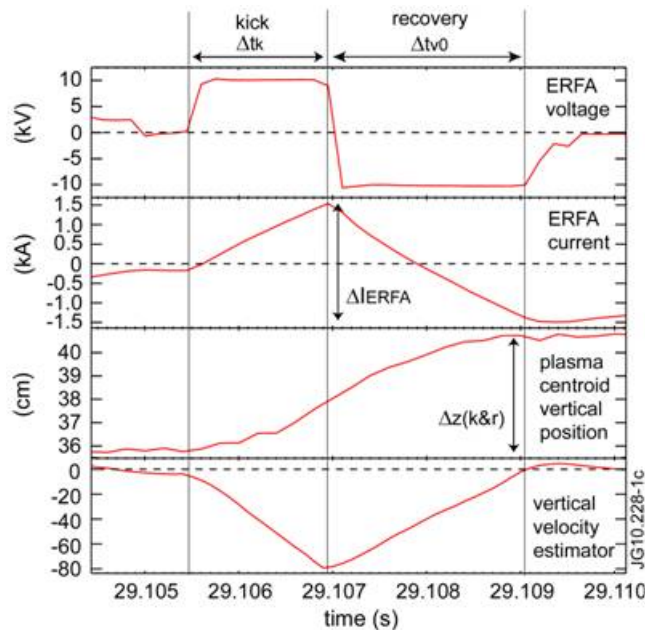- vertical excursion during the recovery : $\Delta z(k\&r)$

Figure 4.21 Time evolution of plasma and ERFA parameters for a vertical kick

106

The turn options have also been compared in terms of quality indexes taking into account the maximum value of Ip*Δz after a kick & recovery test compatible with ERFA current and voltage constraints. The fact that ERFA is capable to operate continuously with a current bias of up to 2.5 kA (yielding the possibility of having a current swing of up to 7.5 kA) was also taken into account.

The result is a better performance in terms of the average quality factor Q at high growth rate, say more than 150-200 s^{-1}, for the reduced and asymmetric options. At lower growth rates, the maximum kick duration is longer, and then the current limit (saturation at 5 kA) privileges the solution at high inductance. For high growth rate plasmas, the experimental analysis has also shown a significant reduction of the recovery time and the vertical excursion during recovery for the configurations at reduced inductance.

Figure 4.22 shows the experimental tests carried out on a high triangularity configuration characterized by a growth rate of 180 s^{-1} (estimate from the linearized model confirmed by the experimental data related to the speed inversion time $\Delta t_k + \Delta t_{v0}$), yielding a maximum kick duration of 3.9 ms at full voltage. These tests confirm that the performance is comparable for a growth rate of 180 s^{-1}, even if in terms of vertical motion there is a preference for the symmetric reduced option.
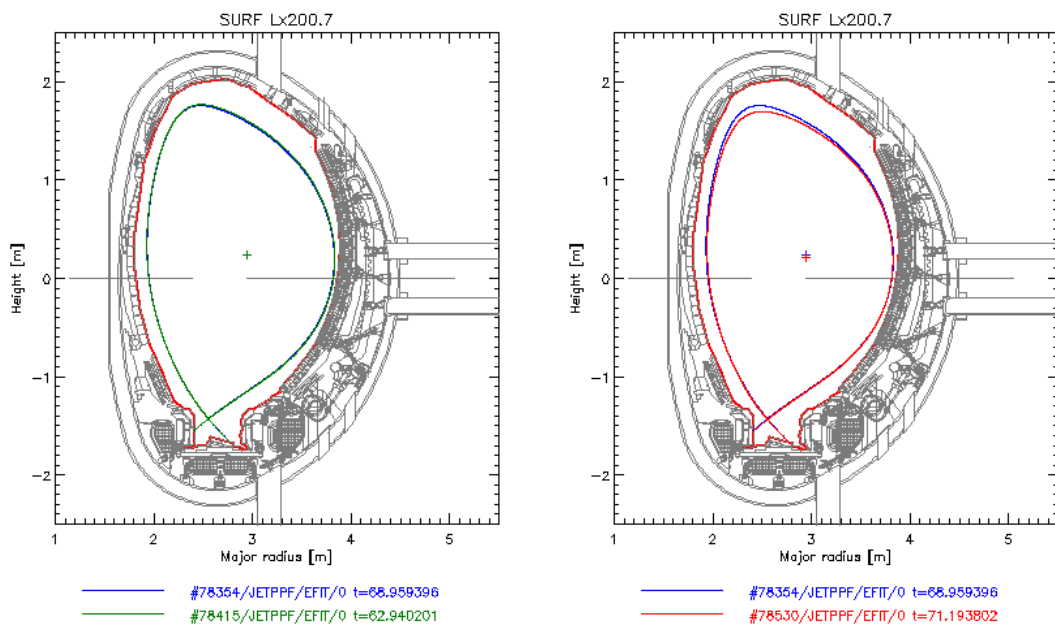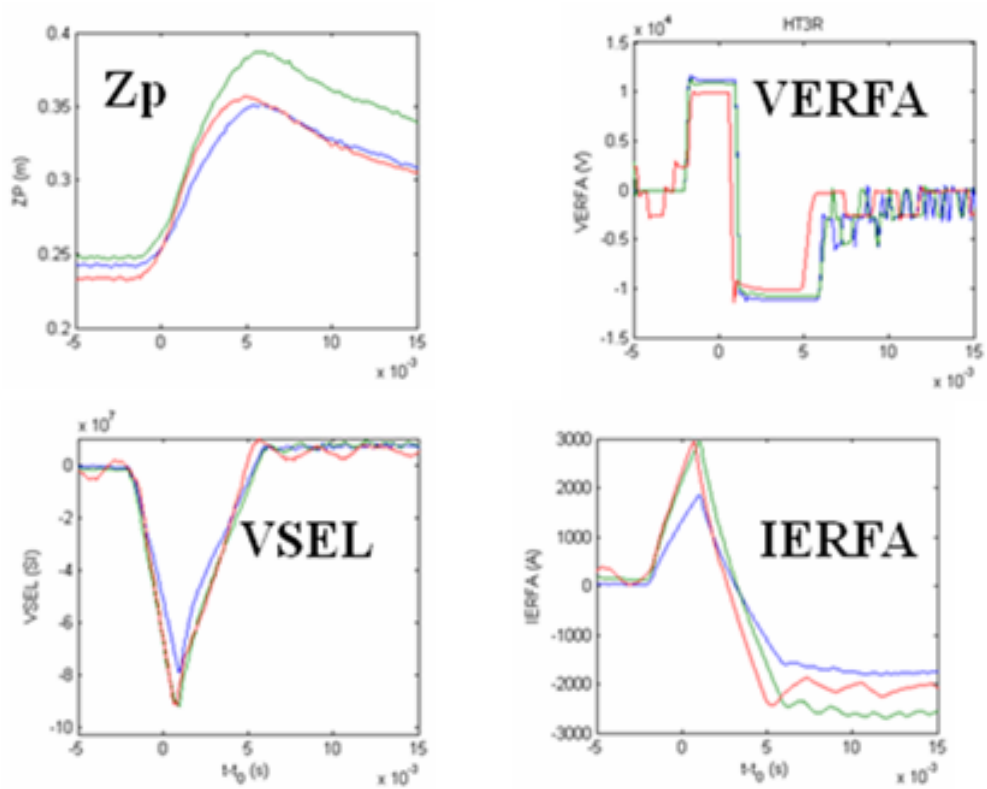
Figure 4.22 Experimental tests carried out on a 1.5 MA plasma at a high triangularity configuration characterized by a growth rate of 180 s^{-1}. Here I_{ERFA} is the amplifier current; V_{ERFA} is the amplifier voltage, Z_p is the vertical position of the plasma current centroid; VSEL is the controlled variable amplifier.

It is interesting to note here that in the asymmetric turns configuration a significant radial movement has been observed, up to 2 cm for a 25 cm kick driven vertical displacement (Fig. 4.23). This could cause problems in controlling the inboard plasma-wall distance.
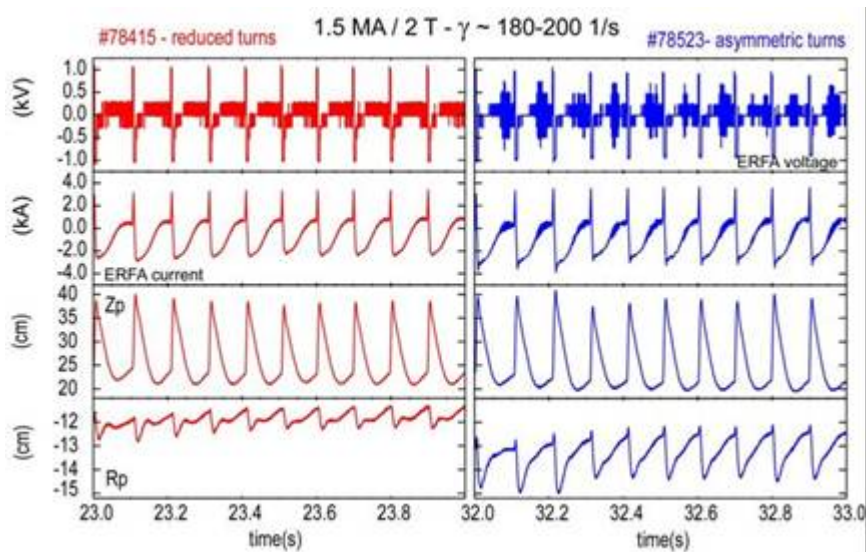
Figure 4.23 Radial and vertical motion during kick and recovery tests. Here R_p (respectively Z_p) is the horizontal (respectively vertical) shift of the plasma current centroid with respect to the center of the plasma chamber.

Moreover the asymmetric configuration was eventually discarded because of interference and control problems with no significant benefits with respect to the reduced symmetric option.

Therefore the reduced symmetric option was finally selected after the experimental kick and recovery tests, which confirmed the theoretical predictions.

5

The Vertical Stabilisation Simulator

5.1 Introduction

To achieve high performance in tokamaks, plasmas with elongated poloidal cross-section, characterized by large vertical instability growth rates, are needed. Such elongated plasmas are vertically unstable, hence position control on a fast time scale is an essential feature of all machines. The achievement of the fast time performance is strictly dependent on the flexibility and reliability of the real-time systems that operate the plant during the experiment. In large experimental plants like JET [2] or ITER [35], it is crucial to have an architecture that supports model-based development to validate software modules against a plant model. Such an architecture permits to minimize the risks related to the development of complex plant control systems. Furthermore, simulation tools can effectively be adopted also during the deployment of real-time systems. Indeed, offline testing of the full real-time system permits to debug the code and validate the real-time version of the control algorithms before running them on the plant [32]. Such an approach permits to minimize the risk of malfunctions and to reduce the time needed for the

commissioning on the plant, yielding a cost reduction. Eventually, by using such a simulation environment, it is possible to perform offline analyses addressed to the fine tuning of the control algorithms for specific operative scenarios. In order to adopt such an approach, the real-time framework has to satisfy some key requirements: in particular it must allow to run the real-time code in an offline (non real-time) environment, interfacing it with a plant simulator. On the other hand, reliable plant models must be available.

A MARTe-based simulator has been recently developed at JET tokamak, and it has been used to validate the new JET Vertical Stabilization (VS) system [40]. MARTe [49] is the multi-thread framework used at JET to deploy hard real time control systems. Thanks to the modularity of its software architecture, MARTe allows to interface the real-time control system with a C++ version of the plasma magnetic linear model. It also allows to use different linear models (corresponding to different plasma equilibria) in different pulse phases, in order to simulate a complete JET pulse.

This chapter describes the software architecture of the MARTe-based simulator. As an example case study, it is shown how this tool has effectively been used to evaluate the effects of Edge Localized Modes (ELMs) on the VS system [75]. In particular, a drop of energy due to an ELM occurrence is simulated by a variation of both poloidal beta and internal inductance [73]. These parameters are considered as a disturbances applied to the plasma linearized model. By using the simulator it is possible to analyze different plasma configurations, extrapolating the operational limit of the new vertical amplifier in term energy of largest rejectable ELM.

5.2 Design of the Vertical Stabilization Simulator

The new VS control system represents the first MARTe based control system that has been successfully developed and deployed at JET [40]. Within the MARTe environment, the end users are required to define and implement algorithms inside a well defined software block named Generic Application Module (GAM), which is executed by a real-time scheduler. The JET VS system was implemented by using MARTe under the Real Time Application Interface (RTAI)/Linux operating system. The adoption of a standard framework for the development of real-time systems, model-based design and validation is effective approach to reduce the time needed for commissioning a new system on the plant.

Exploiting the MARTe modularity it is possible to add different modules to the structure of the VS system, in order to implement a complete closed-loop simulator that permits to study the VS behaviour. In particular, in Fig. 5.1, the four GAMs shown in yellow have specifically been developed to simulate the plant.

The VS simulator has been very useful during the commissioning phase of the new VS system, especially to tune the controller parameters and to study the behaviour of the new control law.

The following sections present the software architecture of the VS simulator and its human machine interface.
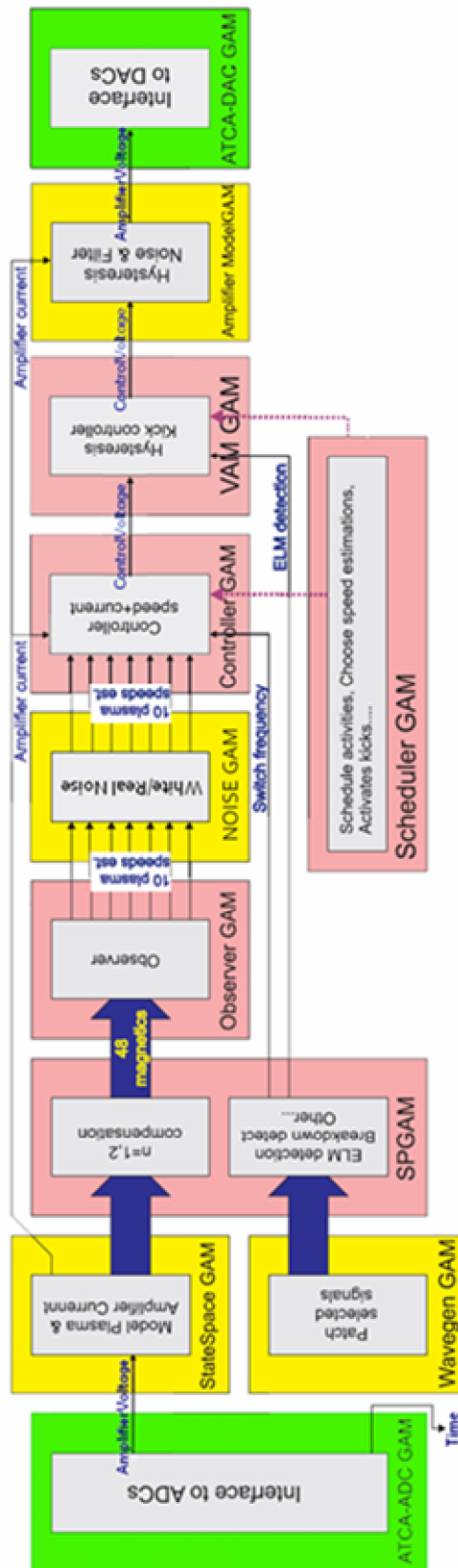
Figure 5.1 Block diagram of the VS software architecture

5.2.1 Software architecture

The VS simulator is MARTe based and mimics the same structure of the VS system. By adding four different modules to the structure of the VS system it is possible to implement a complete closed-loop simulator of the same code that runs on the real plant. In particular the four simulation GAMS depicted in yellow in Fig. 1 have been added:

- *state–space GAM*: it allows to simulate the plant behaviour by receiving the voltage applied by the Enhanced Radial Field Amplifier (ERFA) as input, and produces the estimation of the plasma vertical velocity and the amplifier current as outputs. The state–space model can be configured by using the CREATE–L code. This GAM allows to load different linearized model to take into account the different plasma configurations, allowing to simulate a complete JET pulse.

- *waveform generator GAM*: it allows to add inputs that are not modified by the closed–loop, e.g., the plasma current, which is an input for the simulator and it is not modified by the VS system.

- *ERFA logic GAM*: it allows to simulate hysteretic characteristic of ERFA and adds some noise to simulate a real acquired signal.

- *noise GAM*: the plasma vertical velocity measurement used for the vertical stabilization in JET, is reconstructed by means of a suitable linear combination of flux and field time derivative measurements, This reconstructed signal is obviously affected by error. The main sources of errors are: errors due to the violation of hypotheses assumed by the reconstruction algorithm; noise due to power electronics; noise due to measurement instrumentation & signal conditioning electronics; noise due to *plasma activity*. The *noise GAM* allows to add noise signal to the plasma vertical velocity computed by the model, in order to model all these sources of uncertainty.

5.2.2 Human Machine Interface

At JET the plant control systems are configured using a distributed system named Level-1. This system is utilized by the expert users to set up all the VS system parameters before the experiment.

MARTe provides a web interface which enables the browsing its internal components, allowing the user to navigate into the GAMs' structure and check the values of the parameters loaded in the VS system.

The human-machine interface of the simulator has been designed as similar as possible to the VS Level-1 interface. Thanks to this choice, by using the simulator, the user can access to all the parameters available on the plant during the experiment. The Level-1 interface for MARTe based systems is divided in two levels:

- *Real-time executor level*, which allows the user to load the MARTe skeleton configuration; where the can specify what GAMs are to be executed together with their basic parameters. It is important to note that this level is common to all MARTe-based applications;

- *Application level*, which is customized for the VS system. This level is designed to allow the user to set each controller parameter before the experiment and to configure the GAM parameters using fully featured graphical user-interface.

The user interface of the simulator presents the same structure as the Level 1. This interface is realized by using the Matlab® GUI Application. As shown in Fig. 2 (yellow blocks), this interface is structured in two levels: the former allows to load the machine configuration file, the latter allows to change it by setting the controller parameters and add the different linearized models of plasma.
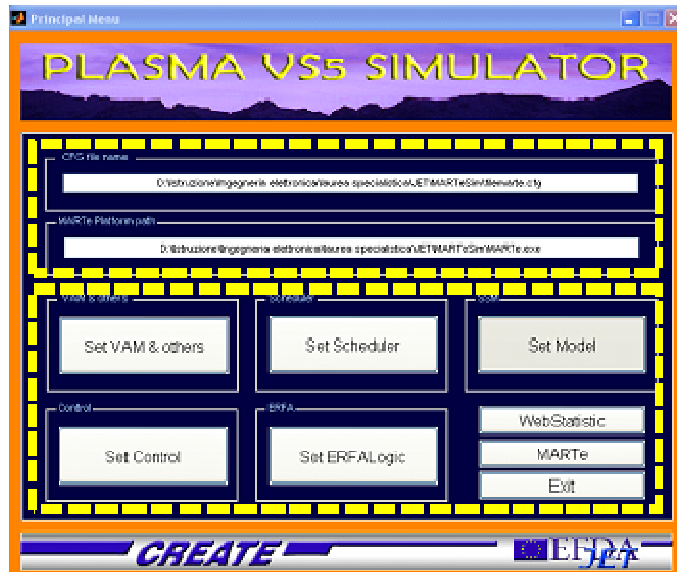
Figure 5.2 MATLAB GUI Interface of the simulator

In particular:

- Set VAM & others: allows to change the parameter of the Vertical Amplifier Manager (VAM) GAM and add the waveforms of the signals that are not modified by the closed–loop.

- Set Scheduler: allows scheduling the experiment because every JET discharge is logically divided into a number of *time windows*. As shown in Fig. 3, for each time windows it is possible to set several control mode and several controlled variables.

- Set Model. allows to load different linear models (corresponding to different plasma scenarios) in different pulse phases, allowing to simulate a complete JET pulse.

- Set Control: allows to set all the parameters of the controller which are independent from the scheduling of the pulse. These global parameters are set by using a waveform editor.

- Set ERFA Logic: allows to set the amplifier parameters.

Figure 5.3 Interface of the simulator to set the controller parameters for each time window.
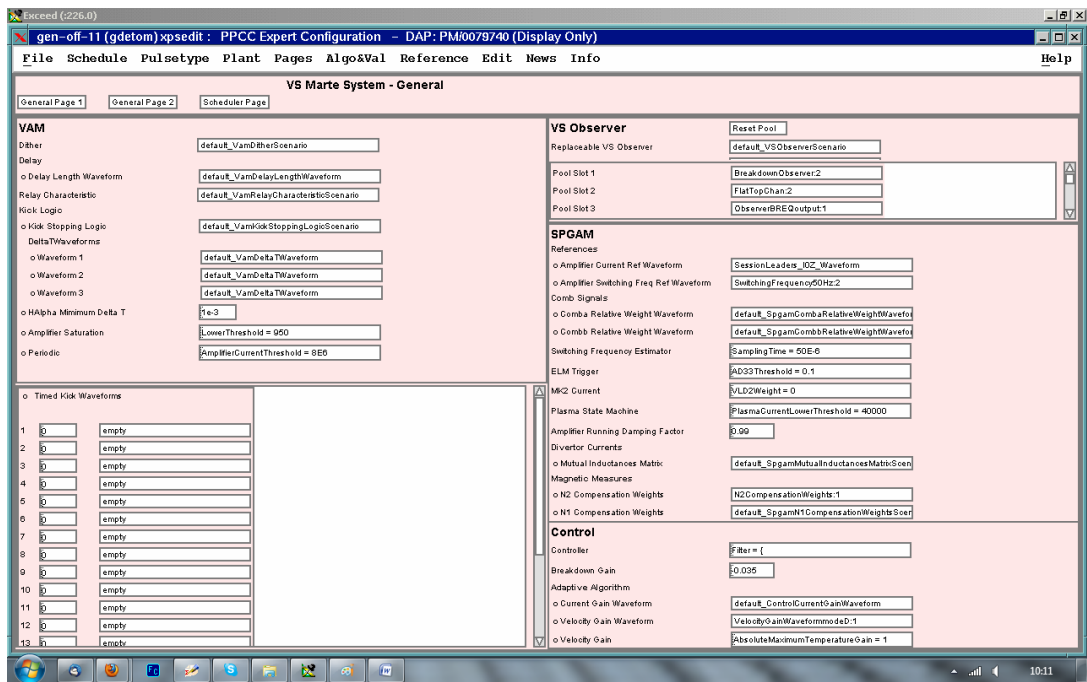
5.3 Study of VS performance: larger rejectable ELM

The VS simulator has useful to study the operational limits of the VS system in the presence of very strong localized MHD plasma instabilities, named ELMs. ELMs manifest themselves as strong magnetic perturbations associated with a burst of D-alpha radiation and a loss of particles and energy from the plasma periphery. Moreover an ELM event is characterized by a loss of the diamagnetic energy that is strictly related to a variation of poloidal beta and the relationship is given by [73]:

$$\Delta W = \frac{3}{8}\mu_0 R_0 I_p^2 \Delta\beta$$

where *Ip* is the plasma current, R_0 is the major radius and *Δβ* is the variation of poloidal beta.

Because the perturbation affects the magnetic fields creating a strong variation in the plasma speed measurement, the VS *sees* an ELM as a rapid increase of plasma speed (ZPDIP) followed by a rapid inversion and a slower decay (Fig. 4). This causes the firing of ERFA and a resulting vertical excursion of the plasma, in some cases associated with loss of control.

For these reason it is very important to characterize the behaviour of the VS system in terms of energy drop of largest rejectable ELM.

Since an ELM event creates a strong variation in the plasma speed measurement, it can be modelled as a disturbance for the VS system. In particular, by using the CREATE-L model, a representation of the plant behaviour is given in the state space form. A characterization of ELMs by means of poloidal beta and internal inductance variations has been carried out via simulation, using both experimental magnetic signals and CREATE-L models. By considering the identified quantities as disturbances for the system, the closed loop simulations have been carried out by using the MARTe simulator. In particular, the inputs of the system are the amplifier voltage and the identified quantities, whereas the outputs are the amplifier current and the estimation of the vertical velocity.
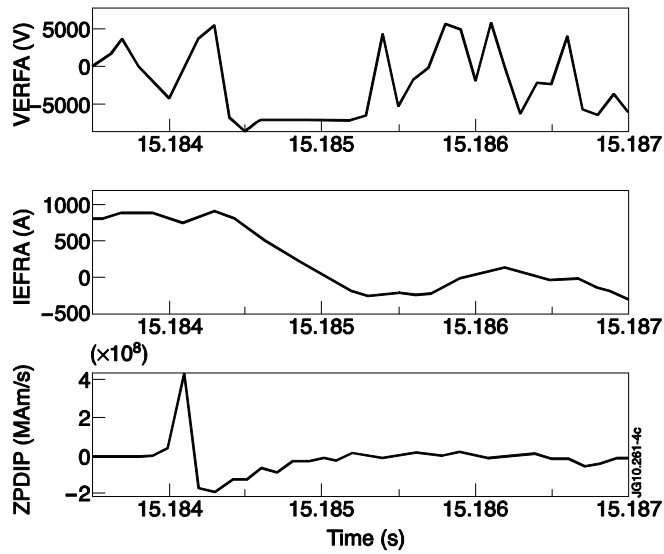
Figure 5.4 Effect of an ELM event on the VS parameters.

Thanks to these simulations it has been possible to find the maximum controllable ELM by multiplying the disturbances for a factor α Since the poloidal beta and internal inductance variations are strictly related to a loss of diamagnetic energy, with this simulations it was possible to find the maximum controllable ELM from the VS system in term of maximum diamagnetic energy loss.

The tolerable poloidal beta drop $\Delta\beta$ scales with $1/I_p$, whereas the tolerable energy drop ($\Delta W \propto \Delta\beta I_p^2$) scales with I_p. ELM transients are characterized by fast dynamics (hundreds of µs) followed by a slow β drop (tens of ms).

In pulse #78452 with *Ip=3 MA*, and a relatively high growth rate of the vertical instability ($\gamma=200$ s^{-1}), the VS system tolerated a considerable energy drop ($|\Delta W|>1.5$ *MJ*) with an excursion of the ERFA current ($|\Delta I_{ERFA}|=2.5$ *kA*) well below its operational limit. Simple extrapolations based on scaling laws and more accurate simulations based on the CREATE-L model show that the tolerable energy drop for a 4 MA plasma would have been well beyond 2 MJ, with a dramatic improvement with respect to the previous VS system with the old radial field amplifier FRFA.

As shown on Fig. 5(a) the ELM effect on the VS system in characterized by two phases. The first one is a fast phase in which the simulated trace is very close to the experimental behaviour.

On the contrary, during the slow phase the simulated behaviour is very different from the experimental one. As shown on Fig. 5(b) this experimental behaviour is

119

essentially due to a shape controller effect that is not taken into account by the VS simulator.

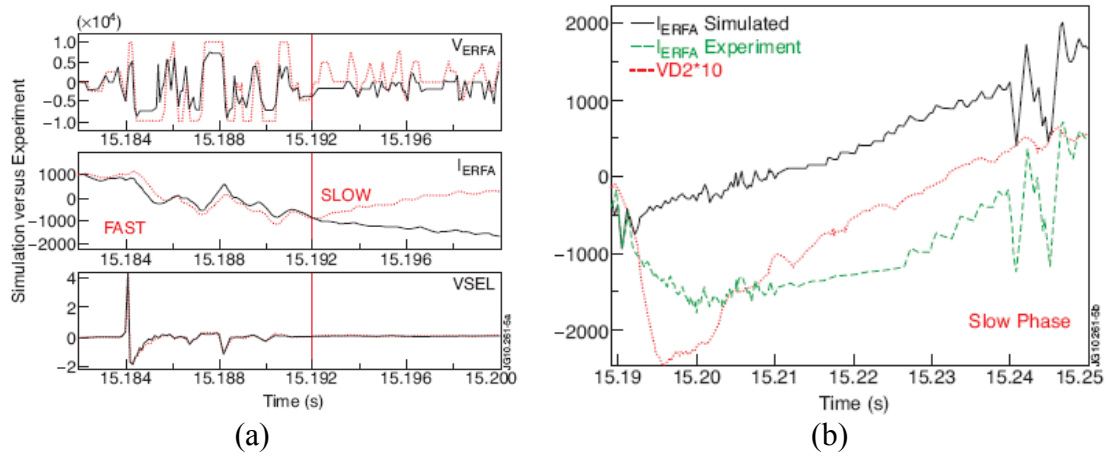(a)   (b)

Figure 5.5 (a) Comparison between experimental data (black line) and simulation (red line) during an ELM event. (b) Experimental behaviour during slow phase is essentially due to a shape controller effect.

6
Conclusions

This thesis discusses problems of plasma control and modelling in Tokamaks, experimental thermonuclear fusion facilities that magnetically confine a fully ionized gas called plasma.

Most of the activities described in this thesis have been carried out in the framework of the Plasma Control Upgrade (PCU) project. The PCU project and the related enhancement of the Radial Field Amplifier [40] aimed at providing the JET tokamak with a significant improvement in its vertical stabilisation capability in high performance conditions. Throughout its life this project relied heavily on modelling activities both to guide the design of the new VS controller and to assess regularly the expected performance of the new system. Eventually, the model-based approach was also used to influence the planning of the integrated commissioning of the system.

My contribution to the project has been in term of both modelling and commissioning activities.

The alternative controlled variable OBS05 [37] has been proposed and successfully tested on the vertical stabilization system of JET. The main motivation of this study

was the need of operating JET in future campaigns with the new ITER-like wall (ILW), which is expected to significantly shield some magnetic diagnostics. This study was also aimed at improving the VS capabilities by reducing the effect of edge localized modes (ELMs) on the vertical position estimator. The alternative controlled variable was also planned to play the role of back-up solution in case of troubles with the standard one after the modifications of the radial field circuit. The new controlled variable OBS05 was successfully tested in JET experimental campaign on a variety of plasma scenarios and was then used as preferred VS controlled variable. The behaviour of OBS05 was better than ZPDIP in the Elm phases of some pulses, yielding a significant reduction (about 40 %) of the excursion of ERFA current.

The modelling approach is fundamental both to guide the design of the new VS controller and to assess regularly the expected performance of the new system. Concerning modelling analysis several tools have been developed in order to:

- evaluate the shielding effects on the magnetic sensors and related new VS controlled variable usable with the new ITER like wall;

- Establish the optimal configuration of radial field coils.

- study the undesired vertical oscillations of the plasma, linked to the plasma shape control [76];

- have an indication of limits for kick duration, to avoid disruption during normal operation;

- provide a method for the experimental estimation of the growth rate of the vertical instability;

- model the new radial field amplifier

All these tools developed and tested for JET VS system could be used in future devices like ITER [35].

Moreover a fully validated closed loop simulator [75] for the JET VS system has been developed. This simulator has effectively been used to test the VS software offline during the commissioning of the system. Furthermore this simulator has been used to assess the system performance by tuning the controller parameters. The VS simulator has been developed in the MARTe framework [49], exploiting its modularity, the coupling between the VS system and the shape controller at JET can

be analyzed in the future by simply adding the shape controller GAM. The VS simulator can also be used in future devices like ITER.

The work has been carried out at JET during the experimental campaign of 2008 - 2009.

The PCU Project, together with the ERFA upgrade, has delivered to JET a significantly improved Vertical Stabilisation system more than capable to meet the future challenges of operation in highly elongated plasmas with large perturbations to the vertical stability.

The integrated plasma commissioning of ERFA and its upgraded control system VS5 has been carried out in a very short period of only 4 experimental weeks [77], [74]. Thanks to the excellent preparation, via modelling and advanced commissioning of some of the VS5 features, the commissioning team succeeded in completing all the essential items and responding positively to the unplanned technical problems that are typical of tokamak operations.

The PCU project and, more specifically, the integrated ERFA/VS5 commissioning has provided a full size test of application of model-based approach to design and implementation of a major and essential subsystem in a complex tokamak environment. Many activities carried out at JET during this commissioning can be regarded as ITER relevant, and can therefore give significant indications for ITER controller design and any possible satellite experiments.

References

[1]   F. F. Chen. Introduction to plasma physics. Plenum Press, 1974.

[2]   J. Wesson. *Tokamaks*. Oxford University Press, 2004.

[3]   J. D. Lawson. Some criteria for a power producing thermonuclear reactor. Proceedings of the Physical Society, 70:6-10, 1957.

[4]   N. J. Fisch. Theory of current drive plasmas. Reviews of Modern Physics, 59(1):175-234, 1987.

[5]   M. Shimada, V. Mukhovatov, G. Federici, Y. Gribov, et al. Performance of ITER as burning plasma experiment. Nuclear Fusion, 44:350-356, 2004.

[6]   R. O. Dendy. Plasma Dynamics. Clarendon Press - Oxford, 1990.

[7]   R. O. Dendy, editor. Plasma Physics - An introductory course. Cambridge University Press, 1993.

[8]   EFDA-JET website. http://www.jet.efda.org.

[9]   L.E. Zakharov, V.D. Shafranov, Equilibrium of a toroidal plasma with non circular cross section, Sov. Phys.-Tech. Phys., 18(2), 151-156, 1973.

[10] J. P. Freidberg, Ideal Magneto-Hydro-Dynamics, Plenum Press, New York, 1987, pp. 59-85.

[11] J. P. Freidberg. Ideal magneto-hydro-dynamics. Plenum Press, 1987.

[12] Zohm H.1996 Edge localized modes(ELMs) Plasma Phys.Control.Fusion38 105–28.

[13] Connor J.W. 1998 A review of models for ELMs Plasma Phys.Control. Fusion 40 191–213.

[14] F. Sartori et al., "The JET PCU project: an international plasma control project," Fus. Eng. Design, vol. 83, no. 2–3, pp. 202– 206, Apr. 2008.

[15] M. Lennholm et al., "Plasma vertical stabilisation at JET using adaptive gain control," in Proc. 17th SOFE Conf., vol. 1, San Diego, CA, 1997, pp. 539–542.

[16] V. Toigo et al., "Conceptual design of the enhanced radial field amplifier for plasma vertical stabilisation in JET," Fus. Eng. Design, vol. 82, no. 5–14, pp. 1599–1606, Oct. 2007.

[17] F. Sartori et al., The system architecture of the new jet shape controller. Fusion Engineering and Design, 74(1-4):587{591, 2005.

[18] J. P. Freidberg, Ideal Magneto-Hydro-Dynamics, Plenum Press, New York, 1987, pp. 59-85.

[19]   V.D. Shafranov, "Plasma equilibrium in a magnetic field, "Reviews of Plasma Physics,vol. 2, no. 1, pp. 103-151, Jan. 1966**.**

[20]   G Ambrosino, R Albanese, Magnetic control of plasma current, position and shape in Tokamaks: a survey of modelling and control approaches, IEEE Control Systems, Vol.25 No.5, pp. 76-92 (Oct.2005).

[21]   E. B. Becker, G. F. Carey and J. T. Oden, Finite Elements, An Introduction, Volume I, Prentice-Hall, Englewood Cliffs, New Jersey, 1981.

[22]   O. C. Zienkiewicz and R. L. Taylor, The Finite Element Method, Fourth Edition, Volumes 1 and 2. New York, McGraw-Hill: (1989), (1991).

[23]   G. Strang & G. Fix, An Analysis of the Finite Element Method, Prentice-Hall, Englewood Cliffs, New Jersey, 1973.

[24]   K Kurihara, Tokamak plasma shape identification on the basis of boundary integral equations, Nuclear Fusion, Vol.33, No.3, 399-412, 1993.

[25]   J. L. Luxon, B. B. Brown, Magnetic analysis of non-circular cross-section tokamak, Nuclear Fusion Vol.22, pp. 813-821,June 1982.

[26]   R. Albanese and F. Villone. The linearized CREATE-L plasma response model for the control of current, position and shape in tokamaks. Nucl. Fusion, 38:723–738, 1998.

[27]   R. Albanese, G. Artaserse, M. Mattei, O. Tudisco, JET – EFDA Contributors. Plasma reconstruction in tokamaks with linearized approaches. International Journal of Applied Electromagnetics and Mechanics 26 (2007) 191-199.

[28]   D.C. Robinson and A.J. Wootton, "An experimental study of tokamak plasmas with vertically elongated cross-sections, "Nuclear Fusion, vol. 18, no. 11, pp. 1555-1567, Nov. 1978.

[29]   M. Okabayashi and G. Sheffield, "Vertical stability of elongated tokamaks, "Nuclear Fusion, vol. 14, no. 2, pp. 263-265, Apr. 1974.

[30]   K. Lacknerand A.B. Macmahon, "Numerical study of displacement instability in elongated tokamak, "Nuclear Fusion, vol. 14, no. 4, pp. 575-577, Sept. 1974.

[31]   E.A. Lazarus, J.B. Lister, and G.H. Neilson, Control of the vertical instability in tokamaks, Nuclear Fusion, vol. 30, no. 1, 111-141, Jan. 1990.

[32]   G. Ambrosino, G. Celentano, V. Coccorese, and F. Garofalo, Controller design for plasma position and current control in NET, in Proc. 15th Symp. Fusion Technology, Utrecht, 1988, pp. 1670–1674.

[33]   R. Albanese, E. Coccorese, G. Rubinacci, Plasma modelling for the control of vertical instabilities, Nuclear Fusion, vol. 29, no. 6, pp. 1013-1023, June 1989.

[34]   R. Albanese. Evoluzione temporale di un plasma confinato magneticamente. PhD thesis, Università degli Studi di Napoli Federico II, 1986.

[35]   J. Paméla et al., "The JET programme in support of ITER", Fusion Eng. and Design, 82(5-14), (2007), 590-602.

[36]   R. Albanese and G. Rubinacci, "Finite element methods for the solution of 3D eddy current problems", Advances in Imaging and Electron Physics, New York: Academic Press, vol. 102, pp. 1–86, 1998.

[37]   R. Albanese and T. Bellizio, "An alternative controlled variable for JET vertical stabilization", to appear on Fusion Science and Technology

[38]   R. Albanese, G. Artaserse, T. Bellizio, G. Rubinacci, R. Fresa, B. Viola, M. Furno Palumbo, F. Villone, Y. Liu and JET-EFDA Contributors, "Coupling plasmas and 3D passive structures in the JET tokamak", Journal International Journal of Applied Electromagnetics and Mechanics Volume 33, Number 1-2 / 2010, Pages 533-540

[39]   R. Albanese, G. Artaserse, F. Maviglia, F.Piccolo, F. Sartori, "Identification of Vertical Instabilities in the JET Tokamak", IEEE Transactions on Magnetics, vol. 44, issue 6, pp. 1650-1653.

[40]   T.Bellizio et al., "The Software Architecture of the new Vertical Stabilization System for the JET tokamak", submitted for publication on IEEE Trans. on Plasma Science.

[41]   M. Ferrara et al., "Plasma inductance and stability metrics on Alcator C-Mod", Nuclear. Fusion, 48 065002, 2008.

[42]   M. Ariola and A. Pironti, Magnetic Control of Tokamak Plasmas. Springer, 2008.

[43] J. Y. Favez, "Enhancing the control of tokamaks via a continuous nonlinear control law," Ph.D. dissertation, CRPP-EPFL, 2004.

[44] F. Sartori et al., "The JET PCU project: an international plasma control project," Fus. Eng. Design, vol. 83, no. 2–3, pp. 202–206, Apr. 2008.

[45] F. Sartori, G. De Tommasi, and F. Piccolo, "The Joint European Torus," IEEE Control Sys. Mag., vol. 26, no. 2, pp. 64–78, Apr. 2006.

[46] M. Becoulet *et al.*, "Edge localized mode physics and operational aspects in tokamaks," *Plasma Phys. Control. Fus.*, vol. 45, no. 12A, pp. A93–A113, Dec. 2003.

[47] R. Albanese, G. Calabrò M. Mattei, and F. Villone, "Plasma response models for current, shape and position control at JET," *Fus. Eng. Des.*, vol. 66–68, pp. 715–718, 2003.

[48] A. Neto et al., "Linux real-time framework for fusion devices", Fus. Eng. Des., vol. 84, no. 7–11, pp. 1408–1411, Jun. 2009.

[49] A. Neto et al., "MARTe: a Multi-platform Real-time Framework," in *Proc. 16th IEEE NPSS Real Time Conference (NPSS-RT2009)*, Beijing, People's Republic of China, May 2009.

[50] M. Ariola and A. Pironti, "The design of the eXtreme Shape Controller for the JET tokamak," IEEE Control Sys. Mag., vol. 25, no. 5, pp. 65–75, Oct. 2005.

[51] R. Albanese *et al.*, "Design, implementation and test of the XSC extreme shape controller in JET," *Fus. Eng. Design*, vol. 74, no. 1–4, pp. 627–632, Nov. 2005.

[52] G. De Tommasi *et al.*, "XSC Tools: a software suite for tokamak plasma shape control design and validation," *IEEE Trans. Plasma Sci.*, vol. 35, no. 3, pp. 709–723, Jun. 2007.

[53] M. Ariola *et al.*, "Integrated plasma shape and boundary flux control on JET tokamak," *Fusion Sci. Technol.*, vol. 53, no. 3, pp. 789–805, Apr. 2008.

[54] M. Lennholm *et al.*, "Plasma vertical stabilisation at JET using adaptive gain control," in *Proc. 17th SOFE Conf.*, vol. 1, San Diego, CA, 1997, pp. 539–542.

[55] A. J. N. Batista, J. Sousa, and C. A. F. Varandas, "ATCA digital controller hardware for vertical stabilization of plasmas in tokamaks," *Rev. Sci. Instruments*, vol. 77, no. 10, p. 10F527, Oct. 2006.

[56] F. Sartori et al., "n=2 compensation and variable gains for the JET vertical stabilisation," Fus. Eng. Design, vol. 66–68, pp. 727–734, Sep. 2003.

[57] G. Franklin, J.D. Powell, and A. Emami-Naeini, Feedback Control of Dynamic Systems, 5th ed. Prentice Hall, 2006.

[58] V Riccardo, T.C. Hender, P.J. Lomas et al., "Analysis of JET halo currents", Plasma Phys. Control. Fusion 46 (2004) 925–934.

[59] R. Albanese, M. Mattei and F. Villone, "Prediction of the growth rates of VDEs in JET", Nucl. Fusion 44 (2004) 999–1007.

[60] F. Sartori, et al., "Synchronous ELM Pacing at JET Using the Vertical Stabilisation Controller", 35th EPS Conference on Plasma Physics, Hersonissos, Crete, Greece, June 2008.

[61] T. Bellizio, et al., "Using Magnetic Diagnostics to Extrapolate Operational Limits in Elongated Tokamak Plasmas", 17th IEEE NPSS Real Time Conference.

[62] D. Ganuza et al., The design and manufacture of the enhanced radial field amplifier (ERFA) for the jet project, Fusion Engineering and Design Volume 84, Issues 2-6, June 2009, Pages 810-814.

[63] V.Toigo et al., Conceptual design of the enhanced radial field amplifier for plasma vertical stabilisation in JET, Fusion Engineering and Design Volume 82, Issues 5-14, October 2007, Pages 1599-1606.

[64] S.R. Shaw et al., The Installation, Testing and Performance on the JET coils of the Enhanced Radial Field Amplifier (ERFA), 26th Symposium on Fusion Technology (SOFT), Porto, Portugal.

[65] G. De Tommasi, "Plasma magnetic and kinetic control in a tokamak," Tesi di dottorato.

[66] F. Maviglia, "Modelling of magnetic diagnostics for tokamak control", Tesi di dottorato.

[67] G. De Tommasi, D. Alves, T. Bellizio, et al.,"Real-time Systems in Tokamak Devices. A case study: the JET Tokamak", 17th IEEE NPSS Real Time Conference.

[68] J. Wesson. The science of JET. JET Joint Undertaking, Abingdon,Oxon, 2000.

[69] F. Sartori, A. Barbalace, A.J.N. Batista, T. Bellizio, P. Card, G. De Tommasi, P. Mc Cullen, A. Neto, F. Piccolo, R. Vitelli, L. Zabeo, "The PCU JET Plasma Vertical Stabilisation Control System", 7th IAEA Technical Meeting on Control, Data Acquisition, and Remote Participation for Fusion Research, Aix-en-Provence, France, June 2009.

[70] T. Bellizio, R. Albanese, G. Artaserse, V. Coccorese, F.Maviglia, F. Villone, "Modellistica per il controllo della posizione verticale nel tokamak JET", Riunione annuale Ricercatori di Elettrotecnica, Napoli, 9-11 Giugno 2010.

[71] F. Sartori, A. Barbalace, A.J.N. Batista, T. Bellizio, P. Card, G. De Tommasi, P. Mc Cullen, A. Neto, F. Piccolo, R. Vitelli, L. Zabeo, "The PCU JET Plasma Vertical Stabilisation Control System", Fusion Engineering and Design 85 (2010) 438-442.

[72] A. J. N. Batista, J. Sousa, and C. A. F. Varandas, "ATCA digital controller hardware for vertical stabilization of plasmas in tokamaks," Rev. Sci. Instruments, vol. 77, no. 10, p. 10F527, Oct. 2006.

[73] O. Barana et al., "Real-time determination of confinement parameters in JET", Fusion Engineering and Design Volumes 66-68, September 2003, Pages 697-701.

[74] M. Ariola, F. Crisanti, F. Rimini, R. Albanese, G. Ambrosino, G. Artaserse, T. Bellizio, V. Coccorese, G. De Tommasi, P.J. Lomas, F. Maviglia, A. Neto, A. Pironti, F. Sartori, R. Vitelli, L. Zabeo, "Commissioning of the New JET Vertical Stabilization System with the Enhanced Radial Field Amplifier", accepted for presentation at the 23rd IAEA Fusion Energy Conference.

[75] T. Bellizio, G. De Tommasi, N. Risoli, R. Albanese, A. Neto, "A MARTe based simulator for Vertical Stabilization System", 26th Symposium on Fusion Technology (SOFT), Porto, Portugal.

[76] R. Albanese, G. Ambrosino, M. Ariola, G. Artaserse, T. Bellizio, V. Coccorese, F. Crisanti, G. De Tommasi, R. Fresa, P.J. Lomas, M. Mattei, F. Maviglia, A. Neto, F. Piccolo, A. Pironti, A. Portone, F.G. Rimini, F. Sartori, A. Sorrentino, V. Toigo, F. Villone, B. Viola, L. Zabeo "Overview of

Modelling Activities for Plasma Control Upgrade in JET", 26th Symposium on Fusion Technology (SOFT), Porto, Portugal .

[77] F. G. Rimini, F. Crisanti, R. Albanese, G. Ambrosino, M. Ariola, G. Artaserse, T. Bellizio, V. Coccorese, G. De Tommasi, P. De Vries, P. J. Lomas, F. Maviglia, A. Neto, I. Nunes, A. Pironti, G. Ramogida, F. Sartori, S. R. Shaw, M. Tsalas, R. Vitelli, L. Zabeo "First Plasma Operation of the Enhanced JET Vertical Stabilisation System", 26th Symposium on Fusion Technology (SOFT), Porto, Portugal.